

Velocity evolution of broad-line Ic supernovae with and without gamma-ray bursts

G. Finneran ^{1,*}, L. Cotter ¹, and A. Martin-Carrillo ¹

School of Physics and Centre for Space Research, University College Dublin, Belfield, Dublin 4, Ireland

ABSTRACT

Context. There are more than 60 broad-line Ic (Ic-BL) supernovae (SNe) which are associated with a long Gamma-ray Burst (GRB). A large population of ‘ordinary’ Ic-BLs for which no GRB component is detected also exists. On average, the expansion velocities of GRB-associated Ic-BLs exceed those of ordinary Ic-BLs, however these results have been drawn from small sample sizes. Energy transfer from the GRB jet may play a role in some Ic-BLs, but it is not certain that jets are absent in ordinary Ic-BLs, so this alone cannot fully explain the discrepancy.

Aims. This work presents the largest spectroscopic sample of Ic-BL SNe with and without GRBs to date, consisting of 61 ordinary Ic-BL SNe and 13 GRBs associated with supernovae, comprising a total of 875 spectra. The goal of this work is to investigate how the expansion velocities evolve in cases where an ultra-relativistic jet has been launched (GRB-SN cases) and compare these to Ic-BL SNe without a GRB detection. This will help us to understand whether the presence of the jet affects the evolution of the expansion velocity, possibly allowing us to infer the existence of jets in cases where GRB emission is not detected.

Methods. We measured the expansion velocities of the Fe II, Si II and Ca II lines observed in the spectra of Ic-BL SNe using a spline fitting method. We fit the expansion velocity evolution with single and broken power-laws, allowing us to quantify any possible similarities or differences between Ic-BL SNe with and without an associated GRB.

Results. The expansion velocities of the Fe II and Si II features reveal considerable overlap between the two populations. It is not clear that GRB-associated supernovae expand more rapidly, though it is clear that Ic-BLs in general expand more rapidly than Ic supernovae. Broken power-law evolution appears to be more common for the Si II feature, which always follows a shallow-steep decay. In contrast the broken power-law Fe II decays are predominantly steep-shallow. The power-law indices for both samples were compared for both Fe II and Si II, and suggest that GRB-SNe decline at a similar rate to non-GRB Ic-BL supernovae. The evolution of the Si II features in PTF12gzk and SN2016coi show a striking similarity to GRB060218-SN2006aj. Both of these supernovae may have been engine-driven, and show a broken power-law decay, which could be explained by a two-component model for the ejecta velocity, i.e. a jet or a cocoon.

Conclusions. Neither the velocities nor their evolution can be used to distinguish between Ic-BLs with and without GRBs. Expansion velocities consistent with broken power-law evolution may indicate the presence of two velocity components, which may be evidence for a jet in some of these explosions. However, it is not possible to rule in or out the presence of a jet in any Ic-BL supernova purely based on the velocities. These results suggest that GRB-SNe and Ic-BLs are drawn from the same underlying population of events.

Key words. supernovae: general – Gamma-ray burst: general – Methods: data analysis

1. Introduction

Gamma-ray bursts have been the subject of extensive theoretical and observational interest from the community for over five decades. The duration of the gamma-ray prompt emission has led to the separation of GRBs into long and short bursts (Kouveliotou et al. 1993). Long GRBs (those with prompt emission longer than 2 seconds) were linked to the death of massive stars by the ‘collapsar’ model (Woosley 1993; MacFadyen & Woosley 1999). This model proposes that long-GRBs are the result of a jet launched by a compact object created when a massive star undergoes core-collapse. The deceleration of this jet in the ambient medium outside of the former star is responsible for the GRB afterglow (Mészáros & Rees 1997), whilst dissipation of energy within the jet powers the prompt emission (Daigne & Mochkovitch 1998; Rees & Meszaros 1994).

The most notable prediction from the collapsar model is that a supernova (SN) should accompany nearly every long GRB, with the star’s outer layers being accelerated by deposition of

energy from the central engine within the stellar material. In 1998, the detection of GRB980425 and its associated supernova SN1998bw (Galama et al. 1998) put the collapsar model at the forefront of long GRB science. In the years since the discovery of GRB980425-SN1998bw, over 60 GRB-SN ‘associations’ have been detected (e.g. Finneran et al. (2024); Cano et al. (2017)).

Nearly all of the supernovae associated with GRBs are broad-line Ic supernovae (Ic-BL SNe)¹. These supernovae lack absorption features of Hydrogen and Helium in their spectra. Their photospheric spectra are dominated by broad absorption features, in particular features created by Fe, Si and Ca (Cano et al. 2017) (for reviews of SNe, see Filippenko (1997); Smart (2009)). These broad features are the result of the rapid expansion of the outer layers of the SN ejecta. Ic-BLs are believed to result from the death of a Wolf-Rayet star, which has been stripped of its hydrogen and helium layers, either through episodic/eruptive mass loss, mass loss due to winds, or interac-

¹ SN2011kl, a super-luminous, magnetar-powered SN associated with GRB111209A is the sole exception to this pattern.

* gabriel.finneran@ucdconnect.ie

tion in a binary system (e.g. [Smith 2014](#); [Crowther 2007](#); [Mokiem et al. 2007](#)).

The association between GRBs and Ic-BLs has been extensively investigated over the past 25 years (for a review of GRBs associated with SNe (hereafter GRB-SNe), see [Cano et al. \(2017\)](#); a review of GRB jets in SNe may be found in [Corsi & Lazzati \(2021\)](#)). Observations of long GRBs at low redshifts indicate that the majority of these events are associated with a supernova, with simulations showing that the same central engine can power both the GRB and the Ic-BL SN ([Barnes et al. 2018](#)). In cases where an extensive follow-up campaign was conducted, supernova-like emission is ruled out for just five events at low redshift: GRB 060505 ([Fynbo et al. 2006](#)), GRB 060614 ([Fynbo et al. 2006](#); [Gal-Yam et al. 2006](#); [Della Valle et al. 2006](#)), GRB 111005A ([Michałowski et al. 2018](#); [Tanga et al. 2018](#)), GRB 211211A ([Rastinejad et al. 2022](#); [Troja et al. 2022](#)), and GRB 230307A ([Levan et al. 2024](#)).

Fewer than one in four Ic-BL supernovae have an associated GRB detection². Despite this, Ic-BLs appear to have very similar parameters regardless of whether or not they are associated with a GRB. Ic-BLs with GRBs synthesise $\sim 0.4 \pm 0.2 M_{\odot}$ of nickel, with ejecta of $\sim 6 \pm 4 M_{\odot}$ (e.g. [Cano et al. 2017](#)), while ordinary Ic-BLs synthesise $\sim 0.3 \pm 0.2 M_{\odot}$ of nickel, with ejecta of $\sim 4 \pm 3 M_{\odot}$ (e.g. [Taddia et al. 2019](#); [Prentice et al. 2016](#); [Lyman et al. 2016](#); [Taddia et al. 2015](#); [Drout et al. 2011](#)). These two populations also have similar supernova kinetic energies (c.f. [Taddia et al. 2019](#); [Cano et al. 2017](#)). A spectroscopic comparison of a small sample of Ic-BLs with and without an associated GRB showed that GRB-SNe seem to have systematically higher expansion velocities (although the velocities of both populations were consistent within one sigma), and broader features than ordinary Ic-BLs ([Modjaz et al. 2016](#)). It is therefore possible that all Ic-BLs occur with a contemporaneous GRB jet.

The presence of relativistic jets in GRBs gives rise to ‘orphan’ afterglows, which are GRB afterglows observed without a corresponding prompt gamma-ray component ([Rhoads 1997](#); [Mészáros et al. 1998](#)). Observers whose line of sight lies outside the beaming cone of the GRB radiation will not see the prompt emission, and will only observe the afterglow radiation as the jet decelerates. In contrast, the radiation emitted by an Ic-BL is visible in all directions. It is therefore possible that many Ic-BL supernovae could have a contemporaneous GRB, invisible because the observer is too far off-axis. Late-time radio observations suggest that there may be hidden GRBs in some Ic-BLs ([Corsi et al. 2023, 2016](#); [Soderberg et al. 2006](#)). At X-ray wavelengths, simulations using the Python package `afterglowpy` ([Ryan et al. 2020](#)) indicate that typical GRBs associated with Ic-BLs may be invisible at observing angles above 25-30 degrees. To date, SN2020bvc is the only candidate off-axis afterglow associated with an Ic-BL ([Izzo et al. 2020](#)).

The lack of GRBs in some Ic-BL events may be a direct result of jet choking. As the GRB jet propagates through the outer layers of the progenitor, it may become stalled, in a scenario known as a choked jet. If this happens, little to no GRB prompt emission will be produced ([Nakar & Piran 2017](#)). This process may transfer energy to the progenitor, producing a high velocity, hot cocoon around the jet ([Nakar & Piran 2017](#); [Ramirez-Ruiz et al. 2002](#)). Such a cocoon has been observed in some GRB-SNe ([Izzo et al. 2019](#)). However, theoretical work by [Barnes et al. \(2018\)](#) suggests that the impact of the dissipation of the jet energy on the supernova spectra and velocities is minimal. For this

reason, it is not clear why there should be a difference in velocity for Ic-BLs with an associated GRB compared with ordinary Ic-BLs.

Previous studies of Ic-BL velocities (e.g. [Taddia et al. 2019](#); [Modjaz et al. 2016](#)) have relied on small sample sizes. With the rapid increase in the detection rate of Ic-BL supernovae enabled by telescopes such as the *Zwicky Transient Facility* (ZTF) ([Dekany et al. 2020](#)), it has become possible to study a much larger dataset than ever before. The abundance of spectral data in online repositories allows for a quantitative investigation of velocity evolution in these supernovae, which has never been attempted before.

This paper investigates the spectral velocity evolution of the largest sample of Ic-BLs and GRB-SNe collected to date, consisting of almost 900 spectra. A spline fitting method is adopted to measure the velocities of the three major absorption features within the Ic-BL spectrum. The focus of the investigation is to determine whether the velocities of these events can help us to distinguish between Ic-BLs with and without GRBs. Section 2 describes the collection of sample data for this research, highlighting some of the challenges involved in the collation of a large heterogeneous dataset. Section 3 details the methodology and its application to the dataset. The results of this analysis are described in Sect. 4, with the discussion and conclusions presented in Sections 5 and 6 respectively.

2. Sample

The supernovae studied in this analysis were collected via an extensive search of the literature and online repositories, in particular the Weizmann Interactive Supernova Data Repository³ (WiSeREP) ([Yaron & Gal-Yam 2012](#)) and the GRBSN webtool⁴ ([Finneran et al. 2024](#)). The data from the WiSeREP archive were initially gathered for supernovae of types Ic and Ic-BL. This was intended to encompass supernovae which were perhaps labelled as a Ic prior to the common usage of the Ic-BL type in the early 2010s. This approach also ensures that supernovae which have an ambiguous type are included in the initial sample; for example, [Prentice et al. \(2016\)](#) found that supernova SN2016P has an intermediate type between Ic and Ic-BL.

The initial search produced 234 Ic/Ic-BL supernovae. Transients are normally classified on WiSeREP based on features visible in their early spectra. In some cases, follow-up observations around maximum light may lead to the re-classification of the transient, which is normally not reported back to WiSeREP. This leads to contamination of the sample with events which do not meet the criteria of a Ic-BL supernova. To confirm the classification provided by WiSeREP, we followed two approaches. First, a literature search was performed for each SN. This method was used to confirm the type for 133 Ic-BL supernovae, including 63 Ic-BL supernovae which were not originally listed as Ic/Ic-BL.

For those cases where no reliable classification was found in the literature, the SNe were re-classified using the Supernova Identification (SNID) tool ([Blondin & Tonry 2007](#)). This re-classification process was restricted to SNe with at least three publicly available spectra so that a more accurate classification could be obtained and the evolution of the SN velocity could be measured. When determining the supernova type, the redshift was fixed, as it had been measured by other analyses. Fig. 1 shows the redshift distribution of Ic-BL SNe with and without GRB associations considered in this study.

² This figure excludes supernovae associated with GRBs for which no spectroscopic confirmation of the supernova type was available.

³ <https://www.wiserep.org/>

⁴ <https://grbsn.watchertelescope.ie>

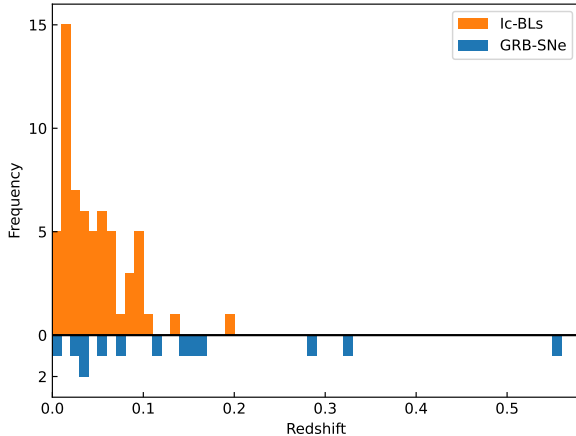


Fig. 1. Redshift distribution of the supernovae used in this analysis. The most distant supernovae are GRB-SNe, as a result of targeted follow-up campaigns after the discovery of their associated GRB. In contrast, the bulk of the Ic-BL population are discovered within redshift 0.1.

The age range of the SNID template spectra used for re-classification was restricted to between -10 and +45 days relative to the peak. Epochs larger than 45 days can show nebular features that are relatively similar among different SN types and can lead to uncertain classification. The -10 day restriction limits the chance that a continuum dominated template spectrum is used during the fitting. Since the default set of templates provided by SNID contains very few Ic-BL supernovae, the stripped envelope supernova templates provided by the NYU supernova group⁵ (Modjaz et al. 2016; Liu et al. 2016) were added to the SNID template database. This is intended to improve the classification accuracy for Stripped-Envelope Supernova candidates, in this case Ic-BL SNe, which otherwise can be classified as Ia SNe by SNID. This analysis ultimately revealed a further 9 Ic-BL supernovae, which as of yet have not been written up in the literature. We also confirmed the classification of 1 Ic-BL which had already been reported elsewhere.

Following these two approaches, a sample of 142 ‘verified’ Ic-BL supernovae was extracted, 29 of them GRB-SNe. This sample was further reduced by imposing a minimum of three spectral observations to allow for investigation the evolution of velocity (ideally spanning a time range around the supernova peak, which is typically 10-20 days since the explosion for Ic-BLs (see e.g. Taddia et al. 2019)) and the need for a known redshift to take into account any possible cosmological effects. The final sample consists of 61 Ic-BL supernovae and 13 GRB-SNe. A list of these SNe may be found in Table B.1.

The supernova spectra, and their metadata, were downloaded from WISEREP using the WiseRep API⁶ (Müller-Bravo 2023). This is a third party tool which was modified to provide both the spectra and their metadata from WISEREP and was also used to automate the SNID classifications. Some of the spectra were found to contain data from the same observation, uploaded multiple times to WISEREP. This was common for telescopes that maintain their own database, since WISEREP downloads the spectra from these repositories as they become available. In a few cases the original observers re-uploaded these spectra following publication of the full dataset. There was also significant

overlap between GRBSN Webtool data and WISEREP data. For all pairs of spectra with the same observation date, a visual examination was performed to remove duplicate spectra. This step was also used to remove any near-identical spectral pairs (for example, when galaxy-subtracted spectra were available these were retained instead of the original spectrum). If emission line removal or de-reddening of the spectrum was detected for one of the spectra in a pair, the spectrum with the highest signal to noise ratio and least evidence of artefacts was retained. The duplicate spectra flagged by this investigation are excluded from velocity measurements. 232 of the initial spectra were rejected based on the search for duplicates. In total, this study includes 875 unique spectra in the final sample analysed, which is the largest to-date for Ic-BLs.

In the case of GRB-SNe, the GRB trigger time was sourced from the GRBSN webtool and used as the explosion time (t_0) (the GRB trigger time is typically accurate to within a few seconds). For non-GRB Ic-BLs, the explosion time needs to be calculated from the rising of their light curve using a low-order polynomial fit. Thus, the precision of t_0 in these cases depends on how well sampled the light curve is. When available, explosion times were sourced from the literature. Otherwise, t_0 was estimated from the light curve using publicly available photometric data. If the resulting fit produced uncertainties larger than 10 days, or in the absence of accessible photometric data, the explosion time was assumed to be the halfway point between a non-detection and the first detection, or the first detection itself depending on the available information.

3. Methods

3.1. Visual examination

A visual examination was performed for all spectra. The purpose of this review was to remove corrupted data, as well as those which show nebular features or are dominated by continuum emission. Supernovae of type Ic-BL enter the nebular phase on a timescale of a few months. During this transition, the optical depth of the supernova decreases due to its continued expansion, and recombination of elements in the ejecta, rendering it transparent to optical radiation. As a result, the supernova spectrum transitions from an absorption dominated regime to an emission dominated one (see e.g. Sahu et al. 2018). In a nebular spectrum, the minimum wavelength of absorption features may be shifted due to contamination by flux from adjacent emission lines, or the feature may disappear entirely. To avoid any contamination of the results for velocity with spectra from the nebular phase, each spectrum was examined for nebular features prior to fitting. This avoids any bias that may be introduced by filtering the spectra based on an arbitrary time when the nebular transition is expected to happen. Likewise, spectra which appear to be dominated by continuum are removed, since they have no clearly identifiable features to fit. This is often the case during the early evolution of a GRB-SN, when the contribution of the GRB afterglow is significant.

3.2. Redshift determination and de-reddening

Following the visual examination, an effort was made to verify the supernova redshift. This was motivated by the fact that some of the spectra available on WISEREP had already been de-redshifted. If a spectrum that has already been corrected for redshift is corrected a second time, the measured velocities will appear larger than their true values. The redshift check was usu-

⁵ <https://github.com/nyusngroup/SESNSpectraLib>

⁶ <https://pypi.org/project/wiserep-api/>

ally performed by searching for the 6553Å H α line, and ensuring that it is centred near its rest wavelength. Since this check was performed by hand, it is only capable of catching larger discrepancies. The redshift was also verified by examining the plotted spectra in the literature for some supernovae. In cases where redshift determination was not made by one of these methods, an attempt to align the spectra based on the evolution of the entire dataset was made. In this case, the velocity evolution of the full spectral sequence is comparable, even if the overall value is shifted slightly with respect to other SNe.

As the supernova light propagates through its host galaxy, and the Milky Way, it is scattered and absorbed by dust grains in a process known as reddening. A correction for this reddening effect may be applied to the spectra of an SN, for example by following the prescription of Cardelli et al. (1989). However, de-reddening typically scales the continuum of the spectrum, rather than affecting the minimum flux of absorption features, which is a function of the feature’s velocity. Liu et al. (2016) found that there was no difference between the de-reddened velocity and the velocity before reddening in their supernovae sample. In this analysis, no correction for reddening was performed, though it should be noted that some SNe may have been de-reddened prior to being uploaded to WISEREP.

3.3. Emission line removal

Emission lines from the host galaxy or the sky, as well as cosmic ray artefacts, are present in some of the sample spectra. These may make it difficult to isolate the continuum, and can affect the location and shape of the absorption lines. Additionally, spectral smoothing is also affected by these phenomena. Since the accurate determination of the wavelength at which the spectral features reach their minimum flux is critical for this analysis, any emission lines in the spectra needed to be removed prior to the fitting of the features.

Typically, emission lines are removed during the initial processing of the observational data. However, for most of the SNe in this sample, the original files are not available, and it would be impractical to perform a full data reduction analysis for such a large dataset. For this reason, an interactive interpolation-based emission line removal code, called `emlineclipper`⁷, was developed. This method can be applied directly to the reduced one-dimensional spectra.

The `emlineclipper` program first displays the input spectrum to the user, allowing them to choose boundaries that bracket the emission features that they wish to remove; this range is known as the ‘bounding region’ and is demarcated by the ‘bounding lines’. The code then fits a spline to the data in two 100Å windows either side of the bounding region. The residuals between the spline fit and the input spectrum are computed within these windows, followed by computation of the mean and standard deviation of the residual array. These values are then used to resample the spectrum by adding noise to the spline within the bounding region. Results from emission line removal using this code are shown in Fig. 2; the residuals are comparable in magnitude to the noise in the spectrum, and the resampled spectrum follows the evolution of the continuum near the emission lines very closely. The program can also handle cases of multiple nearby emission lines.

⁷ This code is freely available on Github <https://github.com/GabrielF98/emlineclipper>

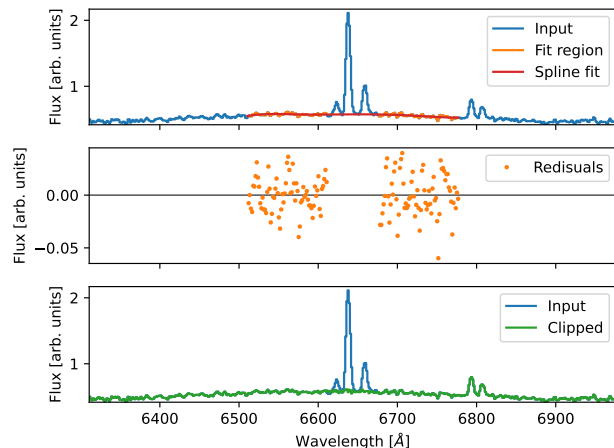


Fig. 2. Emission line removal using the `emlineclipper` Python code. Line selection is performed manually, by selecting the bounding region around the emission lines. The data in a small range either side of the emission line region are fit using a spline. The mean and standard deviation of the spline fit residuals in this region are used to resample the flux in the emission line region.

3.4. Smoothing and mitigation of error sources

Online repositories host spectra from a wide range of instruments and span multiple decades of observations. Thus the dataset contains spectra of varying resolutions and signal to noise ratios. In order to increase the signal to noise ratio, prior to fitting the spectra were smoothed using a Savitzky-Golay (SG) filter (Savitzky & Golay 1964). This increases the likelihood that the minimum wavelength is recovered for an absorption feature, especially if the input data is noisy. An SG filter has two tuneable parameters: the degree of the polynomial and the window length. A cubic polynomial was used to reduce the risk of over-fitting the data, especially near the peaks. As there is no formal method to determine the ideal window length, a statistical analysis was conducted to determine the optimum window length (Finneran et al. 2024, in prep.). This analysis suggests that the optimum window length is between 2-5% of the spectrum length in pixels. This limit proved sufficient to avoid loss of information near the peaks when smoothing spectra in the majority of cases.

Despite efforts to reduce the distortion of the spectrum during smoothing, the results are somewhat sensitive to the exact choice of smoothing parameters. Additionally the fitting of the absorption region may be sensitive to the choice of the endpoints of this region. These effects can be minimised by performing the velocity measurement for a large sample of Monte-Carlo noised spectra and averaging the result.

In general, the spectral uncertainty arrays, which are required for the Monte-Carlo analysis, are not provided by online repositories. These arrays are produced during the sky-subtraction phase of spectral analysis, and cannot be reconstructed without the original data. A method to produce pseudo-uncertainty arrays is described in Appendix A. One benefit of the Monte-Carlo approach is the ability to simultaneously quantify the uncertainty introduced by the signal to noise ratio of the data, the choice of the fitting region and the uncertainty introduced by the fitted function.

3.5. Feature identification

Measuring the velocity of a spectral feature requires a high degree of confidence in the identification of the species responsible for the feature, and hence the rest-frame wavelength used during analysis. Rather than carrying out detailed modelling of the spectra for each SN, line identifications were made based on established patterns within spectra, in combination with comparison to the identifications in the literature where available.

Feature identification is important for each of the three features studied here. The Fe II feature is well known to be a blend of at least three spectral lines, with rest-frame wavelengths of 4924 Å, 5018 Å and 5169 Å, (e.g. Modjaz et al. 2016). Depending on the chosen rest-frame wavelength, the Fe II velocity may differ by up to 15000 km/s once the line becomes de-blended later on in the evolution (c.f. Prentice et al. (2018)). As it is not clear which line is responsible for the minimum in any given spectrum, the 5169 Å line was chosen in order to maintain consistency with previous studies. Although Modjaz et al. (2016) developed a method intended to counteract the effects of Fe II blending, they found it to be inapplicable to the silicon feature. Similar methods to those used here have been applied to GRB-SNe and Ic-BLs before, with the benefit that they can be applied to all the spectral features that we wish to investigate. In cases where the iron line becomes de-blended, the line which most smoothly continues the decaying velocity trend was followed; this choice was informed by reviewing the overall spectral evolution. This avoids having a discontinuity in the velocity evolution as soon as the lines de-blend (e.g. Prentice et al. 2018). Applying this identification in a consistent manner to all SNe in the sample should facilitate comparison of the evolutionary trends between SNe without significant issue.

In the case of the Si II feature, the canonical rest-frame wavelength is 6355 Å. However, it has been proposed that blending with the Na I line may be an issue, as observed by Modjaz et al. (2016) for PTF10qts. There is also an ongoing debate as to whether the feature near 6100 Å, commonly identified with Si II, is in fact entirely due to silicon, or whether it is contaminated by other elements including H-alpha in absorption (Parrent et al. 2016). Once again consistency in identification is the key to studying the evolution.

The Ca II feature is also a triplet, consisting of lines at 8498 Å, 8542 Å, and 8662 Å (e.g. Rho et al. 2021). Following Rho et al. (2021), a mean wavelength of 8567 Å was used as the rest-wavelength for this feature. De-blending of this triplet is not commonly observed for Ic-BL SNe. Indeed, as this triplet is in the near-infrared range of the spectrum it has rarely been studied for a large population of Ic-BLs. Another complication with the Ca II feature is its proximity to the O I feature, with which it may be blended.

3.6. Velocity determination

The velocities of the three absorption features discussed above were determined using the method discussed in Appendix A. This method is very similar to that used by Silverman et al. (2012) for type Ia supernovae. Similar methods have also been applied to stripped envelope supernovae, including those with associated GRBs (e.g. Liu et al. 2016; Patat et al. 2001). Selection of the fitting region was performed manually for all features as shown in Fig. 3. Once the observed wavelength has been determined, Eq. A.1 is used to compute the expansion velocity. An example spline fit is shown in Fig. 4. The fit is performed on

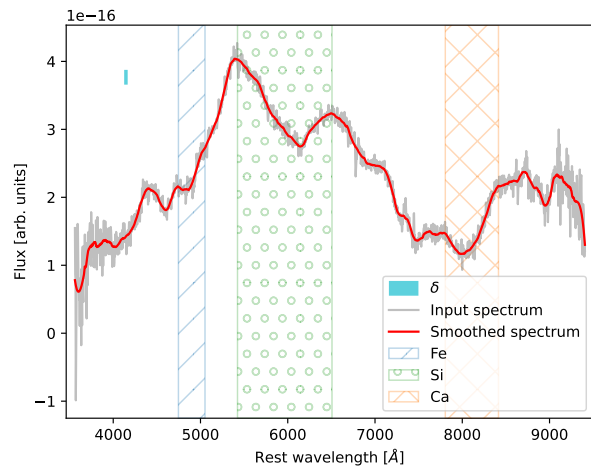


Fig. 3. Selection of the initial boundaries for the Fe II (5169 Å), Si II (6355 Å) and Ca II (8567 Å) features for SN2020bvc. The final boundaries of each feature are determined by locating the local maximum within a range of $\pm\delta$ of the initial boundaries.

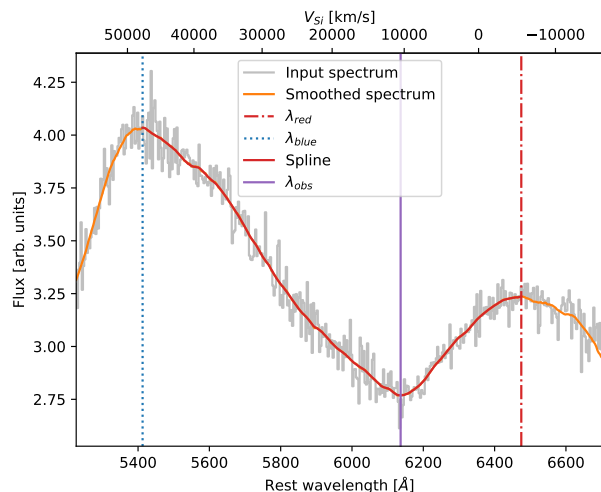


Fig. 4. Spline fit to the Si II feature of 2020bvc. The wavelength at which the spline fit reaches its minimum value is used in the doppler formula to compute the expansion velocity of the feature.

each of the Monte-Carlo spectra and a histogram of velocities is generated. The median and 16th and 84th percentile errors are quoted for all velocities presented in this analysis.

A potential source of error is introduced in the case of noisy spectra, where the smoothing by the SG filter may not be sufficient to produce a smooth feature with a clearly defined minimum. While more aggressive smoothing could be performed, this risks removing information from the spectrum. Instead, the smoothness of the cubic spline used in the fit may be adjusted by changing the number of knots used in the spline (hereafter “knot density”). An analysis of the stability and uncertainty of the measured velocity with different knot densities shows that the optimal knot density is $\sim 10\%$ of the number of pixels within the limits of the feature (Finneran et al. 2024, in prep.). This value was adopted for the majority of spectra in this analysis.

Figure 5 shows an example of visual examination carried out on the results of the spline fitting. Due to the heterogeneity of the data, this is an important step to confirm that the correct feature

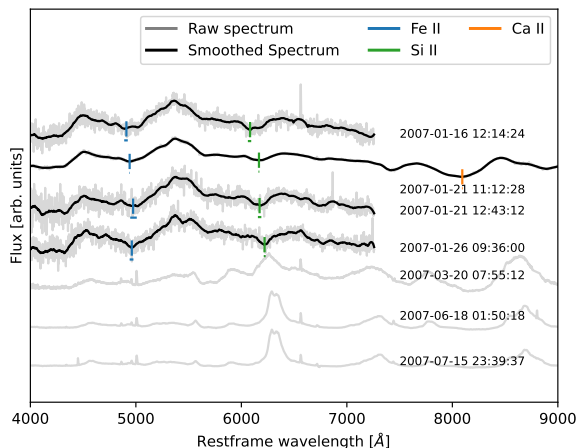


Fig. 5. Spectral sequence of the Ic-BL supernova SN2007D. The raw spectra and smoothed spectra are plotted, along with the minimum wavelength of the Fe II, Si II and Ca II features. This plot was generated for each supernova in the sample; they were used to verify the feature selection and to classify nebular spectra. Also shown in this figure is the uncertainty on the minimum wavelength; the uncertainty is influenced by the S/N of the spectrum. A trend of increasing minimum wavelength with time is visible for Fe II and Si II; this is a direct result of the deceleration of the supernova ejecta. The last three spectra were classified as nebular, as they have a relatively flat continuum and a strong emission feature near 6300 Å. The Ca II feature is only fitted in one epoch, as it lies outside the wavelength range of the other photospheric spectra; this was a common occurrence and resulted in lower statistics overall for Ca II. The spectra were obtained from WISEREP and come from Modjaz et al. (2014); Shivvers et al. (2019).

has been identified in all spectra for each SN. In cases where some misidentifications or poor fits were noticed, the fits were iteratively improved by: changing the delta parameter; selecting different wavelengths for the bounding maxima so that the fitting region was better constrained; refitting the feature using a spline with an increased knot density; or increasing the spline's resolution.

4. Results

The expansion velocities for each feature measured from the spectra can be found in Table B.2 and Table B.3. In all cases, the velocities are only reported for spectra younger than 60 days post explosion (rest-frame time), in order to avoid the nebular phase, where typical assumptions about the formation of the Fe II, Si II and Ca II features, and homologous expansion, break down.

4.1. Trends in the velocity evolution of GRB-SNe and Ic-BL SNe

4.1.1. Fe II

Figure 6 shows the Fe II velocity plotted against the rest-frame time since the supernova explosion. The velocity of this line was measured in at least one spectrum for 12 GRB-SNe and 59 Ic-BL SNe. The absence of an iron velocity measurement for a particular spectrum can be caused by: cases of non-trivial line identification, either due to lack of reference line identification in the literature or multiple features in the region near Fe II; cases where the wavelength range of the SN spectrum did not include the iron

region; cases where the iron feature did not have a well defined minimum, either as a result of noise or there being no minimum value in this region of the spectrum; and cases in which the removal of an emission line altered the minimum of the feature dramatically.

The left panel of Fig. 6 shows that velocities of both GRB-SNe and Ic-BL supernovae decline for 15-20 days prior to entering a plateau phase. The distribution and evolution of velocities among GRB-SNe and Ic-BL supernovae are indistinguishable; as indicated by the significant scatter among the velocities of both populations, which suggests that a continuum of events likely exists. Additionally, supernovae that begin at high velocities tend to plateau at high velocities; this might indicate that the plateau is intrinsic to the expansion of a GRB/Ic-BL, or indeed to SNe in general, rather than being a distinguishing feature of either class.

The right panel of Fig. 6 reveals that a large fraction of the supernova sample, both Ic-BL and GRB-SN, follow power-law decays. It also shows that the velocities, though scaled, still have some scatter, around 1000 km/s at t_0+10 days rest-frame. The scatter becomes larger after 15-20 days partially due to some SNe showing evolutions consistent with a broken power-law decay. These decays tend to follow a steep-shallow evolution. Examples of likely broken power-law decays are GRB980425-SN1998bw, SN2002ap and SN2009bb. The scatter at late times could also be due to the effects of line blending (see Prentice et al. 2018). The lack of early observations for many SNe makes it difficult to determine whether power-laws emerge early in the evolution, or appear later.

4.1.2. Si II

Figure 7 shows the Si II velocity plotted against the rest-frame time since the supernova explosion. The velocity of this line was measured in at least one spectrum for 11 GRB-SNe and 60 Ic-BL supernovae.

The left panel of Fig. 7 shows a steady decline of the silicon velocity from 20000-25000 km/s to below 10000 km/s in the first 30 days, though there are some SNe with velocities larger than this. Some supernovae appear to show a plateau phase after ~25 days, while others simply keep decaying to very low velocities. Similar to the evolution of the iron feature, there does not seem to be a clear distinction between GRB-SNe and Ic-BLs.

The right panel of Fig. 7 shows that, based on their silicon velocity, the supernovae in the sample can be divided between those with broken power-law evolutions and those with power-law decays. Many of those with broken power-law evolution follow a shallow-steep decay, unlike the broken power-laws for iron. In the case of SNe with power-law decays, their slopes appear to match the decay rates of the first segment of the broken power-laws quite well. The breaks in the power-laws appear to occur between 10-20 days rest-frame.

There is some scatter in the velocity when viewed in log-log scale, which can be attributed to intrinsic differences between the supernovae. The scatter is similar in magnitude to that found for iron over the same time periods, and appears to be similar throughout the evolution, though the effect of the log-log scale serves to visually enhance the scatter after 20 days when it the velocity falls below 10000 km/s.

Figure 7 includes four well-sampled high-velocity events: GRB100316D-SN2010bh, GRB980425-SN1998bw, GRB030329-SN2003dh and SN2014ad. The evolution of GRB980425-SN1998bw and SN2014ad seems quite similar, with both declining from a similar initial velocity and plateauing

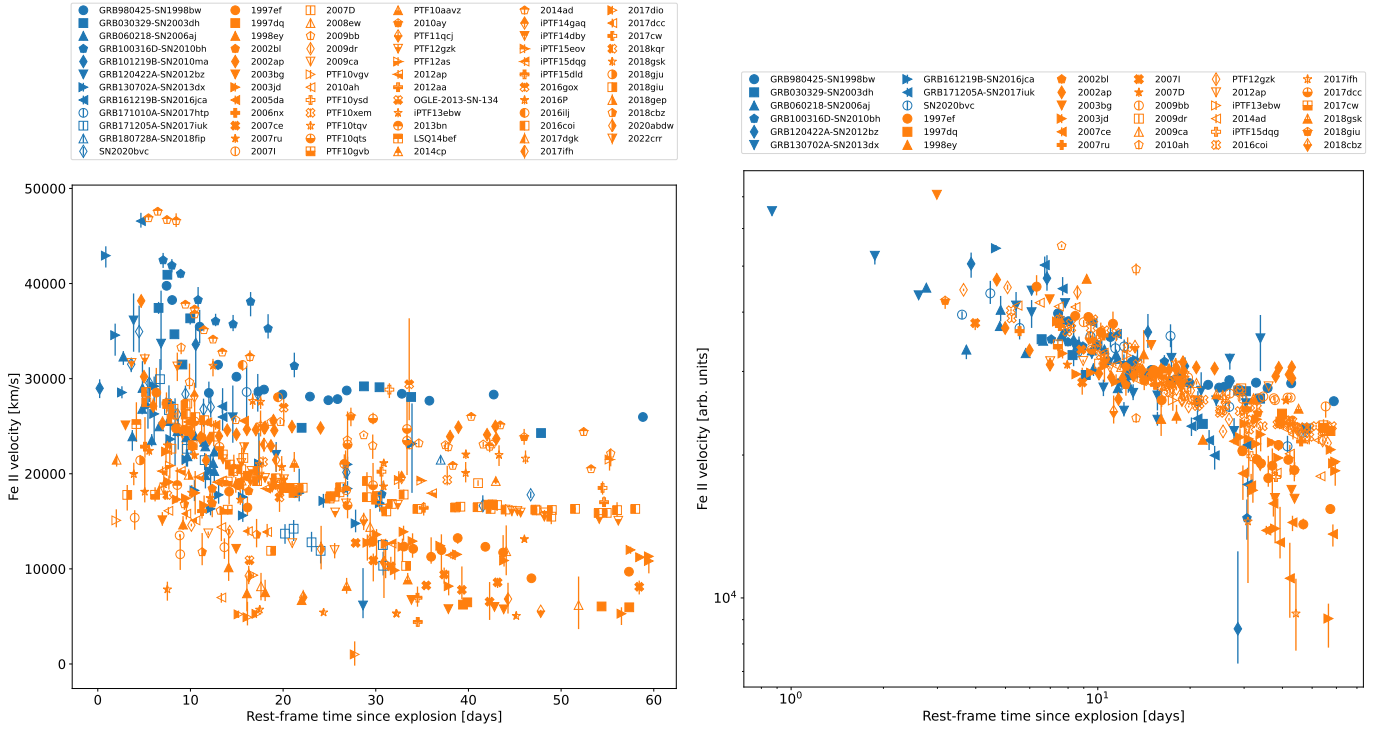


Fig. 6. Velocity evolution of the Fe II feature. *Left:* Plot of all SNe in the sample for which velocities were measured for Fe II. All SNe follow a rapid decay at early times (< 20 days) before beginning to plateau. A continuum of velocities exists for Ic-BLs and GRB-SNe. *Right:* A selection of supernovae for which the velocity evolution has been fitted. The majority show a power-law trend, with others showing broken power-law trends. There are no evolutionary differences between the Ic-BL and GRB-SN samples. The velocities have been scaled to highlight the overall trend. The scaling factor is computed from the fitted velocity at 15 days divided by the fit velocity of GRB980425-SN1998bw at 15 days.

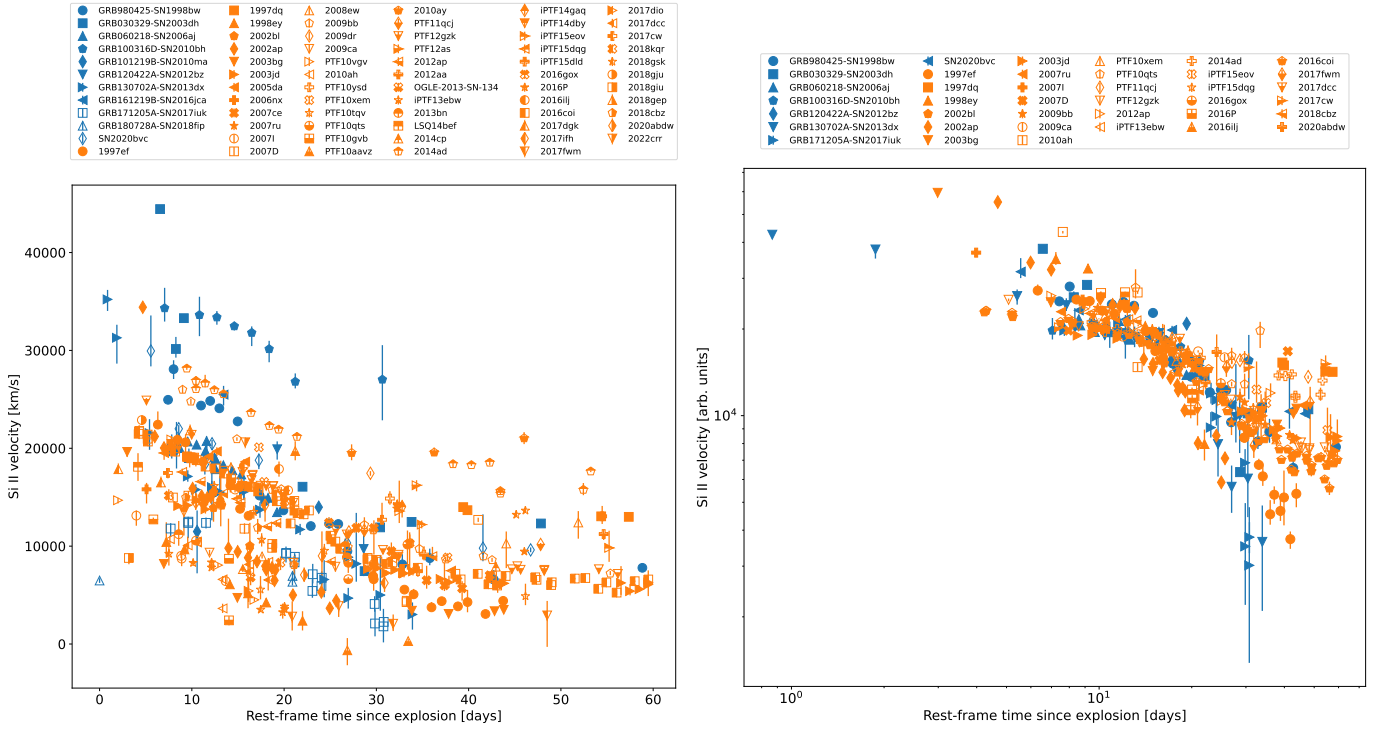


Fig. 7. Velocity evolution of the Si II feature; same sample criteria and graphs as Fig. 6. *Left:* Many Ic-BLs and GRB-SNe evolve rapidly at early times (< 20 days); following this they then begin to plateau. A continuum of velocities exists for Ic-BLs and GRB-SNe. GRB100316D-SN2010bh has a much higher velocity at all epochs studied than the rest of the sample. *Right:* Several Ic-BLs and GRB-SNe can be fitted by power-law decays; supernovae which evolve more rapidly tend to have a higher initial velocity and vice-versa. Some Ic-BL and GRB-SNe show broken power-law decays, with the breaks all being around 15 days.

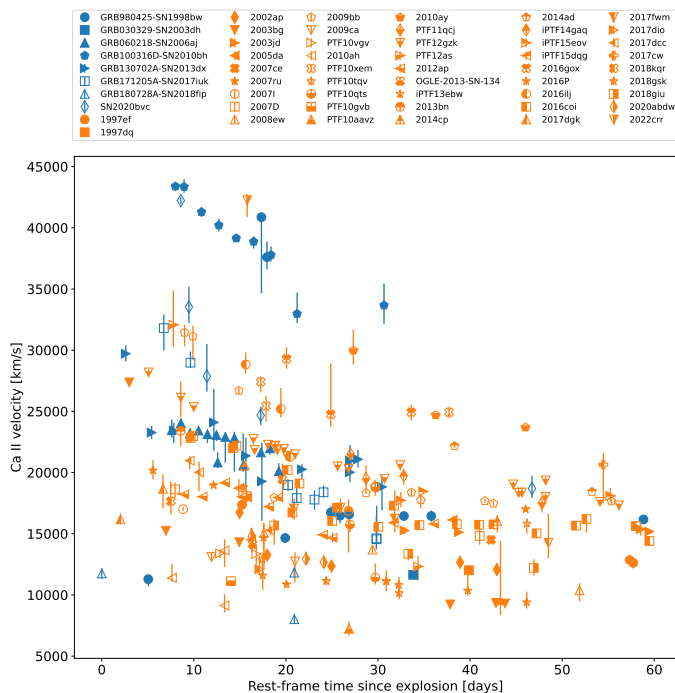


Fig. 8. Velocity evolution of the Ca II feature. A continuum of velocities exists for Ic-BLs and GRB-SNe. The sampling frequency for many of the supernovae is low, and the Ca II feature was often heavily blended; as a result it is difficult to decipher the evolution for many SNe, though some do appear to show a fast decay at early times (<20 days) followed by a plateau. GRB100316D-SN2010bh appears to be an outlier, having a much higher velocity at all epochs studied than the rest of the sample.

at around 20-22 days. However, the final plateau velocity of SN2014ad is larger by nearly a factor of two (~9000 km/s vs ~18000 km/s). GRB100316D-SN2010bh appears to have a shallow velocity decrease before 10 days, followed by a steepening of its decay. GRB030329-SN2003dh achieves the highest silicon velocity (~45000 km/s), which rapidly declines to velocities that are more in line with the general population by day 10.

4.1.3. Ca II

Figure 8 shows the velocity evolution of the Ca II velocity against rest-frame time since the explosion. A velocity measurement was obtained on at least one epoch for 8 GRB-SNe and 47 Ic-BLs. The lower number of detections for this feature can be attributed in part to problems with reliable identification of the feature, either due to heavy blending, lack of near-infrared coverage in spectra, or ringing in red/near-infrared regions which affected the smoothing.

The velocities at 15 days post explosion have a range of over 35000 km/s, which is larger than that measured for Fe II or Si II at a similar epoch. This likely reflects the blending of the Ca II lines, particularly with oxygen in some SNe; resulting in a wide feature whose minimum wavelength is bluer than the underlying Ca II feature. Generally, the evolution shows a decay in the calcium velocity over time, particularly in those better sampled SNe. These SNe also seem to indicate a plateau around 20-30 days, similar to that found for Fe II and Si II. Many of the GRB-SNe included in Fig. 8 are surrounded by Ic-BLs, and there is no clear distinction in the phase space between these two classes.

GRB980425-SN1998bw shows a trend of increasing velocity, likely caused by poor identifications of calcium in the early spectra. A poor calcium identification may also play a role in the low velocities measured for GRB180728A-SN2018fp at 20 days (around 10000 km/s), as it has very noisy spectra.

GRB100316D-SN2010bh is once again an outlier among the SNe presented here, with velocities that are nearly 10000 km/s higher than the bulk of the population at around 10 days post explosion. SN2022crr achieves similar velocities, which is interesting since this SN has a spectrum which is very similar to the spectrum of SN1998bw. As of yet only one early spectrum of SN2022crr is publicly available, so it is impossible to say how similar to SN2010bh it may be.

4.2. Parameterising the velocity evolution

Motivated by the evolutionary trends visible in the log-log velocities of Fe II and Si II, their velocity evolution was fit with either a power-law or broken power-law function⁸. While this is the first analysis of its kind for fully stripped-envelope supernovae, a similar analysis has been carried out for Ia supernovae by Zheng et al. (2017) and for Ib supernovae in Branch et al. (2002).

For the power-law model, the function adopted was

$$v = at^b, \quad (1)$$

where t is the rest-frame time since explosion, a is the velocity of the SN one day after the explosion and b is the slope of the velocity evolution; a negative b value implies a velocity that decreases over time.

The broken power-law adopted is similar to those used in GRB afterglow fitting (e.g. Martin-Carrillo et al. 2014) and SN studies (e.g. Zheng et al. 2017), and can be expressed as:

$$v = A \left[\left(\frac{t}{t_b} \right)^{-\alpha_1 s} + \left(\frac{t}{t_b} \right)^{-\alpha_2 s} \right]^{-1/s}, \quad (2)$$

where A is the SN velocity at the break time, α_1 and α_2 are the slopes of the power-law segments, t_b is the rest-frame time of the break, and s is a parameter which controls the smoothness of the break.

While the power-law fit was performed for all SNe with at least three velocity measurements, the broken power-law fit was only performed if there were five or more velocity measurements, and only if the data showed clear deviation from the single power-law decay. An F-test was used to distinguish between power-law and broken power-law fits; requiring a three sigma confidence level improvement.

Marginalisation of the fit parameters was performed using the emcee Python package⁹ (Foreman-Mackey et al. 2013). A basic check for convergence, based on the autocorrelation time of the walkers was performed for each fit, as recommended by the emcee documentation. Although the uncertainties on the computed feature velocities are asymmetric, the maximum error value was used for the fit as a conservative estimate of the uncertainty.

Similarly to Zheng et al. (2017), the value of the smoothness parameter, s , was fixed during the fitting process, since the fits

⁸ Due to limited confidence in the line identification for Ca II for all SNe in the sample, the velocity evolution of this feature was not fitted.

⁹ <https://emcee.readthedocs.io/en/stable/tutorials/line/>

Table 1. Cardinality of the sample groups for the Fe II and Si II features.

Feature	Gold	Silver	Bronze	Excluded	Total
Fe II	19	7	10	8	44
Si II	17	10	12	9	48

seem to be only weakly dependent on it. In general, a value of ± 20 seemed to produce reasonable results for the majority of fits. However, in a few cases, the s parameter had to be changed to ± 5 , indicating a smoother break. The sign of s dictates whether the power-law evolution is steep-shallow or shallow-steep.

The quality of the fit was estimated based on the posterior distributions generated by `emcee`. Using this information, the data were cast into one of three samples: *Gold*, *Silver*, or *Bronze*.

Gold sample: Fits for which the velocity evolution shows little scatter and which have converged for all parameters¹⁰, showing near-Gaussian posterior distributions. Supernovae for which the t_0 time is constrained via modelling or non-detections to within 3 days.

Silver sample: Fits which have slightly less clear velocity evolution than the *Gold* sample, but which have sufficient number of datapoints to produce a good fit. The requirements on scatter and error size are relaxed compared with the *Gold* sample. Fits which have not converged for all parameters, but whose corner plots show good marginalisation of the posterior parameter distributions. Supernovae for which the t_0 time is constrained via modelling or non-detections to within 5 days.

Bronze sample: Fits which have a less clear velocity evolution than the *Silver* sample, or very few datapoints. The requirements on scatter and error size are relaxed compared with the *Silver* sample. Supernovae for which the t_0 time is constrained via modelling or non-detections with an error of more than 5 days, or where the t_0 time is taken as 48 hours before the last non-detection.

A final *Exclude* sample was created for SNe that seemed to have no clear evolutionary trend in their data; most often due to a very low number of scattered velocities or unrealistic values for the scaling constants (a in Eq. (1)). This sample was not included in the analysis of the evolution parameters.

4.2.1. Fe II evolution parameters

A total of 44 SNe satisfied our criterion for power-law fits in the case of the velocities measured from the Fe II feature¹¹. Table 1 shows the number of SNe assigned to each sample for the Fe II evolution fits. More than half of the events are in the *Gold* or *Silver* samples. For this analysis, SNe falling into the *Bronze* sample were included, as this was caused by their uncertain t_0 , which has little to no effect on the slope of the decay. Thus, SNe from all three samples were considered here.

¹⁰ For GRB-SNe the majority of the fits converged, probably because their evolution tended to be better sampled than that of the Ic-BLs; consequently the convergence criterion was ignored when determining the sample group for a GRB-SN.

¹¹ Although PTF10qts and SN2017dio met the criteria for number of observations, they could not be fit because the large uncertainty on their late-time velocities produced negative values which the fitting pipeline could not handle; they are not included in Table 1.

Table 2. Median decay indices for GRB-SNe, Ic-BLs and Ic.

	GRB-SN	Ic-BL	Ic
Fe II	$-0.27^{+0.05}_{-0.25}$	$-0.29^{+0.11}_{-0.43}$	$-0.38^{+0.13}_{-0.06}$
Si II	$-0.43^{+0.19}_{-0.26}$	$-0.61^{+0.36}_{-0.33}$	-

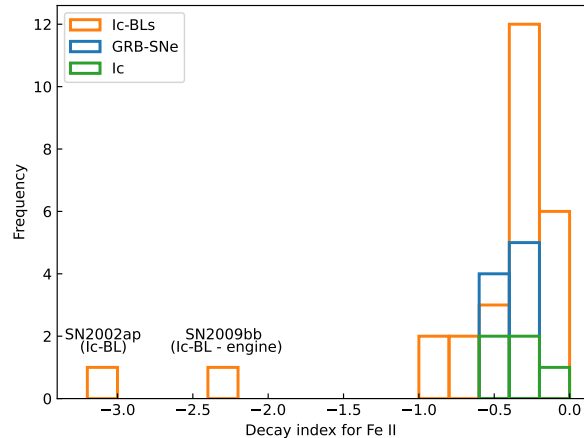


Fig. 9. Distribution of the power-law index for the Fe II velocity of GRB-SNe and Ic-BLs. For broken power-laws the decay index of the first segment is plotted. Fit results for sample of Ic supernovae from Modjaz et al. (2016) are shown for comparison purposes. Allowing for the low population statistics, the decay index appears to be very similar for Ic, Ic-BL and GRB-SNe. This indicates that the presence or absence of a central engine or a relativistic jet has no impact on the rate of velocity evolution of a supernova.

Figure 9¹² shows the distributions of the decay indices for the Fe II feature. A sample of velocities for Ic supernovae taken from Modjaz et al. (2016) is shown for comparison purposes. Regardless of subtype, the Fe II velocities of all SNe experience a similar evolution. The median values of the distributions are presented in Table 2. The decay rate distribution for GRB-SNe lies entirely within the range of the distribution of Ic-BLs, suggesting that the Fe II velocities of both populations decay at comparable rates. Similar decay rates were found for Ic supernovae, suggesting that the decay rate is intrinsic to (stripped-envelope) supernovae, rather than being a distinguishing feature of Ic-BLs or GRB-SNe. Since jet activity is not generally invoked in descriptions of Ic supernovae, this result suggests that jets may not play a significant role in determining the evolution of the iron velocity.

There are two outliers among the SNe in Fig. 9, both of which are Ic-BL supernovae. SN2002ap belongs to the *Bronze* sample and shows evidence of a very extreme power-law decay at early times, as shown in Fig. 10, with a decay index of -3^{+1}_{-1} , based on a broken power-law fit. Although there is clear evidence that SN2002ap is not a pure power-law decay, the fit does not put stringent constraints on the break time (assuming a smooth break, $s=-5$). The velocity of the first datapoint is almost 40000 km/s, which as shown in Fig. 6 is not particularly unusual. However, there is a decay of almost 10000 km/s to the next datapoint less than 1 day later, which results in the high decay index. It should be noted that, although the high decay index of SN2002ap is

¹² For those SNe that are best fit by broken power-laws, the plot shows the index of the first segment of the broken power-law; this paradigm is used for all other plots of the decay index unless stated otherwise.

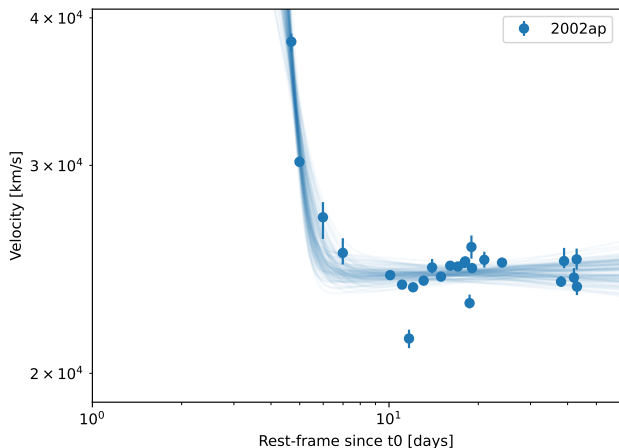


Fig. 10. Fe II velocities of SN2002ap. The best fit is a broken power-law, showing the steep decay at early times. The decay index is poorly constrained, and the break region has been poorly fit; as a result of these issues, SN2002ap was assigned to the *Bronze* sample.

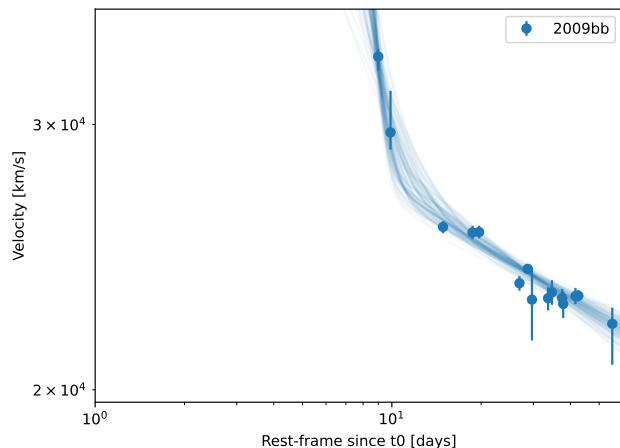


Fig. 11. Fe II velocities of SN2009bb. The best fit is a broken power-law, showing the steep decay at early times. The decay index is poorly constrained, and the break region has been poorly fit; as a result of these issues, SN2002ap was assigned to the *Gold* sample.

abnormal compared with the rest of the sample, it is still consistent within its 2σ error. In the literature SN 2002ap was found to have a spectral shape similar to GRB980425-SN1998bw and SN1997ef (Gal-Yam et al. 2002; Mazzali et al. 2002). Mazzali et al. (2002) also found that the spectral evolution is more rapid than SN1997ef, and that its kinetic energy was similar to those of GRB-SNe, though no GRB was detected. They also found no evidence for asymmetry, suggesting a weak or absent jet. Evidence for Helium in the spectrum was also found by Mazzali et al. (2002), making it interesting that the velocity evolved so rapidly, given the larger mass available within the ejecta to slow down the recession of the photosphere.

The second outlier is SN2009bb, with a decay index of -2^{+1}_{-1} (see Fig. 11). The large uncertainty on the decay index means that it is consistent with the rest of the sample at 2σ . This SN is a member of the *Gold* sample, and has well marginalised parameters, with the fit appearing to capture the break behaviour quite well. Similar to SN2002ap, this SN was fit with $s=-5$, as $s=-20$ produced an unrealistically sharp break. Notably SN2009bb is an example of an engine driven Ic-BL (Pignata et al. 2011), but with no evidence of an aspherical explosion.

4.2.2. Si II evolution parameters

The distributions of the Si II decay indices are shown in Fig. 12, with the average values for GRB-SNe and Ic-BLs shown in Table 2 considering all three samples (see Table 1 for sample details). It seems that GRB-SNe tend to have shallow decays (closer to 0) when compared with the full population of Ic-BLs. The lack of positive decay indices, associated with increasing velocities over time, aligns with assumptions that Si II is linked to the photospheric evolution. In homologous expansion, the greatest velocities are found in material at the edge of the expansion. This means that as the ejecta becomes optically thin and the photosphere recedes, the velocity of the features decrease. If an increasing velocity was detected, it would mean that the photosphere is moving to higher velocities, which would be difficult to explain given the expansion and cooling of the ejecta (it could be true during the very early evolution however, see Liu et al. (2018)).

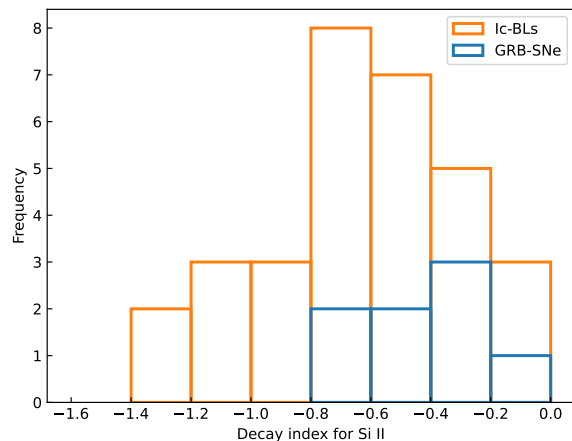


Fig. 12. Same as Fig. 9, but for Si II. The decay indices of GRB-SNe are clustered at lower values than those of Ic-BLs; this implies that the Si II velocities of GRB-SNe decay more slowly than those of Ic-BLs. This could be an indication that the expansion velocity for Si II is affected by central engine or jet activity.

4.3. Broken power-law fits

As mentioned previously, a sub-sample of well sampled SNe, show velocity evolutions that can be better constrained using a broken power-law model. While theoretical studies suggest that the evolution of the photospheric velocity should follow a power-law (Branch et al. 2002), observation of broken power-law evolution may indicate that the spectra are sensitive to the evolution of more than just the photospheric velocity. It may also indicate that for these SNe, the commonly used lines are not appropriate tracers of the photospheric velocity. The results of the broken power-law fits can be found in Table B.4 and Table B.5.

4.3.1. Fe II

There are five SNe consistent with broken power-law evolution for the Fe II feature. Figure 13 shows the decay indices pre and

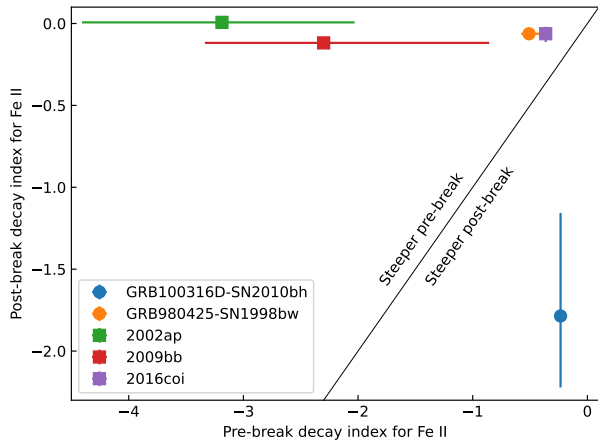


Fig. 13. Fe II decay indices pre and post-break. The majority of Fe II features studied undergo a steep-shallow break.

Table 3. Best fit parameters for the A vs t_b plots.

	A_0	t_b
Fe II	21200 ± 700	590 ± 70
Si II	32000 ± 5000	-900 ± 300

post-break for these cases. Four out of five supernovae follow a steep-shallow evolution (only GRB100316D-SN2010bh follows a shallow-steep decay), and there is no distinction between GRB-SNe and Ic-BLs in this regard. This late shallow evolution indicates that these SNe experience a near-plateau phase, which could potentially suggest that the photosphere is stationary relative to the velocity stratification of the expanding ejecta. In the case of GRB100316D-SN2010bh, the shallow-steep decay is mostly based on the final observation, which shows a greatly reduced iron velocity in comparison to the rest of the evolution.

A comparison between the velocity at break, A , and the break time, t_b , (see Fig. 14) shows that the break velocity is strongly correlated with the break time for 4 of the 5 broken power-laws; with larger break times implying higher velocities at break. The outlier is SN2016coi, which shows a much lower break velocity than expected. A linear fit (excluding SN2016coi) shows a positive correlation (see Table 3 for details on the resulting parameters). This differs from the negative correlation between these parameters seen in the corner plots for the individual fits. It seems that the correlation between the break velocity and the time of the break shown in Fig. 14 is intrinsic to the population, rather than a result of the fitted models. However, a larger dataset is needed to confirm this result. Both Ic-BLs and GRB-SNe lie along this correlation, so it cannot be used as a discriminating test without more data.

4.3.2. Si II

Figure 15 shows that all Si II features for which a broken power-law was the best fit undergo a shallow-steep decay. There appears to be a larger spread in the post-break decay index compared with the pre-break index. Notably, GRB171205A-SN2017iuk has the steepest post-break power-law, and the most aggressive change of index at the break.

As shown in Fig. 16, in contrast with the rest of the sample, SN2016coi and PTF12gzk show evidence for a third power-law

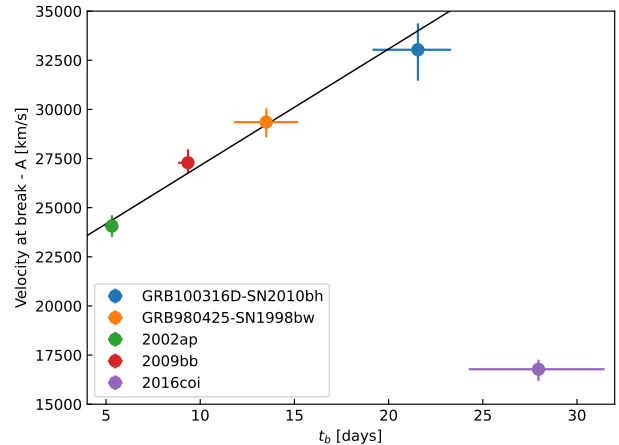


Fig. 14. Break velocity (A) vs rest-frame break time (t_b) for Fe II. The black line shows the line of best fit. A later break time implies a higher break velocity.

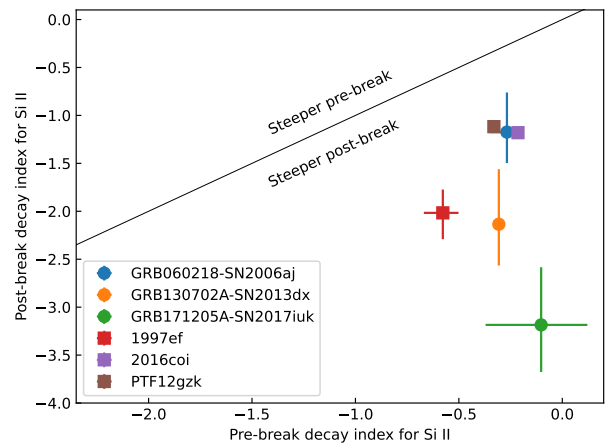


Fig. 15. Same as Fig. 13, but for Si II feature. All SNe have a shallow-steep decay. There is no clustering of GRB-SNe or Ic-BLs that can be used to distinguish the populations.

segment in their Si II velocity evolution. PTF12gzk was found to have a relativistic velocity component by Horesh et al. (2013), who suggested that it may be similar to GRB-SN events, with similar explosion parameters (Ben-Ami et al. 2012)¹³. In the case of SN2016coi, it has a similar radio and X-ray emission to SN2009bb and SN2012ap, two relativistic supernovae; however the velocity of the shockwave is sub-relativistic (Terreran et al. 2019). The classification of Ic-BL (Prentice et al. 2018; Terreran et al. 2019) is robust, though evidence of Helium in the early spectrum was also found (Prentice et al. 2018). Like PTF12gzk, this event appears to be a transitional object between Ic-BLs and GRB-SNe.

Evidence for the third power-law segment appears at t_0+40 days for both events. As such, the fits for these broken power-

¹³ While PTF12gzk is not truly a Ic-BL, Ben-Ami et al. (2012) found that its photospheric evolution is similar to that of most GRB-SNe. However, this SN was included in the sample due to the suggestion that it may be engine driven, an intermediate case between Ic and GRB-SN/Ic-BL.

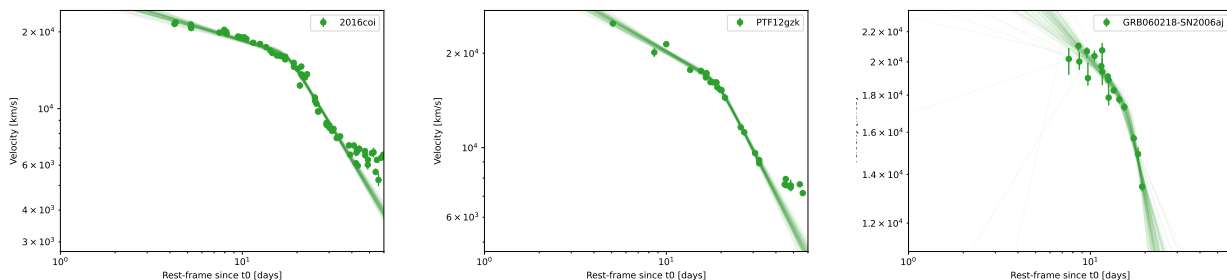


Fig. 16. Broken power-law fits for SN2016coi, PTF12gzk and GRB060218-SN2006aj. All supernovae evolve from a similar maximum velocity of 20000 km/s, initially following a shallow decay before a break at around 18 days. A second break is visible at around 40 days for SN2016coi and PTF12gzk; there is no data beyond 20 days for GRB060218-SN2006aj, so it is not possible to prove or disprove the existence of a second break for this event.

laws were restricted to data prior to 40 days, and no attempt was made to fit the velocities beyond 40 days. Figure 15 shows that these SNe have a similar set of power-law characteristics to GRB060218-SN2006aj. The break times of these SNe are all consistent within their uncertainties with a break at 18 days. Unfortunately, there were no spectra for GRB060218A-SN2006aj beyond ~ 20 days, so it was not possible to confirm the presence or absence of this third decay component in this GRB-SN. The third decay component could indicate the existence of a separate ejecta component that has not yet been studied in detail, and whose influence becomes apparent only after maximum light. The similarity with respect to GRB060218A-SN2006aj supports the conclusion that these events are similar to (some) GRB-SNe.

Figure 17 shows that there is a negative linear correlation between the break velocity and break time for the Si II feature. The slope and intercept values can be found in Table 3. The slope appears to be similar to the slope of the correlation visible in the corner plots of the posterior parameter distributions for the individual fits. Given this, it is difficult to know whether the correlation seen here is something intrinsic to the supernovae considered in this analysis, or whether the result is strongly influenced by the behaviour of the fitted function. Nonetheless, all SNe with Si II velocity measurements exhibit this correlation, regardless of the type of event. Additionally, it can be seen from Fig. 15 that there are vastly different slopes on either side of the break for different events, so it is not clear why the break time should correlate so well with the velocity at the break. Finally, this correlation may also be influenced by the decision to fix the smoothness parameter during fitting. If future SNe exhibit broken power-law evolution then this analysis may produce a more definitive answer as to whether the correlation is intrinsic, or a result of the modelling.

4.4. Comparing the 15-day velocities of Ic-BLs and GRB-SNe

If there is energy injection in GRB-SNe that is not present in (all) Ic-BL SNe, then there should be observable differences in the velocities of the two populations. Based on the results described in Sect. 4.1, this section provides a more quantitative answer to this question.

For this analysis, the velocities computed from the (broken) power-law fits at t_0+15 days were used, since many of the SNe

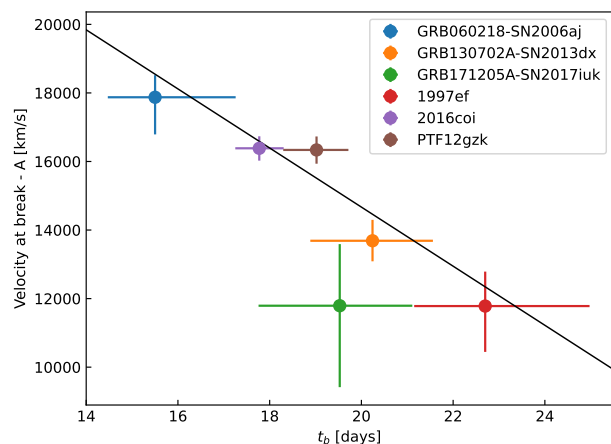


Fig. 17. Same as 14 but for Si II. The black line shows the line of best fit. A later break time implies a lower break velocity.

in this sample have observations around this time, and thus their fits are well constrained¹⁴.

In the case of those SNe with broken power-law fits, the power-law index was determined based on the break time of the broken power-law. Thus, if an SN has a break after t_0+15 days, then the index of the first power-law segment was used; conversely, if the break occurs before the chosen epoch, the index of the second power-law segment was used.

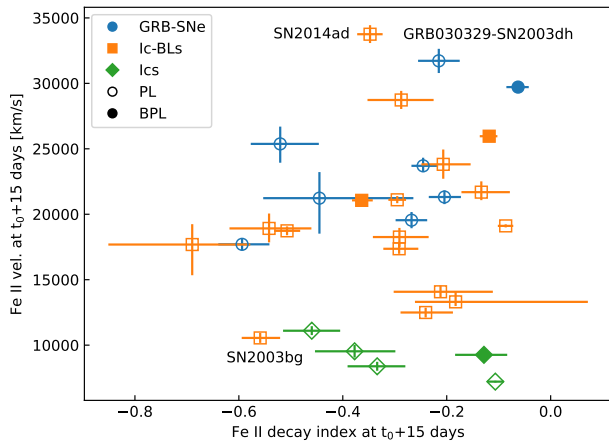
Only SNe from the *Gold* and *Silver* samples were included in this analysis. This decision is justified by the following arguments:

- The velocity evolution begins at t_0 ; if t_0 is not well known, comparisons based on time periods after t_0 are not valid.
- SNe where the evolution is not clear may have poorly constrained fits at the chosen epoch, which would make it hard to compare their velocities
- SNe in the *Gold* and *Silver* samples tend to have better sampled evolutionary curves, increasing the level of confidence in the prediction of velocity for any given epoch.

¹⁴ This well covered epoch time is likely a direct consequence of the light-curve of Ic-BLs, that typically peaks at ~ 15 days (e.g. Taddia et al. 2019; Cano et al. 2017; Taddia et al. 2015)

Table 4. Median velocities for GRB-SNe, Ic-BLs and Ics at t_0+15 days (rest-frame).

	GRB-SN	Ic-BL	Ic
Fe II	23000 ⁷⁰⁰⁰ ₃₀₀₀	19000 ⁶⁰⁰⁰ ₃₀₀₀	9300 ⁸⁰⁰ ₁₃₀₀
Si II	18000 ⁴⁰⁰⁰ ₃₀₀₀	14000 ³⁰⁰⁰ ₅₀₀₀	-

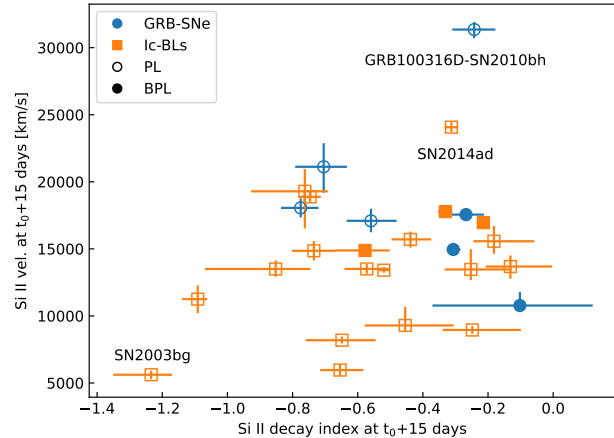

Fig. 18. Fe II velocity vs decay index at t_0+15 days. A sample of Ic supernovae from Modjaz et al. (2016) are shown for comparison purposes. Both Ic-BLs and GRB-SNe have higher velocities than the Ic population, but there is no clear distinction between the GRB-SNe and Ic-BL velocities.

4.4.1. Fe II

Figure 18 shows the relationship between the Fe II velocity and the decay index at t_0+15 days¹⁵. The velocities of GRB-SNe and Ic-BLs show significant overlap, although some Ic-BLs are located at lower velocities. This is also reflected by the overlapping median values of the populations shown in Table 4. There appears to be no correlation between decay index and velocity for Ic-BLs or GRB-SNe. The three SNe presented here that are consistent with broken power-law fits seem to have velocities consistent with the other, single power-law SNe. These broken power-law SNe have relatively shallow decay indices, indicating that they have all transitioned to the slow decay segment of their velocity evolution.

There is a population of low-velocity Ic-BLs, with similar velocity to the Ic population. Among these is SN2003bg, whose type is ambiguous. Some authors have proposed that it evolves from a BL-like SN to a type IIb, before becoming similar to a Ibc supernova in the nebular phase (Hamuy et al. 2009; Soderberg et al. 2006; Mazzali et al. 2009). Its spectral evolution is certainly very different to classical Ic-BL supernovae, with more narrow features than expected after the early epochs. This SN may be more similar to Ic supernovae, both in terms of its decay index and velocity at t_0+15 days. The other members of this group are: SN2018giu, which was classified using SNID as a Ic-BL based on a single spectrum, so the classification may not be definitive; SN2017dcc, which both Taddia et al. (2019) and Prentice et al. (2019) found to be a Ic-BL; and SN2009ca, which may be an SLSN according to (Stritzinger et al. 2023). The fastest

¹⁵ We show Ic supernovae from the *Bronze* sample for comparison; several Ic supernovae are in the *Bronze* sample due to uncertainties in t_0 , but have good fits.


Fig. 19. Same as Fig. 18, but for Si II. GRB-SNe show similar velocities to some Ic-BLs but evolve more slowly.

SNe are SN2014ad and GRB030329-SN2003dh; both of these supernovae also have similar decay indices.

4.4.2. Si II

Figure 19 shows the relationship between the Si II velocity and the decay index at t_0+15 days. There is no clear distinction between Ic-BLs and GRB-SNe. The velocities of GRB-SNe are not universally higher than those of Ic-BL supernovae, and there is significant overlap both visually and statistically speaking (see Table 4). Once again the fastest SNe are SN2014ad and GRB030329-SN2003dh; both of these supernovae also have similar decay indices. SN2003bg is once again the slowest SN in this sample, which could be due to the same reasons as listed in the case of the Fe II feature.

Many of the SNe with broken power-law fits show a shallow index Figure 19. Since the majority of silicon feature fits show a shallow-steep decay, this indicates that many supernovae have a break after 15 days. There is no evidence that SNe that follow broken power-law evolution have higher velocities than SNe that are consistent with a single power-law model.

4.5. Comparison of the Fe II and Si II decay indices

The range of the decay index distribution for Ic-BLs is larger for both Fe II and Si II compared with the distributions for GRB-SNe. This could perhaps be intrinsic, but the more likely explanation is that there are a larger number of Ic-BLs than GRB-SNe in this sample, and so it is more likely that events with a wider range of indices may be observed.

In Figure 20 supernovae from the *Gold*, *Silver* and *Bronze* samples are presented, showing the decay indices of both features. The majority of the supernovae show an Si II decay index above -1 and an Fe II index larger than -0.8. Within this cluster there appears to be no division between GRB-SNe and Ic-BLs. The velocity of the iron feature decays faster than the silicon feature in just three cases: GRB171205A-SN2017iuk, SN2009bb and SN2002ap.

Izzo et al. (2019) propose that GRB171205A-SN2017iuk has a spectrum characterised by an excess of high velocity material (>30000 km/s in the first few days); with the high velocity material attributed to a cocoon around the GRB jet. They find that the

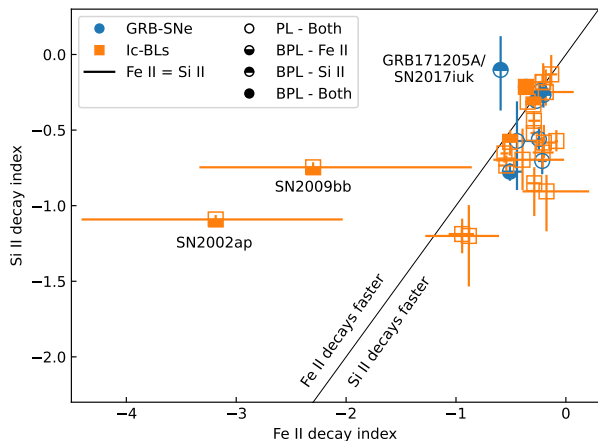


Fig. 20. Si II decay index vs the Fe II decay index. For the majority of supernovae, the silicon velocity decreases more rapidly than the iron velocity. There appears to be no significant differences between GRB-SNe and Ic-BL supernovae in this regard. For broken power-laws the decay index of the first segment is plotted.

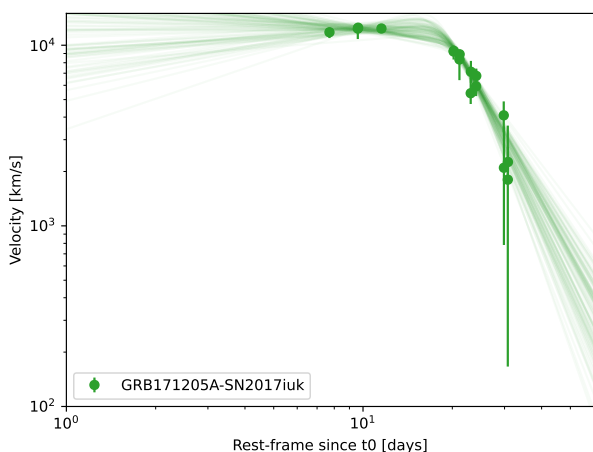


Fig. 21. Broken power-law fit to GRB171205A-SN2017iuk.

early spectra are consistent with Si II velocities of up to 115000 km/s one day after the burst, and declining to around 20000 km/s at t_0+10 days in the rest frame of the GRB-SN. The spectra in this sample for this event begin at t_0+8 days, at which time the velocity is in a plateau at 10000 km/s. The velocity then reduces in the following weeks. Wang et al. (2018) also fit the Si II velocity, and find a result similar to that presented here around the same epoch. As the spectrum is relatively featureless, the discrepancy between the velocities reported here and those of Izzo et al. (2019) are difficult to explain.

GRB171205A-SN2017iuk is best fit with a broken power-law (Fig. 21). In contrast with many SNe in the sample, the decay index is nearly flat for the first segment of the fit, with a value of $-0.1_{-0.3}^{0.2}$. The presence of a cocoon was also suggested by D’Elia et al. (2018). If the cocoon is active during the first few days of the explosion, it is unlikely that the (relatively) late-time spectra presented here are influenced by its activity. Additionally the velocity space of these observations is well below the 30000 km/s which may be associated with cocoons.

4.6. Co-evolution of Fe II and Si II

Figure 22 shows the change in the difference between the Fe II and Si II velocity over time¹⁶. There is no clear difference between the GRB-SN and Ic-BL populations. The Fe II lines are thought to be a good tracer of the photospheric velocity (e.g. Branch et al. 2002), while Si II lines are believed to form above the photosphere. As such it is possible that there may be some difference in their evolution as the ejecta become optically thin. Figure 22 shows that the Fe II (photospheric) velocity is larger than the velocity in the Si II forming region for the majority of SNe, regardless of their type; with the difference normally in the range of 0-10000 km/s.

It seems that the iron feature often maintains a high velocity relative to silicon at late times, and also that this velocity difference is relatively constant throughout the evolution. The relative difference between the features could be due to misidentification of the underlying feature responsible for the emission in iron, likely due to the effects of blending. It has been shown by Prentice et al. (2018) that none of the iron lines are perfect tracers of the photospheric velocity, and that large velocity differences may emerge between the blended feature velocity and the velocities of its component lines at late times when deblending occurs. The choice to follow the 5169 Å line, which is most affected by this issue, could explain the large velocity discrepancies seen at late time.

As shown in the right panel of Fig. 22, the log-log scale shows that for many SNe, there is an early period prior to 10 days where the Fe II velocity is declining more rapidly than the Si II velocity; this manifests as a decrease from a delta of around 20000 km/s at early times to below 10000km/s between 10-20 days. Following this, the difference between the two velocities rises again. For some SNe this velocity difference exceeds 20000 km/s after 30 days, while for others a range of around 5000-10000 km/s is maintained out to day 60. The behaviour of both the GRB-SNe and Ic-BL SNe appears to be very similar in this regard.

Some of the SNe in Fig. 22 show evolution that is unusual. GRB130702A shows an increasing delta between Fe II and Si II out to around 35 days. This appears to be driven by a sharp decline in the silicon velocity around this time. On the opposite side of the distribution around this time is GRB100316D-SN2010bh, whose sharp decline in Fe II velocity results in a negative delta at this time.

5. Discussion

5.1. Comparison with previous work

Modjaz et al. (2016) studied the Fe II velocity evolution of 11 GRB-SNe and 10 Ic-BL supernovae. For Ic-BLs, this sample represents a six-fold increase in the number of Ic-BL supernovae with measured Fe II velocity, compared to Modjaz et al. (2016). This is in part due to the explosion in Ic-BL classification rates since 2018 with the advent of ZTF (Dekany et al. 2020). Differences between the GRB-SNe in the sample and those of the Modjaz et al. (2016) sample can be explained by the selection criteria: only those SNe which had at least 3 epochs of spectral data in online repositories are presented here.

¹⁶ The propagation of asymmetric uncertainties for this plot where computed using the `asymmetric_uncertainties` Python package, available at: https://github.com/muryelgp/asymmetric_uncertainties

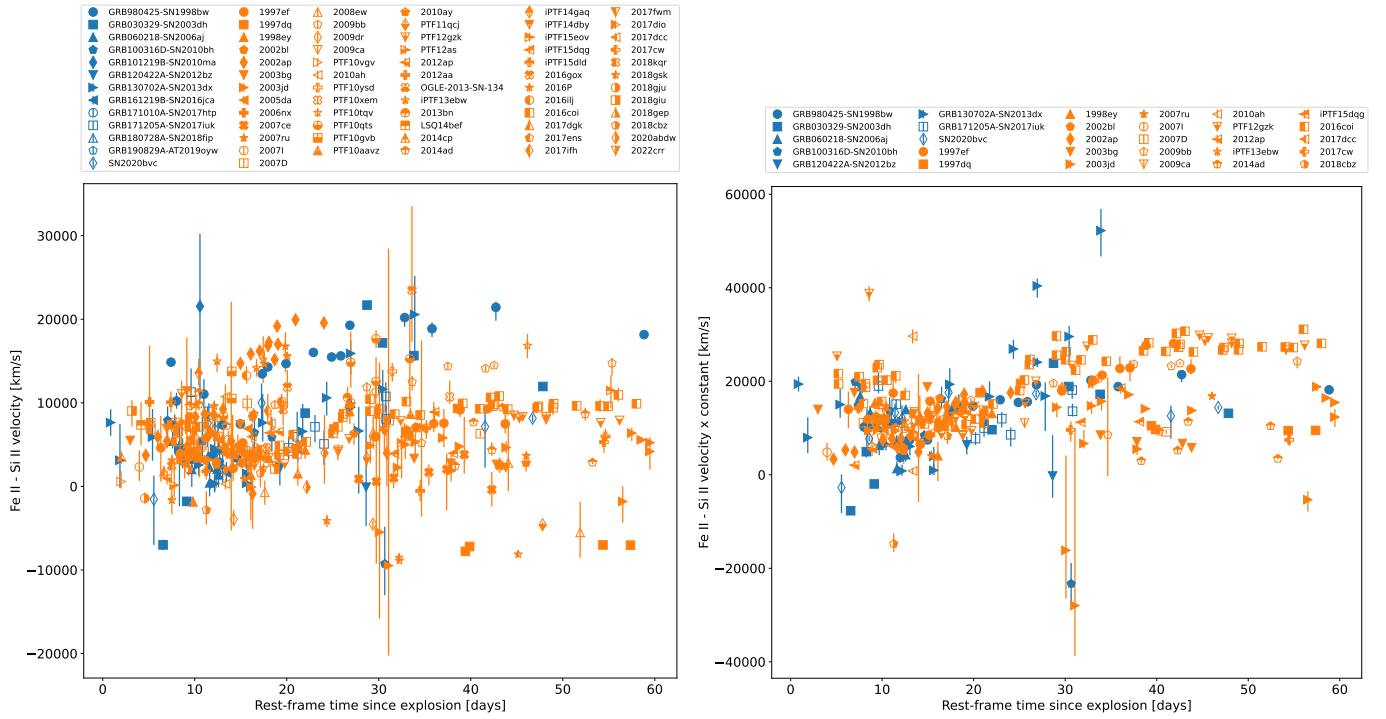


Fig. 22. Difference between the Fe II and Si II velocities over time for Ic-BLs and GRB-SNe. *Left:* Full sample of SNe shown in log-log scale. *Right:* SNe from the *Gold*, *Silver* and *Bronze* samples; the result is scaled by the difference between the Fe II and Si II velocity for each SN divided by the result for GRB980425-SN1998bw at t_0+15 days.

Qualitatively, the evolutionary trend for Fe II feature velocity seen by Modjaz et al. (2016) is confirmed. However, the quantitative analysis reveals an insignificant difference between the average velocities of GRB-SNe and Ic-BLs. This may be a result of the larger number of Ic-BL SN spectra presented here, or it could be due to issues with line blending. Overall the range of velocities for both studies seems to be quite similar, with all SNe lying between 5000-50000 km/s. In contrast with the results of Modjaz et al. (2016), the velocities of GRB100316D-SN2010bh are similar to GRB980425-SN1998bw, though it is still the highest velocity GRB-SN. The remaining GRB-SNe are surrounded by Ic-BLs, in a band that evolve from 25-35000 km/s to 5-20000 km/s. This could be evidence for jet activity in both Ic-BLs and GRB-SNe, or it could mean that jet activity has no impact on the magnitude or evolution of the velocities.

SN2014ad seems to be an outlier among Ic-BLs; its velocities and their evolution are similar to those of GRB980425-SN1998bw and GRB100316D-SN2010bh. Sahu et al. (2018) corroborate this finding, observing that SN2014ad is characterised by higher expansion velocities than typical GRB-SNe and Ic-BL supernovae (measured from the Si II line); they also concluded that parameters derived from its lightcurve make it similar to GRB-SNe.

The sample of Si II and Ca II features presented here are the largest of their kind for GRB-SNe and Ic-BL SNe. As such, no direct population-level comparisons can be drawn with previous research. Overall the behaviour of the Si II and Ca II features are consistent with the idea that GRB-SNe and Ic-BL supernovae arise from a population of similar progenitors.

5.2. Are jets active in all Ic-BL supernovae?

It appears that neither the velocity, nor its evolution are distinguishing characteristics between GRB-SNe and Ic-BL super-

novae. Previous studies have ruled out GRBs (or put very stringent constraints on the phase space of the explosion) for several SNe in this sample (e.g. Soderberg et al. 2006; Corsi et al. 2016, 2023). Despite this, there is significant overlap between the Ic-BLs and GRB-SNe studied here, including for some which are known not to harbour a GRB. This overlap exists for all lines studied here, and therefore cannot purely be attributed to issues with line-identification or blending, since these issues do not affect every event or every feature in the spectrum.

Jetted emission is inferred to power the afterglow lightcurves of GRB-SNe, thus the supernovae observed in association with GRBs must contain a jet. To form a GRB the jet must have sufficient energy to break out of the stellar envelope without choking (e.g. Corsi & Lazzati 2021). It is thought that energy injection from a central engine may be the source of the high velocities observed in GRB-SNe. However, models of the spectra of GRB-SNe suggest that the velocity increases due to a jet are small, and are present at early times (Barnes et al. 2018). The results of this study suggest that jet energy injection does not have a significant influence on the velocity of the ejecta. Thus, it is not possible to conclude that jets are present in all Ic-BL SNe, or infer the frequency with which these jets may become choked and be seen as non-GRB Ic-BLs.

5.3. Factors influencing the velocity evolution

The velocities of all three absorption features studied show evidence for a plateau phase beginning around 20 days; although for Ca II the decay in velocity is more shallow than for Fe II/Si II and the plateau is less significant. Li et al. (2023) shows that a similar plateau observed for SN2020bvc may be modelled assuming an r-process component within the ejecta, rather than the classical model of a supernova powered by the decay of nickel produced by the supernova shock or a GRB jet. However, a study

by Anand et al. (2024) ruled out r-process enrichment in a sample of 25 Ic-BL supernovae discovered by ZTF. Given the weight of this large sample it is difficult to conclude that the plateaus are all due to r-process elements.

It is also possible that plateaus may be a natural result of the underlying ejecta's density profile. Liu et al. (2018) presents the theoretical framework for the evolution of the photospheric velocity. Out of all the density profiles studied in this work, only the broken power-law model shows evidence for a rapid decline in velocity followed by a slower decline phase. In this model there is an inner core where the density falls off more slowly with increasing radius, and an outer shell where the density declines more rapidly. Liu et al. (2018) points out that the actual photospheric radius evolves more slowly than their theoretical prediction; it is then possible that plateaus could be a consequence of this.

Mixing of the radioactive nickel in the ejecta can also impact the photospheric velocity evolution and the magnitude of those velocities. Moriya et al. (2020) performed simulations of SESN progenitors, finding that the greater the degree of mixing in the ejecta, the smoother and more rapid the decline in the photospheric velocity is. They found evidence for plateaus in the photospheric velocity around 15 days prior to the bolometric luminosity peak. There is no evidence for early plateaus such as these in this sample, and so qualitatively it appears that many of the supernovae studied here are highly mixed, in line with the results of studies performed on supernova lightcurves.

5.4. Physical interpretation of power-law and broken power-law fits

A power-law decline is anticipated for the photospheric velocity, and likely also for absorption features formed near the photosphere (e.g. Branch et al. 2002). The majority of supernovae in this sample can be fit with a power-law decline during their photospheric evolution. Differences between the decay indices for the Fe II and Si II lines may be put down to differences in the optical depths for these lines, though in most cases they appear to follow similar declining trends, with the Si II feature appearing to decline more rapidly than the Fe II one in most cases.

Interpretation of the broken power-law fits is more difficult. These fits cannot be purely due to identification or blending issues, as they are observed for both the Fe II feature (often heavily blended) and the Si II feature (usually not heavily blended) in a handful of SNe. It is possible that these fits reveal the presence of another ejecta component, whose velocity evolution may differ due to differences in temperature, composition, or orientation relative to the observer. Broken power-laws may be linked to aspherical explosion geometry, however in this case it is difficult to explain why they are not observed in all GRB-SNe. One possibility is that the cocoon formed by the GRB jet as it tunnels through the star may be responsible for this break. However, the times of the breaks, and their velocities, are not consistent with the proposed cocoon properties (e.g. Izzo et al. 2019). Additionally, there is only one observation of cocoon emission for any of the events in this sample: GRB171205A-SN2017iuk (Izzo et al. 2019), which does not stand out significantly from the overall population. For all Si II features, the broken power-law fits follow a shallow-steep decay, whereas for Fe II the decays tended to be steep-shallow. It is difficult to explain why different velocity components would be present for different lines in the same SN. Only SN2016coi showed a similar broken power-law evolution for both Fe II and Si II, though the break times and slopes are not compatible.

6. Conclusions

This paper has presented measurements of the expansion velocities for a large sample of Ic-BL supernovae. These events were drawn from online archives, and are split between a population of Ic-BLs with an associated GRB detection, and Ic-BLs where no GRB component was found. This sample of 61 ordinary Ic-BLs and 13 GRB-SNe represents the largest sample of velocity measurements for these types of events to date. The velocities have been measured using a spline fitting method.

The presence of a GRB component has no impact on the expansion velocity of a Ic-BL supernova. For all three features, there is no separation between the two populations in velocity-time space. This is in line with expectations from theory which show that the interaction of the jet with the stellar mantle should have little impact on the supernova observables. For this reason the analysis presented here is not capable of ruling out a GRB component for Ic-BLs where no such component has been observed.

The velocity evolution of a Ic-BL may be fit with either a power-law or broken power-law model. A single power-law fit is in agreement with the expectations for a single component photosphere, while those with broken power-law fits may indicate the presence of a second (or even third) velocity component in the ejecta of some Ic-BL supernovae. This could be evidence for asphericity in the explosion. However, there is no particular preference for broken power-laws among Ic-BLs with an associated GRB, again making it difficult to rule out jets in non-GRB associated Ic-BLs. The decay slopes of the Fe II and Si II features are also identical for both populations. This is likely further evidence that the jet has no direct impact on the expansion velocity of the supernova.

There is some evidence that broken power-law fits may be related to engine driven explosions. Both PTF12gzk and SN2016coi show strong similarities to GRB060218-SN2006aj in terms of their velocity and velocity evolution. Emission from a GRB cocoon is expected to peak within ~ 1 day of the explosion (Izzo et al. 2019). Since breaks are observed at around 15 days post explosion, this raises the question of what the origin of this additional velocity component could be.

These results demonstrate there is structure within the velocity evolution which has not yet been explored before now. It is likely that a greater number of broken power-law fits may be found in data with a higher sampling rate. If all Ic-BL supernovae harbour a GRB jet, the impacts of this may only be found at very early times (< 10 days), which are not probed in detail by this study. Both of these issues can be addressed by changes to observing strategies, with greater emphasis placed on rapid classification and targeted spectral follow-up of new Ic-BLs. Classifications are ideally needed within hours to days rather than weeks as is currently the case for Ic-BLs. With upcoming facilities such as the *Vera Rubin Observatory* (Ivezić et al. 2019) observing many more Ic-BLs, it is vital that we continue to classify suspected Ic-BLs as accurately and as rapidly as possible, to ensure that follow-up observations are as beneficial as possible. In tandem with this, efforts should be made to follow-up all Ic-BLs across the spectrum, to search for signatures of off-axis jets. Better labelling of a dataset like this one may reveal a clearer distinction between Ic-BLs with and without jets.

Acknowledgements. GF and AMC acknowledge support from the UCD Ad Astra programme. LC and AMC acknowledge support from the Irish Research Council Postgraduate Scholarship No GOIPG/2022/1008. This work has made extensive use of WISEREP (available at: <https://www.wiserep.org>) as one source for our Ic-BL spectra. In order to access data from WISEREP we used the WISEREP API, created by Tomás E. Müller Bravo; we thank them for

providing a modified code from which we built our data-collection pipeline. GRB-SN data was gathered from the GRBSN webtool, which can be found at <https://grbsn.watchertelescope.ie/>. We also cross checked the list of Ic and Ic-BL supernovae using the Transient Name Server (available at: <https://www.wis-tns.org/>). We have made use of the Rochester Astronomy List of Bright Supernovae to gather data about the detection dates of OGLE-2013-SN-134 and LSQ14bef. We also make use of the Central Bureau for Astronomical Telegrams (available at: <http://tamkin2.eps.harvard.edu/cbet/RecentCBETs.html>) to locate some of the legacy data for SNe.

References

- Anand, S., Barnes, J., Yang, S., et al. 2024, *ApJ*, 962, 68
- Arbour, R. & Schwartz, M. 1998, *IAU Circ.*, 7065, 1
- Armstrong, M. 2002, *IAU Circ.*, 7845, 1
- Barnes, J., Duffell, P. C., Liu, Y., et al. 2018, *ApJ*, 860, 38
- Ben-Ami, S., Gal-Yam, A., Filippenko, A. V., et al. 2012, *ApJ*, 760, L33
- Blondin, S. & Tonry, J. L. 2007, *ApJ*, 666, 1024
- Branch, D., Benetti, S., Kasen, D., et al. 2002, *ApJ*, 566, 1005
- Bright, J. S., Horesh, A., van der Horst, A. J., et al. 2019, *MNRAS*, 486, 2721
- Bufano, F., Pian, E., Sollerman, J., et al. 2012, *ApJ*, 753, 67
- Cano, Z., Wang, S.-Q., Dai, Z.-G., & Wu, X.-F. 2017, *Advances in Astronomy*, 2017, 8929054
- Cardelli, J. A., Clayton, G. C., & Mathis, J. S. 1989, *ApJ*, 345, 245
- Chen, T. W., Inserra, C., Fraser, M., et al. 2018, *ApJ*, 867, L31
- Childress, M. J., Tucker, B. E., Yuan, F., et al. 2016, *PASA*, 33, e055
- Chornock, R., Berger, E., Rest, A., et al. 2013, *ApJ*, 767, 162
- Corsi, A., Gal-Yam, A., Kulkarni, S. R., et al. 2016, *ApJ*, 830, 42
- Corsi, A., Ho, A. Y. Q., Cenko, S. B., et al. 2023, *ApJ*, 953, 179
- Corsi, A. & Lazzati, D. 2021, *New A Rev.*, 92, 101614
- Corsi, A., Ofek, E. O., Frail, D. A., et al. 2011, *ApJ*, 741, 76
- Corsi, A., Ofek, E. O., Gal-Yam, A., et al. 2014, *ApJ*, 782, 42
- Corsi, A., Ofek, E. O., Gal-Yam, A., et al. 2012, *ApJ*, 747, L5
- Crowther, P. A. 2007, *ARA&A*, 45, 177
- Daigne, F. & Mochkovitch, R. 1998, *MNRAS*, 296, 275
- De, K. 2020, *Transient Name Server Discovery Report*, 2020-3604, 1
- De, K., Kasliwal, M. M., Tzanidakis, A., et al. 2020, *ApJ*, 905, 58
- Dekany, R., Smith, R. M., Riddle, R., et al. 2020, *PASP*, 132, 038001
- D’Elia, V., Campana, S., D’Ai, A., et al. 2018, *A&A*, 619, A66
- D’Elia, V., Pian, E., Melandri, A., et al. 2015, *A&A*, 577, A116
- Della Valle, M., Chincarini, G., Panagia, N., et al. 2006, *Nature*, 444, 1050
- Drott, M. R., Soderberg, A. M., Gal-Yam, A., et al. 2011, *ApJ*, 741, 97
- Filippenko, A. V. 1997, *ARA&A*, 35, 309
- Finneran, G., Cotter, L., & Martin-Carrillo, A. 2024, *arXiv e-prints*, arXiv:2411.08866
- Foley, R. J., Papenkova, M. S., Swift, B. J., et al. 2003, *PASP*, 115, 1220
- Foreman-Mackey, D., Hogg, D. W., Lang, D., & Goodman, J. 2013, *PASP*, 125, 306
- Fynbo, J. P. U., Watson, D., Thöne, C. C., et al. 2006, *Nature*, 444, 1047
- Gal-Yam, A., Fox, D. B., Price, P. A., et al. 2006, *Nature*, 444, 1053
- Gal-Yam, A., Ofek, E. O., & Shemmer, O. 2002, *MNRAS*, 332, L73
- Galama, T. J., Vreeswijk, P. M., van Paradijs, J., et al. 1998, *Nature*, 395, 670
- Gangopadhyay, A., Misra, K., Sahu, D. K., et al. 2020, *MNRAS*, 497, 3770
- Gomez, S., Berger, E., Nicholl, M., Blanchard, P. K., & Hosseinzadeh, G. 2022, *ApJ*, 941, 107
- Griffith, C., Li, W., & Filippenko, A. V. 2008, *Central Bureau Electronic Telegrams*, 1469, 1
- Gutierrez, C., Cartier, R., & Yaron, O. 2017, *Transient Name Server Classification Report*, 2017-474, 1
- Hamuy, M., Deng, J., Mazzali, P. A., et al. 2009, *ApJ*, 703, 1612
- Ho, A. Y. Q., Kulkarni, S. R., Perley, D. A., et al. 2020, *ApJ*, 902, 86
- Horesh, A., Kulkarni, S. R., Corsi, A., et al. 2013, *ApJ*, 778, 63
- Ivezić, Ž., Kahn, S. M., Tyson, J. A., et al. 2019, *ApJ*, 873, 111
- Izzo, L., Auchettl, K., Hjorth, J., et al. 2020, *A&A*, 639, L11
- Izzo, L., de Ugarte Postigo, A., Maeda, K., et al. 2019, *Nature*, 565, 324
- Kosugi, G., Mizumoto, Y., Kawai, N., et al. 2004, *PASJ*, 56, 61
- Kouveliotou, C., Meegan, C. A., Fishman, G. J., et al. 1993, *ApJ*, 413, L101
- Kuncarayakti, H., Maeda, K., Ashall, C. J., et al. 2018, *ApJ*, 854, L14
- Lee, E. & Li, W. 2005, *IAU Circ.*, 8570, 1
- Lee, N. & Li, W. 2007, *Central Bureau Electronic Telegrams*, 807, 1
- Levan, A. J., Gompertz, B. P., Salafia, O. S., et al. 2024, *Nature*, 626, 737
- Li, L., Zhong, S.-Q., & Dai, Z.-G. 2023, *ApJ*, 952, L39
- Liu, L.-D., Zhang, B., Wang, L.-J., & Dai, Z.-G. 2018, *ApJ*, 868, L24
- Liu, Y.-Q., Modjaz, M., Bianco, F. B., & Graur, O. 2016, *ApJ*, 827, 90
- Liu, Z., Zhao, X.-L., Huang, F., et al. 2015, *Research in Astronomy and Astrophysics*, 15, 225
- Lyman, J. D., Bersier, D., James, P. A., et al. 2016, *MNRAS*, 457, 328
- MacFadyen, A. I. & Woosley, S. E. 1999, *ApJ*, 524, 262
- Martin-Carrillo, A., Hanlon, L., Topinka, M., et al. 2014, *A&A*, 567, A84
- Matheson, T., Filippenko, A. V., Li, W., Leonard, D. C., & Shields, J. C. 2001, *AJ*, 121, 1648
- Matheson, T., Garnavich, P. M., Stanek, K. Z., et al. 2003, *ApJ*, 599, 394
- Mazzali, P. A., Deng, J., Hamuy, M., & Nomoto, K. 2009, *ApJ*, 703, 1624
- Mazzali, P. A., Deng, J., Maeda, K., et al. 2004, *ApJ*, 614, 858
- Mazzali, P. A., Deng, J., Maeda, K., et al. 2002, *ApJ*, 572, L61
- Mazzali, P. A., Iwamoto, K., & Nomoto, K. 2000, *ApJ*, 545, 407
- Mazzali, P. A., Walker, E. S., Pian, E., et al. 2013, *MNRAS*, 432, 2463
- Melandri, A., Pian, E., Ferrero, P., et al. 2012, *A&A*, 547, A82
- Mészáros, P. & Rees, M. J. 1997, *ApJ*, 476, 232
- Mészáros, P., Rees, M. J., & Wijers, R. A. M. J. 1998, *ApJ*, 499, 301
- Michałowski, M. J., Xu, D., Stevens, J., et al. 2018, *A&A*, 616, A169
- Milisavljevic, D., Margutti, R., Parrent, J. T., et al. 2015, *ApJ*, 799, 51
- Modjaz, M., Blondin, S., Kirshner, R. P., et al. 2014, *AJ*, 147, 99
- Modjaz, M., Liu, Y. Q., Bianco, F. B., & Graur, O. 2016, *ApJ*, 832, 108
- Modjaz, M., Stanek, K. Z., Garnavich, P. M., et al. 2006, *ApJ*, 645, L21
- Mokiem, M. R., de Koter, A., Vink, J. S., et al. 2007, *A&A*, 473, 603
- Moriya, T. J., Suzuki, A., Takiwaki, T., Pan, Y.-C., & Blinnikov, S. I. 2020, *MNRAS*, 497, 1619
- Müller-Bravo, T. E. 2023, *temuller/wiserep_api: First Official Release!*
- Nakar, E. & Piran, T. 2017, *ApJ*, 834, 28
- Parrent, J. T., Milisavljevic, D., Soderberg, A. M., & Parthasarathy, M. 2016, *ApJ*, 820, 75
- Patat, F., Cappellaro, E., Danziger, J., et al. 2001, *ApJ*, 555, 900
- Pian, E., Amati, L., Antonelli, L. A., et al. 1999, *A&AS*, 138, 463
- Pian, E., Mazzali, P. A., Masetti, N., et al. 2006, *Nature*, 442, 1011
- Pian, E., Tomasella, L., Cappellaro, E., et al. 2017, *MNRAS*, 466, 1848
- Pignata, G., Stritzinger, M., Soderberg, A., et al. 2011, *ApJ*, 728, 14
- Polshaw, J., Benitez, S., Taubenberger, S., et al. 2014, *The Astronomer’s Telegram*, 6094, 1
- Prentice, S. J., Ashall, C., James, P. A., et al. 2019, *MNRAS*, 485, 1559
- Prentice, S. J., Ashall, C., Mazzali, P. A., et al. 2018, *MNRAS*, 478, 4162
- Prentice, S. J., Mazzali, P. A., Pian, E., et al. 2016, *MNRAS*, 458, 2973
- Pritchard, T. A., Bensch, K., Modjaz, M., et al. 2021, *ApJ*, 915, 121
- Quimby, R., Kasliwal, M. M., Nugent, P., et al. 2009, *Central Bureau Electronic Telegrams*, 1783, 1
- Quimby, R. M., De Cia, A., Gal-Yam, A., et al. 2018, *ApJ*, 855, 2
- Ramirez-Ruiz, E., Celotti, A., & Rees, M. J. 2002, *MNRAS*, 337, 1349
- Rastinejad, J. C., Gompertz, B. P., Levan, A. J., et al. 2022, *Nature*, 612, 223
- Rees, M. J. & Meszaros, P. 1994, *ApJ*, 430, L93
- Rho, J., Evans, A., Geballe, T. R., et al. 2021, *ApJ*, 908, 232
- Rhoads, J. E. 1997, *ApJ*, 487, L1
- Roy, R., Sollerman, J., Silverman, J. M., et al. 2016, *A&A*, 596, A67
- Ryan, G., van Eerten, H., Piro, L., & Troja, E. 2020, *ApJ*, 896, 166
- Sáhu, D. K., Anupama, G. C., Chakradhari, N. K., et al. 2018, *MNRAS*, 475, 2591
- Sahu, D. K., Tanaka, M., Anupama, G. C., Gurugubelli, U. K., & Nomoto, K. 2009, *ApJ*, 697, 676
- Sanders, N. E., Soderberg, A. M., Levesque, E. M., et al. 2012a, *ApJ*, 758, 132
- Sanders, N. E., Soderberg, A. M., Valenti, S., et al. 2012b, *ApJ*, 756, 184
- Savitzky, A. & Golay, M. J. E. 1964, *Analytical Chemistry*, 36, 1627
- Schulze, S., Yaron, O., Sollerman, J., et al. 2021, *ApJS*, 255, 29
- Shi, D.-W., Wang, S.-Q., Gan, W.-P., & Liang, E.-W. 2024, *ApJ*, 969, 32
- Shivvers, I., Filippenko, A. V., Silverman, J. M., et al. 2019, *MNRAS*, 482, 1545
- Silverman, J. M., Kong, J. J., & Filippenko, A. V. 2012, *MNRAS*, 425, 1819
- Smartt, S. J. 2009, *ARA&A*, 47, 63
- Smith, N. 2014, *ARA&A*, 52, 487
- Soderberg, A. M., Nakar, E., Berger, E., & Kulkarni, S. R. 2006, *ApJ*, 638, 930
- Sonbas, E., Moskvitin, A. S., Fatkhullin, T. A., et al. 2008, *Astrophysical Bulletin*, 63, 228
- Sparre, M., Sollerman, J., Fynbo, J. P. U., et al. 2011, *ApJ*, 735, L24
- Stritzinger, M. D., Holmbo, S., Morrell, N., et al. 2023, *A&A*, 675, A82
- Taddia, F., Sollerman, J., Fremling, C., et al. 2019, *A&A*, 621, A71
- Taddia, F., Sollerman, J., Leloudas, G., et al. 2015, *A&A*, 574, A60
- Taddia, F., Stritzinger, M. D., Bersten, M., et al. 2018, *A&A*, 609, A136
- Tanga, M., Krühler, T., Schady, P., et al. 2018, *A&A*, 615, A136
- Terreran, G., Margutti, R., Bersier, D., et al. 2019, *ApJ*, 883, 147
- Tonry, J., Stalder, B., Denneau, L., et al. 2017, *Transient Name Server Discovery Report*, 2017-440, 1
- Tonry, J., Stalder, B., Denneau, L., et al. 2018a, *Transient Name Server Discovery Report*, 2018-727, 1
- Tonry, J., Stalder, B., Denneau, L., et al. 2018b, *Transient Name Server Discovery Report*, 2018-1384, 1
- Tonry, J., Stalder, B., Denneau, L., et al. 2018c, *Transient Name Server Discovery Report*, 2018-1390, 1
- Tonry, J., Stalder, B., Denneau, L., et al. 2018d, *Transient Name Server Discovery Report*, 2018-1429, 1
- Troja, E., Fryer, C. L., O’Connor, B., et al. 2022, *Nature*, 612, 228
- Valenti, S., Benetti, S., Cappellaro, E., et al. 2008, *MNRAS*, 383, 1485
- Volnova, A. A., Pruzhinskaya, M. V., Pozanenko, A. S., et al. 2017, *MNRAS*, 467, 3500
- Walker, E. S., Mazzali, P. A., Pian, E., et al. 2014, *MNRAS*, 442, 2768
- Wang, J., Zhu, Z. P., Xu, D., et al. 2018, *ApJ*, 867, 147
- Wang, S.-Q., Cano, Z., Li, L., et al. 2019, *ApJ*, 877, 20
- Woosley, S. E. 1993, *ApJ*, 405, 273
- Wyrykowski, L., Udalski, A., Kozłowski, S., & Soszynski, I. 2013, *The Astronomer’s Telegram*, 5663, 1
- Yaron, O. & Gal-Yam, A. 2012, *PASP*, 124, 668
- Zheng, W., Filippenko, A. V., Mauerhan, J., et al. 2017, *ApJ*, 841, 64
- Zheng, W., Stahl, B. E., de Jaeger, T., et al. 2022, *MNRAS*, 512, 3195

Appendix A: Measuring the velocities of spectral features using splines

An absorption feature is characterised by its width, depth (strength) and the wavelength at which it reaches its minimum flux. Absorption features in supernovae are generated above the photosphere, when some of the photons from the photosphere are absorbed by electrons bound within the atoms of the ejecta, forming a spectral line. The lines observed in supernovae do not appear at only one wavelength value, instead they show a broadened profile across a range of wavelengths. This occurs due to the bulk motion of the particles of the gas relative to the photons. This leads to several narrow lines side by side in the spectrum, producing a broadened line. If the rest-wavelength of a spectral line can be identified, then the expansion velocity of the gas can be measured using the doppler shift formula for wavelength,

$$v = \frac{1 - \beta}{1 + \beta} \times c, \quad (\text{A.1})$$

where c is the speed of light and β is given by

$$\beta = \frac{\lambda_{obs}^2}{\lambda_{true}^2}, \quad (\text{A.2})$$

where λ_{obs} is the wavelength of the absorption feature measured from the spectrum, and λ_{true} is the wavelength of the same line emitted from a gas at rest with respect to the observer.

Silverman et al. (2012) proposed a method of determining the doppler-shifted wavelength of an absorption feature in the spectrum of a Ia supernova. The basic tenet of this method is to fit a smooth function to the spectrum in the region of an absorption feature. The wavelength is determined from the point at which the fit reaches its minimum. This method has also been used for SESN in the past (Liu et al. 2016), and a similar idea was used to measure the silicon 6355 Å feature for GRB130702A-SN2013dx (D’Elia et al. 2015), a Ic-BL with a GRB.

For this analysis, a method similar to those in the literature was implemented in Python. The spectrum is first smoothed using a Savitzky-Golay filter as described in Sect. 3.4. The user can adjust the smoothing window length, and a comparison of the result is displayed graphically.

In order to estimate the error on the velocity, a Monte-Carlo analysis was conducted. Once the smoothed spectrum is generated, it is used to generate an uncertainty array for the analysis, in a similar manner to Liu et al. (2016). First, the residuals between the input and smoothed spectra are calculated. Then, a noise array is generated, where the noise at each pixel is drawn from a Gaussian distribution with zero mean and standard deviation computed from the residual array. Samples from the noise array are added to the smoothed spectrum to produce 1000 mock spectra.

Prior to fitting, the user selects the region of interest in the spectrum, in the case of Ic-BL spectra, the features are: Iron at 5169 Å, silicon at 6355 Å and calcium at 8567 Å. The red and blue boundaries of the features are selected manually on the spectrum by clicking the plot. The ultimate location of the boundaries is determined from the peaks in the smoothed mock spectra which are nearest to the user-selected points. A delta value can also be specified, which defines the region (in pixels) in which the code searches for a local maximum relative to the user’s input. The value of δ is kept low, typically 30-50 pixels

and is chosen so as to ensure the selection of the most appropriate local maximum for the feature in question (see Fig. 4). This approach facilitates setting an approximate starting boundary, allowing the wavelength to vary based on the exact maxima in the Monte-Carlo spectra. In any case, the method is relatively insensitive to the choice of the bounding region, a conclusion which was also made by Silverman et al. (2012).

Once the boundaries are determined for a given spectral feature, a cubic spline is fit to each smoothed mock spectrum (see Fig. 4), producing a distribution of velocities. The median velocity and the 16th and 84th percentiles are taken as the estimate for velocity and its error respectively. The cubic spline is agnostic to the shape of the complex absorption and emission processes that may shape a spectral feature. For example, the absorption in a P-Cygni profile would not produce the same feature as pure absorption would. The wavelength of the spline fit at its minimum is converted to a doppler velocity using Eq. A.1. Figure 4 shows a detailed example of this method applied to one of the SNe analysed in this paper.

Appendix B: Tables

Table B.1. List of Ic-BLs and GRB-SNe used for velocity measurements, showing their type, redshift (z), explosion time (t_{exp}) and its error (Δt_{exp}). In some instances, Δt_{exp} was not known for an SN, while for the GRB-SNe t_{exp} is taken from the GRB trigger time, meaning that the error is just a few seconds. For cases where the SN type is ambiguous, the second-most likely type is shown. The number of spectra for each SN is also shown; with the number in brackets indicates the number of these spectra that show evidence of nebular features.

Event name	Type	z	t_{exp} [UTC]	Δt_{exp} [days]	Num. Spectra	Sources
GRB980425-SN1998bw	GRB-SN	0.008499	1998-04-25T21:49:11		29 (5)	Patat et al. (2001); Pian et al. (1999)
GRB030329-SN2003dh	GRB-SN	0.1685	2003-03-29T11:37:14		16 (0)	Matheson et al. (2003); Kosugi et al. (2004)
GRB060218-SN2006aj	GRB-SN	0.033023	2006-02-18T03:34:31		34 (3)	Modjaz et al. (2014, 2006); Pian et al. (2006); Sonbas et al. (2008) GRB-NASASwift
GRB100316D-SN2010bh	GRB-SN	0.0593	2010-03-16T12:44:50		16 (0)	Bufano et al. (2012) GRBNASASwift
GRB101219B-SN2010ma	GRB-SN	0.55185	2010-12-19T16:27:53		6 (0)	Sparre et al. (2011) GRBNASASwift
GRB120422A-SN2012bz	GRB-SN	0.283	2012-04-22T07:12:03		13 (0)	Melandri et al. (2012) GRBNASASwift
GRB130702A-SN2013dx	GRB-SN	0.15	2013-07-02T00:05:23		29 (0)	D'Elia et al. (2015); Taddia et al. (2019); Schulze et al. (2021); Volnova et al. (2017)
GRB161219B-SN2016jca	GRB-SN	0.1475	2016-12-19T18:48:39		3 (0)	GRBNASASwift
GRB171010A-SN2017htp	GRB-SN	0.328	2017-10-10T19:00:50		5 (0)	Bright et al. (2019)
GRB171205A-SN2017iuk	GRB-SN	0.0368	2017-12-05T07:20:43		26 (0)	GRBNASASwift
GRB180728A-SN2018fip	GRB-SN	0.117	2018-07-28T17:29:00		14 (0)	GRBNASASwift
GRB190829A-AT2019oyw	GRB-SN	0.0785	2019-08-29T19:56:44		10 (0)	GRBNASASwift
SN2020bvc	GRB-SN	0.025235	2020-02-03T16:04:48		14 (0)	Ho et al. (2020)
1997ef	Ic-BL	0.011805	1997-11-20T00:00:00		38 (7)	Modjaz et al. (2014); Matheson et al. (2001); Mazzali et al. (2000)
1997dq	Ic-BL	0.003196	1997-09-29T00:00:00		15 (5)	Modjaz et al. (2014); Matheson et al. (2001); Mazzali et al. (2004)
1998ey	Ic-BL	0.016	1998-12-02T15:37:26	2.0	6 (0)	Arbour & Schwartz (1998)
2002bl	Ic-BL	0.016	2002-02-22T10:48:00	8.4	4 (0)	Shivvers et al. (2019); Armstrong (2002)
2002ap	Ic-BL	0.002108	2002-01-27T00:00:00	2.0	43 (12)	Modjaz et al. (2014); Foley et al. (2003); Chornock et al. (2013); Gal-Yam et al. (2002)
2003bg	Ic-BL/IIb	0.004403	2003-02-25T00:00:00		14 (6)	Hamuy et al. (2009); Mazzali et al. (2009)
2003jd	Ic-BL	0.01886	2003-10-20T12:00:00	4.5	29 (4)	Modjaz et al. (2014); Shivvers et al. (2019); Valenti et al. (2008)
2005da	Ic-BL	0.01501	2005-07-16T08:38:24	2.0	4 (0)	Modjaz et al. (2014); Shivvers et al. (2019); Lee & Li (2005)
2006nx	Ic-BL	0.137	2006-11-11T05:02:24	0.71	3 (0)	Taddia et al. (2015)
2007ce	Ic-BL	0.046	2007-04-10T02:24:00	5.2	11 (0)	Modjaz et al. (2014); Shivvers et al. (2019); Gomez et al. (2022)
2007ru	Ic-BL	0.015464	2007-11-25T12:00:00	3.0	5 (0)	Modjaz et al. (2014); Shivvers et al. (2019); Sahu et al. (2009)
2007I	Ic-BL	0.021638	2007-11-12T10:33:36	2.0	7 (3)	Modjaz et al. (2014); Shivvers et al. (2019); Lee & Li (2007)
2007D	Ic/Ic-BL	0.023146	2007-01-05T07:12:00	0.3	4 (0)	Modjaz et al. (2014); Shivvers et al. (2019); Drout et al. (2011); Wang et al. (2019)
2008ew	Ic/Ic-BL	0.02026	2008-08-08T05:16:48	2.0	4 (0)	Shivvers et al. (2019); Griffith et al. (2008), SNID
2009bb	Ic-BL (pec.)	0.0104	2009-03-19T02:24:00	0.6	28 (2)	Stritzinger et al. (2023); Pignata et al. (2011)
2009dr	Ic-BL	0.199	2009-04-15T06:00:00	2.0	6 (1)	Quimby et al. (2009)
2009ca	Ic-BL/SLSN	0.0957	2009-03-25T08:38:24	3.35	4 (0)	Stritzinger et al. (2023); Taddia et al. (2018)
PTF10vgv	Ic-BL	0.015	2010-09-13T23:16:48	2.0	10 (3)	Corsi et al. (2012); Taddia et al. (2019)
2010ah	Ic-BL	0.0498	2010-02-21T00:00:00		4 (0)	Corsi et al. (2011); Taddia et al. (2019); Mazzali et al. (2013)
PTF10ysd	Ic-BL	0.0963	2010-09-25T12:00:00	2.0	3 (0)	Taddia et al. (2019)
PTF10xem	Ic-BL	0.0567	2010-09-22T03:36:00	2.0	5 (2)	Taddia et al. (2019)
PTF10tqv	Ic-BL	0.0795	2010-08-14T04:04:48	2.0	3 (0)	Taddia et al. (2019)
PTF10qts	Ic-BL	0.0907	2010-08-03T14:24:00	2.0	13 (2)	Walker et al. (2014); Taddia et al. (2019)
PTF10gvb	Ic/Ic-BL	0.098	2010-04-29T14:24:00	2.0	6 (0)	Taddia et al. (2019); Quimby et al. (2018)
PTF10aavz	Ic-BL	0.062	2010-11-07T11:31:12	2.0	4 (1)	Taddia et al. (2019)
2010ay	Ic-BL	0.0671	2010-02-21T07:12:00	1.3	3 (0)	Sanders et al. (2012a); Shivvers et al. (2019); Sanders et al. (2012b)
PTF11qcj	Ic-BL	0.028	2011-10-08T12:00:00		6 (1)	Corsi et al. (2014)
PTF12gzk	Ic/Ic-BL	0.01377	2012-07-23T07:12:00	0.6	55 (12)	Childress et al. (2016); Shivvers et al. (2019); Ben-Ami et al. (2012)

Continued on next page

Table B.1. List of Ic-BLs and GRB-SNe used for velocity measurements, continued.

Event name	Type	z	t_{exp} [UTC]	Δt_{exp} [days]	Num. Spectra	Sources
PTF12as	Ic-BL	0.033	2011-12-25T12:14:24	2.0	3 (1)	Taddia et al. (2019)
2012ap	Ic-BL (pec.)	0.01224	2012-02-07T17:02:23	2.5	15 (4)	Milisavljevic et al. (2015); Liu et al. (2015)
2012aa	Ic-BL/SLSN	0.0799	2011-12-26T12:00:00	10.0	4 (1)	Shivvers et al. (2019); Roy et al. (2016)
OGLE-2013-SN-134	Ic/Ic-BL	0.039	2013-12-08T07:29:48	2.0	2 (0)	Wyrzykowski et al. (2013), SNID
iPTF13ebw	Ic-BL	0.069	2013-11-15T17:02:24	2.0	6 (0)	Schulze et al. (2021); Taddia et al. (2019)
2013bn	Ic-BL	0.054	2013-04-03T23:02:24	2.0	5 (0)	Taddia et al. (2019); Shivvers et al. (2019)
LSQ14bef	Ic-BL	0.05	2014-04-20T00:00:00	2.0	1 (0)	Polshaw et al. (2014)
2014cp	Ic-BL	0.016164	2014-06-23T00:00:00		10 (6)	Childress et al. (2016); Zheng et al. (2022)
2014ad	Ic-BL	0.005	2014-03-08T12:00:00	3.0	31 (5)	Sahu et al. (2018)
iPTF14gaq	Ic-BL	0.0826	2014-09-19T17:02:24	2.0	3 (0)	Taddia et al. (2019)
iPTF14dby	Ic-BL	0.074	2014-06-19T13:55:12	2.0	4 (1)	Taddia et al. (2019)
iPTF15eov	Ic-BL	0.0535	2015-12-02T05:16:48	2.0	17 (0)	Taddia et al. (2019)
iPTF15dqq	Ic-BL	0.065	2015-11-02T05:31:12	2.0	4 (0)	Taddia et al. (2019)
iPTF15dld	Ic-BL	0.047	2015-10-03T00:00:00	1.0	6 (0)	Pian et al. (2017)
2016gox	Ic-BL	0.042	2016-09-10T02:09:36	2.0	4 (0)	Taddia et al. (2019)
2016P	Ic/Ic-BL	0.0146	2016-01-16T00:00:00	2.0	19 (1)	Prentice et al. (2019); Gangopadhyay et al. (2020)
2016ilj	Ic-BL	0.039711	2016-11-08T18:00:00	2.0	3 (0)	Taddia et al. (2019)
2016coi	Ic/Ic-BL	0.0036	2016-05-23T21:36:00	1.5	100 (26)	Prentice et al. (2018); Terreran et al. (2019)
2017dgk	Ic/Ic-BL	0.065	2017-04-21T22:31:42	2.0	2 (0)	Gutierrez et al. (2017), SNID
2017ens	Ic-BL	0.1086	2017-06-03T19:12:00	1.5	17 (14)	Chen et al. (2018)
2017ifh	Ic-BL	0.039	2017-10-30T00:15:50	7.5	5 (0)	Prentice et al. (2019)
2017fwm	Ib/Ic-BL	0.016	2017-07-26T18:37:26	0.2	6 (0)	WISeREP, SNID
2017dio	Ic-BL/IIin	0.037	2017-04-14T06:00:00	0.25	15 (0)	Kuncarayakti et al. (2018); Shi et al. (2024)
2017dcc	Ic-BL	0.0245	2017-04-12T11:45:38	3.96	9 (2)	Tonry et al. (2017)
2017cw	Ic-BL	0.093	2016-12-29T21:36:00	2.0	3 (0)	Taddia et al. (2019)
2018kqr	Ic-BL	0.045	2018-12-06T12:07:19	3.0	2 (0)	De et al. (2020), SNID
2018gsk	Ic-BL	0.0116	2018-09-15T15:15:50	2.0	13 (1)	Tonry et al. (2018d), SNID
2018gju	Ic-BL	0.05	2018-09-13T12:30:14	2.0	1 (0)	Tonry et al. (2018c), SNID
2018giu	Ic-BL	0.026	2018-09-13T21:23:45	1.5	7 (0)	Tonry et al. (2018b), SNID
2018gep	Ic-BL (pec.)	0.033	2018-09-09T02:24:00	0.95	7 (0)	Pritchard et al. (2021)
2018cbz	Ic-BL	0.0223	2018-05-29T08:54:14	2.0	6 (0)	Prentice et al. (2019); Tonry et al. (2018a)
2020abdw	Ic/Ic-BL	0.0327790007	2020-11-21T06:02:28	4.0	3 (0)	De (2020), SNID
2022crr	Ic-BL	0.0188	2022-02-08T06:11:31	0.94	3 (0)	WISeREP, SNID

Table B.2. Measured velocities of Fe II, Si II and Ca II for the Ic-BL supernovae analysed here. Each line in the table represents one observation. The name of the event, SG filter width, redshift (z), observation date of the spectrum and rest-frame time relative to the explosion date (ΔT_{rest}) are all given. The velocities (and uncertainties) of the Fe II (v_{FeII}), Si II (v_{SiII}) and Ca II (v_{CaII}) features are reported for each observation. In some cases, no velocity is reported for a feature, for example because the wavelength range of the feature in question was not covered by the spectrum.

Event name	SG filter width	z	Obs. date [UT]	ΔT_{rest} [days]	v_{FeII} [km/s]	v_{SiII} [km/s]	v_{CaII} [km/s]
1997ef	65	0.011805	1997-12-24 10:33:36.00	34.04	12106 ⁻⁵⁰³ ₊₄₂₁	5073 ⁻⁵⁵⁵ ₊₄₅₃	
1997ef	80	0.011805	1997-12-29 07:12:00.00	38.84	13240 ⁻³⁶⁸ ₊₆₀₃	3845 ⁻⁴⁶⁷ ₊₃₅₈	
1997ef	63	0.011805	1997-11-26 09:21:36.00	6.32	28533 ⁻²⁵⁹⁷ ₊₁₈₇₆	22417 ⁻¹³⁴⁷ ₊₄₅₀	
1997ef	63	0.011805	1997-12-04 08:09:36.00	14.17	18127 ⁻¹⁰⁵⁹ ₊₁₃₅₂	16192 ⁻⁴⁶⁷ ₊₇₀₈	
1997ef	65	0.011805	1997-12-23 10:19:12.00	33.04	12341 ⁻⁵¹⁵ ₊₄₆₃	5559 ⁻³³⁷ ₊₂₃₇	
1997ef	121	0.011805	1997-12-30 08:24:00.00	39.88		4283 ⁻¹²⁴⁹ ₊₁₀₃₉	
1997ef	67	0.011805	1998-01-20 05:31:12.00	60.52	9031 ⁻⁵³⁷ ₊₅₄₈		
1997ef	65	0.011805	1998-01-01 07:40:48.00	41.83	12322 ⁻³⁰³ ₊₃₀₉	3069 ⁻²³⁵ ₊₂₇₈	
1997ef	63	0.011805	1997-12-05 07:26:24.00	15.13	18815 ⁻²⁵⁸ ₊₃₀₆	16012 ⁻³⁴⁸ ₊₄₂₉	
1997ef	60	0.011805	1998-01-17 09:41:46.00	57.72			12616 ⁻⁴³⁵ ₊₄₄₉
1997ef	63	0.011805	1997-12-01 08:09:36.00	11.21	23833 ⁻²³⁰⁵ ₊₁₀₆₃	18632 ⁻⁵²⁹ ₊₇₃₉	
1997ef	100	0.011805	1997-11-28 12:57:36.00	8.44	24762 ⁻⁵⁹³ ₊₆₄₆	20867 ⁻⁵⁷⁰ ₊₆₂₂	
1997ef	153	0.011805	1998-01-17 00:00:00.00	57.32	9704 ⁻²⁷⁰ ₊₃₂₁		12850 ⁻²⁷⁴ ₊₃₁₄
1997ef	100	0.011805	1997-11-30 08:24:00.00	10.23	22900 ⁻¹⁶⁹⁸ ₊₁₃₄₃	19085 ⁻³⁴⁷ ₊₃₅₅	
1997ef	63	0.011805	1997-12-20 00:00:00.00	29.65	12846 ⁻⁵⁹ ₊₅₅	6922 ⁻⁶⁷ ₊₆₄	
1997ef	31	0.011805	1997-12-20 00:00:00.00	29.65	12893 ⁻⁸⁰ ₊₆₆	6905 ⁻⁷⁵ ₊₇₈	
1997ef	63	0.011805	1998-01-06 08:24:00.00	46.80	9011 ⁻³⁴⁷ ₊₃₉₇		
1997ef	90	0.011805	1998-01-03 06:14:24.00	43.74	11721 ⁻¹⁸²⁹ ₊₉₈₃	4412 ⁻⁴⁷⁰ ₊₅₄₈	
1997ef	67	0.011805	1998-01-24 06:28:48.00	64.51	8631 ⁻¹¹⁰⁹ ₊₂₄₅₉		
1997ef	63	0.011805	1997-11-29 10:19:12.00	9.32	24629 ⁻³⁵¹ ₊₃₅₀	20616 ⁻⁷⁸⁶ ₊₁₃₀₈	
1997ef	73	0.011805	1998-01-26 06:14:24.00	66.48	5551 ⁻³⁵⁰ ₊₂₆₉		11300 ⁻²⁴⁵¹ ₊₅₀₆
1997ef	71	0.011805	1997-12-05 09:50:24.00	15.23	19032 ⁻⁴³⁵ ₊₄₄₆	13814 ⁻²³⁴ ₊₂₂₁	17361 ⁻²⁵⁶ ₊₂₄₃
1997ef	65	0.011805	1997-12-26 09:36:00.00	35.98	11272 ⁻²⁰⁴⁶ ₊₇₂₈	3745 ⁻⁵⁴³ ₊₃₆₄	
1997ef	133	0.011805	1998-03-26 06:10:05.00	124.78	5086 ⁻⁸³ ₊₈₃	13532 ⁻¹⁴⁸ ₊₁₄₇	9650 ⁻¹⁴⁰ ₊₁₃₆
1997ef	100	0.011805	1997-12-27 12:28:48.00	37.08	11970 ⁻¹⁶⁶³ ₊₂₈₄₂	4378 ⁻³⁶⁶ ₊₃₇₃	
1997ef	100	0.011805	1997-12-06 08:09:36.00	16.15	16455 ⁻¹¹⁰⁵ ₊₈₅₄	13103 ⁻³²² ₊₂₆₅	
1997ef	87	0.011805	1998-01-28 06:05:46.00	68.45	7248 ⁻³¹⁴ ₊₃₁₄	13289 ⁻⁶² ₊₆₂	11915 ⁻²⁹² ₊₁₈₉
1997ef	71	0.011805	1998-01-28 05:02:24.00	68.40	7728 ⁻⁴⁸⁰ ₊₆₅₀		14296 ⁻⁷³² ₊₁₈₄₄
1997ef	173	0.011805	1998-01-28 00:00:00.00	68.19	7067 ⁻³⁷¹ ₊₃₈₂		11891 ⁻²⁵⁰ ₊₂₂₀
1997dq	63	0.003196	1997-11-22 12:57:36.00	54.37	6050 ⁻¹⁰⁷ ₊₉₄	13046 ⁻⁶¹ ₊₅₁	
1997dq	65	0.003196	1998-01-01 13:12:00.00	94.25	5200 ⁻⁵⁶ ₊₅₆	12198 ⁻⁶⁹ ₊₆₈	
1997dq	65	0.003196	1997-12-31 00:00:00.00	92.70	5200 ⁻⁵² ₊₄₈	12197 ⁻⁶⁹ ₊₆₈	
1997dq	63	0.003196	1997-12-20 00:00:00.00	81.74	6059 ⁻²¹ ₊₂₇	12209 ⁻¹⁵ ₊₁₅	
1997dq	63	0.003196	1997-11-25 12:57:36.00	57.36	5959 ⁻⁸³ ₊₈₅	12995 ⁻⁵³ ₊₅₈	
1997dq	63	0.003196	1997-12-04 12:00:00.00	66.29	5798 ⁻⁹³ ₊₉₆	12837 ⁻⁷³ ₊₆₉	
1997dq	181	0.003196	1997-11-08 00:00:00.00	39.87	6483 ⁻¹¹⁹ ₊₁₁₂	13674 ⁻⁷¹ ₊₆₆	12013 ⁻¹⁴⁵ ₊₁₄₇
1997dq	63	0.003196	1997-11-29 12:57:36.00	61.34	5859 ⁻⁶⁷ ₊₆₆	12678 ⁻⁴³ ₊₅₇	
1997dq	63	0.003196	1997-11-07 12:57:36.00	39.41	6238 ⁻¹⁸¹ ₊₁₇₁	13987 ⁻⁷⁵ ₊₆₀	
1997dq	73	0.003196	1997-12-05 12:57:36.00	67.32	5901 ⁻¹¹⁵ ₊₁₁₀	12782 ⁻⁶⁷ ₊₇₇	10223 ⁻³⁹³ ₊₃₁₄
1998ey	100	0.016	1998-12-21 00:00:00.00	18.06	7542 ⁻¹³¹⁴ ₊₉₂₇	4238 ⁻⁴⁴² ₊₄₆₁	
1998ey	63	0.016	1998-12-10 00:00:00.00	7.23		10421 ⁻²⁰¹⁹ ₊₁₅₇₉	
1998ey	63	0.016	1998-12-25 00:00:00.00	22.00	6711 ⁻⁴⁵⁰ ₊₄₀₁	2375 ⁻⁹⁷⁴ ₊₉₈₉	
1998ey	63	0.016	1998-12-12 00:00:00.00	9.20	14652 ⁻⁸⁹² ₊₅₅₈	9664 ⁻²⁹³ ₊₃₃₃	
1998ey	151	0.016	1998-12-19 00:00:00.00	16.09	7425 ⁻¹⁸⁸⁰ ₊₁₈₉₀	5174 ⁻³⁴⁵⁹ ₊₁₅₁₅	

Continued on next page

Table B.2. Measured velocities of Fe II, Si II and Ca II for the Ic-BL supernovae analysed here, continued.

Event name	SG filter width	z	Obs. date [UT]	ΔT_{rest} [days]	$v_{Fe II}$ [km/s]	$v_{Si II}$ [km/s]	$v_{Ca II}$ [km/s]
1998ey	121	0.016	1998-12-17 00:00:00.00	14.12	10156 ⁻⁴⁰⁷² ₊₁₄₂₀	6097 ⁻³⁸⁴ ₊₃₉₃	
2002ap	89	0.002108	2002-02-11 00:00:00.00	14.97	24150 ⁻¹³³ ₊₁₂₉	9425 ⁻⁸⁰ ₊₈₇	16742 ⁻¹⁴⁸ ₊₁₇₃
2002ap	61	0.002108	2002-03-07 00:00:00.00	38.92	24895 ⁻⁶⁴⁷ ₊₃₄₃		12664 ⁻⁶⁹ ₊₅₆
2002ap	50	0.002108	2002-02-06 02:38:24.00	10.09	24220 ⁻⁹⁷ ₊₉₇	15886 ⁻¹⁴⁷ ₊₁₂₇	
2002ap	63	0.002108	2002-02-15 02:09:36.00	19.05	24555 ⁻¹⁰⁴ ₊₈₇	7559 ⁻⁶⁵ ₊₇₄	
2002ap	63	0.002108	2002-02-13 02:24:00.00	17.06	24631 ⁻⁹⁵ ₊₉₉	8428 ⁻⁷⁸ ₊₇₉	
2002ap	131	0.002108	2002-02-14 17:27:54.00	18.69	22935 ⁻³⁸² ₊₂₃₂	7784 ⁻¹⁴⁰ ₊₁₂₉	
2002ap	63	0.002108	2002-02-07 02:09:36.00	11.07	23776 ⁻⁹⁴ ₊₈₆	15113 ⁻¹⁵⁷ ₊₁₄₉	
2002ap	63	0.002108	2002-03-06 02:24:00.00	38.02	23911 ⁻²³³ ₊₂₅₄		
2002ap	25	0.002108	2002-02-10 00:00:00.00	13.97	24587 ⁻⁴¹¹ ₊₂₈₁	9797 ⁻³⁰¹⁴ ₊₅₅₀	
2002ap	63	0.002108	2002-03-11 02:24:00.00	43.01	23682 ⁻³⁶⁵ ₊₃₈₈		
2002ap	120	0.002108	2002-02-07 16:52:41.00	11.68	21404 ⁻³⁷² ₊₃₉₀	14939 ⁻¹⁴⁰ ₊₁₇₄	
2002ap	63	0.002108	2002-02-08 01:55:12.00	12.05	23653 ⁻¹²⁰ ₊₁₁₉	15035 ⁻⁸⁰ ₊₈₀	
2002ap	89	0.002108	2002-03-11 00:00:00.00	42.91	24979 ⁻⁵²⁸ ₊₄₉₈		12075 ⁻³²⁰ ₊₃₄₉
2002ap	63	0.002108	2002-02-12 02:52:48.00	16.09	24669 ⁻¹⁰⁷ ₊₁₃₁	8820 ⁻⁸⁵ ₊₈₅	
2002ap	63	0.002108	2002-02-09 02:38:24.00	13.08	23962 ⁻¹²⁸ ₊₁₂₈	14728 ⁻⁸⁹ ₊₈₇	
2002ap	63	0.002108	2002-02-14 02:24:00.00	18.06	24879 ⁻¹⁷⁶ ₊₁₈₁	7618 ⁻³⁸² ₊₃₉₅	
2002ap	83	0.002108	2002-02-14 00:00:00.00	17.96	24806 ⁻¹¹⁹ ₊₁₃₄	7964 ⁻³⁶ ₊₃₉	13257 ⁻⁵¹ ₊₄₇
2002ap	63	0.002108	2002-03-10 02:24:00.00	42.01	24108 ⁻⁴⁴³ ₊₄₀₅		
2002ap	81	0.002108	2002-02-21 00:00:00.00	24.95		3654 ⁻²⁰² ₊₂₁₆	12357 ⁻²⁵⁰ ₊₁₅₇
2002ap	50	0.002108	2002-02-15 00:00:00.00	18.96	25589 ⁻⁵⁷⁸ ₊₅₇₉	6499 ⁻³³⁶ ₊₄₀₇	
2002ap	46	0.002108	2002-02-03 00:00:00.00	6.99	25292 ⁻⁷³⁹ ₊₅₆₁	20033 ⁻⁶²⁴ ₊₇₂₂	
2002ap	25	0.002108	2002-02-17 00:00:00.00	20.96	24954 ⁻³⁹⁷ ₊₃₇₂	4998 ⁻⁴⁵⁷ ₊₄₀₅	
2002ap	147	0.002108	2002-02-01 00:00:00.00	4.99	30210 ⁻³⁰⁹ ₊₃₁₂		
2002ap	200	0.002108	2002-01-31 16:39:56.00	4.68	38186 ⁻⁶⁰⁵ ₊₇₄₂	34411 ⁻²⁴¹ ₊₂₃₁	
2002ap	63	0.002108	2002-02-20 02:09:36.00	24.04	24820 ⁻¹⁵⁵ ₊₁₃₇	5308 ⁻¹³⁰ ₊₁₈₃	
2002ap	35	0.002108	2002-02-02 00:00:00.00	5.99	27114 ⁻⁸¹³ ₊₁₁₂₂	21207 ⁻²⁷⁴ ₊₃₀₁	
2002ap	121	0.002108	2002-02-21 16:53:40.00	25.65		4432 ⁻²¹⁰ ₊₁₇₈	
2002bl	61	0.016	2002-03-07 00:00:00.00	12.35	18440 ⁻²⁰⁸ ₊₁₈₀	15520 ⁻⁴⁸ ₊₆₃	
2002bl	121	0.016	2002-03-07 00:00:00.00	12.35	16884 ⁻¹⁴⁶⁷ ₊₁₄₅₄	13909 ⁻²¹²⁸ ₊₁₄₀₉	
2002bl	89	0.016	2002-03-11 00:00:00.00	16.29	18190 ⁻⁶²⁶ ₊₄₇₀	10036 ⁻⁴⁷⁹ ₊₅₆₄	
2003bg	43	0.004403	2003-03-31 00:00:00.00	33.85	6737 ⁻⁸⁹ ₊₈₁	3402 ⁻⁴² ₊₄₉	
2003bg	45	0.004403	2003-04-04 00:00:00.00	37.83	5766 ⁻⁹⁰ ₊₅₅	3074 ⁻⁴⁹ ₊₀	9224 ⁻¹⁰⁶ ₊₁₀₈
2003bg	25	0.004403	2003-04-09 00:00:00.00	42.81	5997 ⁻¹¹⁴ ₊₁₂₈	3353 ⁻⁴⁴ ₊₃₇	9344 ⁻¹⁷⁴ ₊₁₉₄
2003bg	20	0.004403	2003-04-10 00:00:00.00	43.81	5745 ⁻⁵⁹ ₊₃₄	3493 ⁻⁵² ₊₈₂	9302 ⁻²⁴⁵ ₊₂₆₂
2003bg	45	0.004403	2003-03-12 00:00:00.00	14.93	12109 ⁻⁷⁶ ₊₇₈	4718 ⁻³⁰ ₊₂₉	14307 ⁻³⁰⁸ ₊₃₁₂
2003bg	45	0.004403	2003-03-04 00:00:00.00	6.97	15116 ⁻⁸⁵⁵ ₊₅₈₂	8181 ⁻⁴⁸ ₊₄₅	15245 ⁻¹²¹ ₊₁₅₄
2003bg	79	0.004403	2003-02-28 00:00:00.00	2.99	25092 ⁻²²⁰ ₊₂₁₅	19631 ⁻⁴³³ ₊₅₁₄	27364 ⁻¹⁹⁵ ₊₂₀₆
2003jd	100	0.01886	2003-11-27 03:50:24.00	36.96	12428 ⁻³²⁸ ₊₃₇₉	6640 ⁻²⁵¹ ₊₂₉₆	
2003jd	100	0.01886	2003-11-19 03:21:36.00	29.09	12744 ⁻⁸⁶⁶ ₊₁₈₇₄	7674 ⁻⁴¹⁶ ₊₃₇₅	
2003jd	100	0.01886	2003-11-23 00:00:00.00	32.88	12333 ⁻⁸⁴⁶ ₊₁₅₉₅	7257 ⁻²⁴¹ ₊₂₂₀	15271 ⁻²⁴⁸ ₊₂₉₆
2003jd	100	0.01886	2003-12-20 02:09:36.00	59.47	10828 ⁻⁷³¹ ₊₁₂₉₉	6285 ⁻¹²⁴⁰ ₊₁₃₈₉	
2003jd	100	0.01886	2003-11-23 02:52:48.00	33.00	13898 ⁻⁶⁴⁰ ₊₉₃₂	7212 ⁻³⁸⁸ ₊₃₉₃	
2003jd	89	0.01886	2003-10-28 00:00:00.00	7.36	22332 ⁻¹⁰⁵⁹ ₊₁₇₇		
2003jd	63	0.01886	2003-12-22 01:55:12.00	61.42	11640 ⁻⁶⁰⁵ ₊₁₀₉₁	8338 ⁻²⁵⁹ ₊₂₄₆	
2003jd	63	0.01886	2003-10-28 07:40:48.00	7.68	19129 ⁻⁶⁸⁸ ₊₇₈₇		

Continued on next page

Table B.2. Measured velocities of Fe II, Si II and Ca II for the Ic-BL supernovae analysed here, continued.

Event name	SG filter width	z	Obs. date [UT]	ΔT_{rest} [days]	$v_{Fe II}$ [km/s]	$v_{Si II}$ [km/s]	$v_{Ca II}$ [km/s]
2003jd	100	0.01886	2003-12-25 03:50:24.00	64.44	10019 ⁻⁵¹⁹ ₊₅₀₈	5433 ⁻¹⁴¹¹ ₊₉₃₈	
2003jd	79	0.01886	2003-11-29 00:00:00.00	38.77	11523 ⁻¹⁸² ₊₁₉₀	6725 ⁻⁹³ ₊₈₅	15121 ⁻⁹⁷ ₊₁₁₂
2003jd	63	0.01886	2003-11-24 02:38:24.00	33.97	12914 ⁻⁴⁶¹ ₊₁₇₃₉	7419 ⁻⁴⁰⁶ ₊₆₇₄	
2003jd	120	0.01886	2003-11-28 01:55:12.00	37.87	8180 ⁻¹⁶⁴⁰ ₊₉₆₃	6302 ⁻⁶⁷⁴ ₊₅₅₄	
2003jd	65	0.01886	2003-12-20 02:09:36.00	59.47	11317 ⁻⁶⁸ ₊₇₄	6078 ⁻²⁷⁹ ₊₃₀₉	15179 ⁻¹⁷⁴ ₊₂₁₁
2003jd	63	0.01886	2003-11-01 04:33:36.00	11.47	16684 ⁻¹⁰³⁰ ₊₄₂₈	13766 ⁻³⁵⁴ ₊₄₃₆	
2003jd	65	0.01886	2003-12-19 03:07:12.00	58.53	11224 ⁻¹⁵³ ₊₁₇₂	5604 ⁻³³⁷ ₊₂₇₇	15375 ⁻³⁸⁵ ₊₅₂₀
2003jd	63	0.01886	2003-11-20 03:36:00.00	30.08	13609 ⁻⁵⁷¹ ₊₃₁₈₉	7741 ⁻²⁵⁸ ₊₂₅₀	
2003jd	100	0.01886	2003-11-21 03:36:00.00	31.06	12639 ⁻⁵²⁶ ₊₃₁₉	7259 ⁻²⁶⁸ ₊₂₆₀	
2003jd	63	0.01886	2003-12-18 01:55:12.00	57.50	11996 ⁻³³² ₊₄₀₄	5404 ⁻⁴³³ ₊₂₆₀	
2003jd	63	0.01886	2003-10-29 04:19:12.00	8.52	17297 ⁻⁴⁰⁰ ₊₃₁₅	14112 ⁻²⁶⁵ ₊₂₄₃	
2003jd	100	0.01886	2003-12-04 04:04:48.00	43.84	10877 ⁻⁷⁰⁷ ₊₆₃₄	6201 ⁻²⁷⁰ ₊₂₅₇	
2003jd	100	0.01886	2003-10-30 04:33:36.00	9.51	17420 ⁻²⁷³ ₊₂₂₈	14178 ⁻²⁴³ ₊₂₅₁	
2003jd	100	0.01886	2003-12-17 01:55:12.00	56.51	5287 ⁻⁶⁷⁸ ₊₁₁₈₉	6242 ⁻¹⁷¹⁶ ₊₁₂₂₀	
2003jd	63	0.01886	2003-10-31 05:02:24.00	10.51	17986 ⁻²³⁰¹ ₊₂₂₆₉	14725 ⁻⁶⁰⁸ ₊₇₅₀	
2003jd	63	0.01886	2003-11-22 03:36:00.00	32.05	9848 ⁻²⁹³¹ ₊₉₈₆	7582 ⁻¹⁴⁴ ₊₁₅₁	
2005da	67	0.01501	2005-07-28 08:38:24.00	11.82	25404 ⁻³⁸³ ₊₃₆₅	19165 ⁻³³⁴ ₊₄₄₁	
2005da	100	0.01501	2005-07-26 06:28:48.00	9.76	25453 ⁻³⁵⁸ ₊₃₇₀	18893 ⁻⁴³⁰ ₊₈₄₈	
2005da	61	0.01501	2005-08-01 09:08:38.00	15.78	25572 ⁻¹⁸⁸ ₊₁₉₄	18632 ⁻²⁵⁷ ₊₂₂₂	17966 ⁻³³¹ ₊₂₃₇
2005da	61	0.01501	2005-07-29 06:14:24.00	12.71	25121 ⁻¹³¹ ₊₄₉₁	19689 ⁻⁴¹⁴ ₊₅₀₇	
2006nx	43	0.137	2006-11-24 00:00:00.00	11.25	16072 ⁻⁷²³ ₊₇₇₈	14362 ⁻³⁵¹ ₊₇₅₀	
2006nx	49	0.137	2006-11-17 00:00:04.00	5.09	22849 ⁻³¹⁰⁴ ₊₁₆₃	15806 ⁻⁶⁵⁵ ₊₁₄₄₄	
2007I	100	0.021638	2007-01-16 12:14:24.00	3.98	15380 ⁻⁷⁸⁸ ₊₁₂₇₂	13121 ⁻⁵³¹ ₊₁₀₃₅	
2007I	67	0.021638	2007-01-26 09:36:00.00	13.66	12278 ⁻⁹³² ₊₁₂₂₆	6426 ⁻³⁰¹ ₊₃₉₀	
2007I	75	0.021638	2007-01-21 11:12:28.00	8.84	13518 ⁻¹³⁷ ₊₁₄₉	9009 ⁻¹⁹⁶ ₊₂₁	17001 ⁻¹⁶⁰ ₊₁₂₀
2007I	100	0.021638	2007-01-21 12:43:12.00	8.90	11535 ⁻²⁰⁹⁷ ₊₁₆₄₈	8725 ⁻⁸¹⁹ ₊₇₇₁	
2007ru	67	0.015464	2007-12-03 03:21:36.00	7.52	22987 ⁻⁴⁵⁰ ₊₄₇₅	19976 ⁻³²⁰ ₊₄₉₂	
2007ru	67	0.015464	2007-12-06 02:24:00.00	10.44	21946 ⁻⁴¹⁵ ₊₄₁₇	18669 ⁻⁵⁴⁷ ₊₅₂₂	
2007ru	151	0.015464	2007-12-01 03:28:47.00	5.56	22414 ⁻⁵²³ ₊₅₁₃		20171 ⁻⁸³⁷ ₊₇₃
2007ru	67	0.015464	2008-01-11 06:00:00.00	46.04	13128 ⁻²⁷⁹ ₊₂₈₈	9450 ⁻¹⁰⁸ ₊₁₁₇	17007 ⁻²⁰⁷ ₊₂₁₀
2007ru	89	0.015464	2007-12-11 02:54:14.00	15.38	17276 ⁻⁹⁷⁸ ₊₅₃₆	16436 ⁻¹⁶⁵ ₊₁₆₈	18802 ⁻¹⁹⁷ ₊₂₀₇
2007D	75	0.023146	2007-01-21 08:54:14.00	15.71	21660 ⁻⁸⁵⁷ ₊₇₀₃	11782 ⁻³⁴⁸ ₊₃₃₁	18088 ⁻⁵⁷⁶ ₊₅₆₁
2007D	73	0.023146	2007-01-13 10:30:43.00	7.95	22635 ⁻²⁹⁶ ₊₆₆₁	14969 ⁻³³¹ ₊₃₆₅	18620 ⁻³⁰⁶ ₊₇₂₀
2007D	151	0.023146	2007-02-16 06:54:43.00	41.04	19015 ⁻³⁰⁵ ₊₂₉₆	12688 ⁻²²² ₊₂₁₁	14818 ⁻¹²⁶⁵ ₊₇₀₂
2007D	100	0.023146	2007-01-15 03:36:00.00	9.63	25466 ⁻¹³⁸⁴ ₊₁₇₇	15161 ⁻⁴⁷⁸ ₊₄₈₉	
2007ce	67	0.046	2007-05-11 04:48:00.00	29.73	10888 ⁻⁷²⁵ ₊₂₂₀₃	11857 ⁻⁷⁸³ ₊₂₇₂₂	
2007ce	67	0.046	2007-05-09 05:02:24.00	27.83	12728 ⁻³⁹⁰ ₊₃₁₅	11864 ⁻⁶⁰⁷ ₊₄₉₆	
2007ce	67	0.046	2007-06-10 05:16:48.00	58.43	8114 ⁻⁶⁵³ ₊₈₀₀		
2007ce	67	0.046	2007-05-19 04:48:00.00	37.38	9408 ⁻⁷²⁸ ₊₉₆₇	5995 ⁻²³⁰⁵ ₊₅₈₂	
2007ce	100	0.046	2007-05-25 05:31:12.00	43.15	8584 ⁻⁴⁷⁶ ₊₅₉₄	6072 ⁻⁶⁵⁷ ₊₈₃₇	
2007ce	67	0.046	2007-05-21 04:48:00.00	39.29	7792 ⁻²⁴⁶⁴ ₊₉₇₇	5690 ⁻⁷²⁸ ₊₁₂₅₄	
2007ce	100	0.046	2007-05-13 04:19:12.00	31.63	10269 ⁻¹⁰⁰⁰ ₊₇₃₈	9493 ⁻⁸⁸² ₊₉₇₇	
2007ce	89	0.046	2007-05-24 07:55:12.00	42.28	6547 ⁻²⁰⁶⁸ ₊₁₉₁₆	7023 ⁻³¹⁸ ₊₃₃₆	14500 ⁻³⁸³ ₊₃₆₉
2007ce	67	0.046	2007-05-17 04:19:12.00	35.45	8259 ⁻³⁰⁹ ₊₂₉₀	6511 ⁻¹⁴⁸⁶ ₊₈₅₇	
2008ew	91	0.02026	2008-08-26 04:35:02.00	17.61	8167 ⁻¹⁴¹¹ ₊₁₄₇₃	8948 ⁻¹⁹⁹ ₊₃₁₂	15061 ⁻⁷⁸⁷ ₊₃₀₀₅
2008ew	91	0.02026	2008-09-07 05:03:50.00	29.40	14404 ⁻¹⁸⁸⁹ ₊₁₈₉₆	7889 ⁻³¹⁰ ₊₄₆₀	13701 ⁻²²² ₊₃₂₃

Continued on next page

Table B.2. Measured velocities of Fe II, Si II and Ca II for the Ic-BL supernovae analysed here, continued.

Event name	SG filter width	z	Obs. date [UT]	ΔT_{rest} [days]	$v_{Fe II}$ [km/s]	$v_{Si II}$ [km/s]	$v_{Ca II}$ [km/s]
2008ew	181	0.02026	2008-09-22 04:36:28.00	44.08	11860 ⁻²⁷¹² ₊₂₅₂₉	10273 ⁻¹²²⁶ ₊₂₅₁₄	
2008ew	171	0.02026	2008-09-30 03:47:31.00	51.89	6196 ⁻²⁹⁹⁸ ₊₂₅₃₀	12418 ⁻¹¹⁶³ ₊₁₆₅₅	10375 ⁻⁵⁸⁴ ₊₈₈₃
2009bb	101	0.0104	2009-04-18 01:55:12.00	29.67	22954 ⁻¹¹⁷² ₊₁₃₈₉	11629 ⁻²⁵⁰ ₊₂₆₀	18900 ⁻⁵⁰⁶ ₊₄₄₄
2009bb	25	0.0104	2009-04-26 07:26:24.00	37.82	22807 ⁻⁴⁴² ₊₄₈₇		
2009bb	77	0.0104	2009-04-26 00:00:00.00	37.51	23014 ⁻³²⁰ ₊₂₇₇	8656 ⁻²⁶⁵ ₊₂₃₈	
2009bb	33	0.0104	2009-04-07 23:55:29.00	19.69	25454 ⁻²⁴⁹ ₊₂₄₉	15829 ⁻²⁰⁷ ₊₃₂₆	
2009bb	45	0.0104	2009-03-29 02:24:00.00	9.90	29641 ⁻¹⁹⁴⁴ ₊₇₆₅	24786 ⁻²⁸² ₊₂₉₁	31137 ⁻⁸⁶⁷ ₊₁₉₆₃
2009bb	51	0.0104	2009-04-15 07:26:24.00	26.93	23540 ⁻²⁵⁸ ₊₂₆₇		
2009bb	45	0.0104	2009-03-28 04:33:36.00	9.00	33286 ⁻³⁸⁵ ₊₂₁₀	25991 ⁻³⁵⁸ ₊₂₅₈	31436 ⁻⁶²⁷ ₊₁₁₁₂
2009bb	71	0.0104	2009-05-01 01:55:12.00	42.54	23092 ⁻²⁰⁷ ₊₂₀₂	8584 ⁻⁵²² ₊₁₈₉	17470 ⁻²¹⁴ ₊₁₉₃
2009bb	45	0.0104	2009-05-14 00:43:12.00	55.35			17651 ⁻²⁰⁸ ₊₂₇₇
2009bb	71	0.0104	2009-04-30 03:07:12.00	41.60	23083 ⁻²⁹⁰ ₊₂₀₃	8969 ⁻²⁰⁹ ₊₂₄₃	17681 ⁻¹⁷² ₊₁₇₆
2009bb	51	0.0104	2009-04-22 01:55:12.00	33.63	23005 ⁻³⁹³ ₊₄₂₇	10348 ⁻³⁴³ ₊₅₂₁	18371 ⁻²⁶⁵ ₊₂₅₇
2009bb	33	0.0104	2009-04-07 00:00:00.00	18.71	25437 ⁻²⁵⁹ ₊₂₅₈	15757 ⁻²³⁸ ₊₃₆₂	
2009bb	45	0.0104	2009-04-07 00:00:00.00	18.71			17952 ⁻⁵² ₊₅₃
2009bb	71	0.0104	2009-04-17 02:24:00.00	28.70	24062 ⁻¹⁵⁸ ₊₁₆₅	12166 ⁻⁷⁸⁵ ₊₅₅₅	18326 ⁻¹⁰³ ₊₇₆
2009bb	60	0.0104	2009-04-03 03:21:36.00	14.89	25654 ⁻²³⁰ ₊₂₄₅	20940 ⁻¹⁸² ₊₁₈₀	26693 ⁻²⁶⁴ ₊₂₇₇
2009bb	25	0.0104	2009-04-15 07:26:24.00	26.93	9907 ⁻¹¹⁵⁵ ₊₉₁₂		
2009bb	51	0.0104	2009-04-23 02:38:24.00	34.65	23213 ⁻⁴³⁴ ₊₄₃₆	9726 ⁻²⁸²³ ₊₆₃₄	17745 ⁻⁵³⁹ ₊₇₀₃
2009bb	33	0.0104	2009-05-14 00:43:12.00	55.35	22124 ⁻⁵⁴⁶ ₊₁₃₄₃	7209 ⁻²⁴³ ₊₁₇₃	
2009dr	81	0.199	2009-05-02 07:44:29.00	14.24	13918 ⁻²⁷⁰ ₊₂₉₄	17837 ⁻⁷³¹ ₊₁₀₆₁	
2009dr	55	0.199	2009-04-27 08:40:39.00	10.10	14599 ⁻¹³⁵ ₊₁₃₉		
2009dr	55	0.199	2009-05-20 10:46:46.00	29.36	12948 ⁻¹⁶⁹ ₊₃₉₁	17448 ⁻²¹⁹ ₊₂₅₃	
2009ca	71	0.0957	2009-04-17 08:23:59.00	20.98	12706 ⁻²²¹ ₊₂₃₂	8290 ⁻¹⁵⁰ ₊₁₄₈	12731 ⁻⁷⁵⁸ ₊₁₇₀₈
2009ca	51	0.0957	2009-04-22 08:52:48.00	25.56	11977 ⁻⁷³⁹ ₊₈₄₀	7903 ⁻⁴³⁶ ₊₅₀₇	
2009ca	33	0.0957	2009-04-07 10:04:48.00	11.92	13736 ⁻¹⁹⁰ ₊₁₈₆		
2009ca	45	0.0957	2009-04-07 10:04:48.00	11.92		9338 ⁻²⁷⁵ ₊₂₈₂	13099 ⁻⁴³⁰ ₊₃₄₉
PTF10vgv	61	0.015	2010-10-01 00:00:00.00	16.78	9339 ⁻²⁶⁵ ₊₂₉₂	4514 ⁻²⁰⁹ ₊₁₈₁	13333 ⁻⁸⁴⁴ ₊₈₄₅
PTF10vgv	83	0.015	2010-09-16 00:00:00.00	2.00	15101 ⁻¹¹⁶⁰ ₊₇₃₂	14690 ⁻²⁶³ ₊₃₂₆	
PTF10vgv	33	0.015	2010-09-27 00:00:00.00	12.84		8058 ⁻²¹⁴ ₊₁₉₀	13388 ⁻³¹³ ₊₃₇₇
PTF10gvb	51	0.098	2010-05-06 09:21:36.00	6.18	17789 ⁻⁷⁹⁰ ₊₆₉₄		
PTF10gvb	21	0.098	2010-07-08 00:00:00.00	63.21	15812 ⁻⁴⁶⁸ ₊₄₆₂	2392 ⁻⁷¹⁷ ₊₄₆₂	11963 ⁻³²⁷⁵ ₊₃₇₈
PTF10gvb	25	0.098	2010-07-08 00:00:00.00	63.21	18548 ⁻²⁸² ₊₂₆₈	9240 ⁻²¹³ ₊₂₁₀	14053 ⁻⁸¹ ₊₄₁
PTF10gvb	27	0.098	2010-05-06 00:00:00.00	5.83		12727 ⁻¹⁸⁹ ₊₁₇₆	
PTF10gvb	133	0.098	2010-05-15 00:00:00.00	14.03	16221 ⁻³⁹³ ₊₇₁₁	2417 ⁻⁴²⁷ ₊₅₉₃	
PTF10gvb	29	0.098	2010-05-15 00:00:00.00	14.03	19184 ⁻⁷¹¹ ₊₁₈₈	8710 ⁻⁶⁵ ₊₁₁₁	11122 ⁻⁹⁶ ₊₁₁₁
2010ah	137	0.0498	2010-03-01 00:00:00.00	7.62	16109 ⁻³⁸⁹ ₊₄₂₁		
2010ah	65	0.0498	2010-03-07 00:00:00.00	13.34	6985 ⁻⁴⁸⁴ ₊₂₉₁	6604 ⁻³³² ₊₂₉₁	9135 ⁻⁹²⁷ ₊₅₇₃
2010ah	61	0.0498	2010-03-07 00:00:00.00	13.34	14391 ⁻⁵³⁸ ₊₁₂₆₃	3635 ⁻⁴⁸² ₊₄₆₁	13633 ⁻³²⁷ ₊₁₃₅₇
2010ah	181	0.0498	2010-03-01 00:00:00.00	7.62		10718 ⁻³⁴⁵ ₊₅₂₉	11390 ⁻¹¹⁶¹ ₊₃₁₇
PTF10qts	51	0.0907	2010-08-13 00:00:00.00	8.62	24773 ⁻⁹¹⁰ ₊₉₂₈		
PTF10qts	51	0.0907	2010-09-05 00:00:00.00	29.71	18789 ⁻²⁵⁴⁶ ₊₁₄₃₃	6618 ⁻¹¹³¹ ₊₁₁₇₄	11422 ⁻¹¹⁴⁸ ₊₅₈₂
PTF10qts	41	0.0907	2010-09-05 00:00:00.00	29.71	25794 ⁻⁶²⁸ ₊₅₈₇	8175 ⁻⁸⁸⁵ ₊₈₂₅	18786 ⁻⁴⁶¹ ₊₆₈₀
PTF10qts	35	0.0907	2010-09-02 00:00:00.00	26.96	16678 ⁻⁸³¹ ₊₁₃₆₃	6625 ⁻²³⁵ ₊₂₄₆	
PTF10qts	61	0.0907	2010-09-02 00:00:00.00	26.96	23068 ⁻³⁴⁹ ₊₂₇₉	8300 ⁻¹⁰⁸² ₊₁₀₃₃	15749 ⁻⁵⁸³ ₊₆₀₇
PTF10qts	101	0.0907	2010-08-15 00:00:00.00	10.45	25504 ⁻²¹⁴⁴ ₊₁₀₆₂		

Continued on next page

Table B.2. Measured velocities of Fe II, Si II and Ca II for the Ic-BL supernovae analysed here, continued.

Event name	SG filter width	z	Obs. date [UT]	ΔT_{rest} [days]	$v_{Fe II}$ [km/s]	$v_{Si II}$ [km/s]	$v_{Ca II}$ [km/s]
PTF10qts	267	0.0907	2010-08-15 00:00:00.00	10.45		10568 ⁻⁴⁵⁵	
PTF10qts	91	0.0907	2010-08-17 22:11:34.00	13.13	22826 ⁻⁶²²	14333 ⁺³⁶⁰	
PTF10qts	121	0.0907	2010-09-09 00:00:00.00	33.37	24707 ⁺³⁶⁷	10160 ⁺²³⁰⁸	
PTF10qts	66	0.0907	2010-09-09 00:00:00.00	33.37	23466 ⁺⁴⁸⁴¹	10160 ⁺²⁵⁶⁶	
PTF10xem	29	0.0567	2010-11-01 00:00:00.00	37.71	19362 ⁻⁶⁰⁸	8845 ⁻⁴²⁵	24930 ⁻⁴⁷¹
PTF10xem	33	0.0567	2010-10-10 09:36:00.00	17.27	19362 ⁺⁷⁶⁴	20102 ⁻¹⁴⁷¹	27413 ⁺⁴⁹⁶
PTF10xem	51	0.0567	2010-10-11 00:00:00.00	17.84	21249 ⁺⁵⁸³	16565 ⁺⁴³⁵	25439 ⁻⁸¹⁹
PTF10tqv	66	0.0795	2010-09-02 00:00:00.00	17.44	21009 ⁻²¹⁴	5565 ⁺¹⁸⁴	12893 ⁻⁸⁶⁴
PTF10tqv	101	0.0795	2010-11-01 00:00:00.00	73.02	19826 ⁻²⁴⁸²	5565 ⁺²²⁰	12893 ⁺¹²⁵⁸
PTF10tqv	33	0.0795	2010-10-03 00:00:00.00	46.16	19826 ⁺²²⁵⁶	4892 ⁻¹³⁷⁴	15830 ⁻⁵⁶⁶
PTF10aavz	33	0.062	2010-12-06 00:00:00.00	26.85	21596 ⁺⁴⁴²⁴	4892 ⁺¹⁰⁰¹	15830 ⁺⁶²⁰
PTF10aavz	51	0.062	2010-11-30 00:00:00.00	21.21	21596 ⁻³⁴⁸⁷	4892 ⁻¹²⁶⁹	15830 ⁻⁴³²
PTF10aavz	173	0.062	2010-12-13 00:00:00.00	33.45	8198 ⁺⁵⁵⁸	19712 ⁺⁹²¹	7232 ⁻⁸²²
2010ay	91	0.0671	2010-03-22 10:48:00.00	27.32	8198 ⁻⁸⁵²	19712 ⁻¹⁰⁰⁷	7232 ⁻⁶²¹
2010ay	121	0.0671	2010-04-01 00:00:00.00	36.27	21144 ⁺⁸⁰⁷	299 ⁺⁹³⁹	29971 ⁺⁵⁵¹
2010ay	135	0.0671	2010-04-11 09:36:00.00	46.01	8875 ⁻⁶⁹⁵	299 ⁺²⁵²	29971 ⁻¹⁷⁰⁷
PTF10ysd	101	0.0963	2010-10-30 00:00:00.00	31.47	26036 ⁻⁹¹²	19533 ⁻⁸⁶⁸	24692 ⁺¹¹³⁸
PTF11qcj	143	0.028	2011-11-26 15:22:35.00	47.80	23867 ⁺⁷⁵⁸	19577 ⁻⁴⁹⁶	24692 ⁻¹⁸⁹
PTF11qcj	83	0.028	2011-11-07 00:00:00.00	28.70	23867 ⁺³⁷²	21034 ⁻⁶¹⁶	23690 ⁺²⁷⁸
PTF11qcj	17	0.028	2011-11-05 06:37:10.00	27.02	28845 ⁺⁸¹⁹	14865 ⁻⁷⁴⁷	23690 ⁻¹⁴⁵
PTF11qcj	101	0.028	2011-12-31 00:00:00.00	81.23	5543 ⁻⁶⁷¹	10173 ⁺⁶⁰⁷	17514 ⁺¹⁵⁷
PTF12gzk	147	0.01377	2012-08-13 14:01:53.00	21.00	5543 ⁺⁸⁸⁶	11457 ⁻¹⁸⁹	21508 ⁻²²⁸
PTF12gzk	25	0.01377	2012-08-18 06:26:32.00	25.62	15128 ⁻¹⁵⁶	11457 ⁺²⁰¹	21508 ⁺¹⁷⁴
PTF12gzk	71	0.01377	2012-09-25 04:46:33.00	63.03	15128 ⁺¹⁴⁹	6523 ⁻²²³	13735 ⁻⁴²⁰
PTF12gzk	59	0.01377	2012-07-28 10:46:15.00	5.08	15128 ⁻⁷⁷⁷	14435 ⁺¹⁹⁶	13735 ⁺³⁹⁴
PTF12gzk	173	0.01377	2012-08-19 10:58:04.00	26.79	16884 ⁺⁶⁰⁷	11620 ⁻²⁶⁶	21495 ⁻¹²¹
PTF12gzk	147	0.01377	2012-09-23 12:50:51.00	61.39	16884 ⁻¹⁵⁰	8377 ⁻⁵⁰³	20512 ⁻¹³⁵
PTF12gzk	101	0.01377	2012-09-23 07:36:28.00	61.17	14510 ⁺⁹⁸³	8377 ⁺⁵⁶⁷	16946 ⁺³²⁴
PTF12gzk	87	0.01377	2012-07-27 00:00:00.00	3.65	32039 ⁻⁶⁰⁹	24881 ⁻²⁵⁰	28178 ⁺²⁵²
PTF12gzk	101	0.01377	2012-08-12 16:12:15.00	20.10	16884 ⁺²⁰¹	11193 ⁻⁹⁶	20324 ⁺¹⁴⁴
PTF12gzk	25	0.01377	2012-08-09 02:32:40.00	16.58	13571 ⁻⁵⁸⁰	7436 ⁻³⁶⁹	17055 ⁻³³⁴
PTF12gzk	121	0.01377	2012-09-18 05:55:40.00	56.17	14510 ⁺⁴⁸⁹	6876 ⁺³²²	16768 ⁺⁴⁷²
PTF12gzk	159	0.01377	2012-08-09 00:00:00.00	16.47	14510 ⁻²⁴⁰	6876 ⁻³⁴¹	16768 ⁻¹⁶⁵
PTF12gzk	43	0.01377	2012-08-08 00:00:00.00	15.49	31656 ⁺²²¹	15262 ⁻¹¹¹	21356 ⁻⁴⁰⁷
PTF12gzk	109	0.01377	2012-08-10 00:00:00.00	17.46	31656 ⁻²⁵⁷	15262 ⁺¹¹²	21356 ⁺³¹⁶
PTF12gzk	43	0.01377	2012-08-06 00:00:00.00	13.51	19421 ⁺²⁸⁹	17174 ⁻⁵⁵	
PTF12gzk	147	0.01377	2012-08-10 14:26:53.00	18.05	20301 ⁻⁴²⁰	7166 ⁻¹¹⁷	17327 ⁻¹⁵³
PTF12gzk	23	0.01377	2012-08-25 03:37:54.00	32.41	20301 ⁺⁴⁸¹	16750 ⁺⁷⁷	22746 ⁺¹⁵²
PTF12gzk	25	0.01377	2012-08-25 03:12:03.00	32.39	15061 ⁻¹⁰⁹	16750 ⁻³⁴	22746 ⁻⁷⁵
PTF12gzk	101	0.01377	2012-09-06 14:27:06.00	44.69	15061 ⁺¹¹⁵	17573 ⁻⁷¹	22746 ⁺⁸⁸
PTF12gzk	21	0.01377	2012-08-01 00:00:00.00	8.58	19203 ⁻¹¹⁴	17573 ⁺⁶⁵	
PTF12gzk	51	0.01377	2012-09-07 04:52:19.00	45.28	21124 ⁺¹¹²	16178 ⁻⁵⁴	
PTF12gzk	25	0.01377	2012-08-11 08:55:48.00	18.81	19700 ⁻¹⁵⁶	16178 ⁺⁵¹	
PTF12gzk	25	0.01377	2012-08-11 08:55:48.00	18.81	21527 ⁺¹⁸³	17710 ⁺¹⁵⁸	
PTF12gzk	147	0.01377	2012-08-11 14:43:41.00	19.05	21527 ⁻²²³	17710 ⁺¹⁷⁴	
PTF12gzk	81	0.01377	2012-08-02 10:05:28.00	9.98	19558 ⁺²²¹	16153 ⁻³⁷	22276 ⁻¹⁷⁵
					19558 ⁻¹⁵⁸	16153 ⁺¹⁷⁶	20597 ⁺¹⁰⁰
					16744 ⁻⁹⁸	8915 ⁺¹⁹³	
					16744 ⁺⁹⁶	8915 ⁻¹¹⁶	
					16113 ⁻⁵⁹⁷	7637 ⁻¹²⁷	19030 ⁻²²⁹
					16113 ⁺⁵⁷⁸	7637 ⁺¹³³	19030 ⁺³⁴⁵
					31283 ⁻¹⁴⁵⁷	20122 ⁻⁷¹³	26123 ⁻¹³³⁴
					31283 ⁺¹⁵³⁷	20122 ⁺⁶⁴⁷	26123 ⁺¹⁶⁰⁶
					16081 ⁻²⁰⁶	7948 ⁻⁷⁵	18343 ⁻¹⁹⁹
					16081 ⁺¹⁹⁰	7948 ⁺⁸⁸	18343 ⁺²⁴
					18541 ⁻³⁹⁶	16102 ⁻⁴⁶	22203 ⁻²⁴¹
					18541 ⁺²⁰⁶	16102 ⁺¹⁹	22203 ⁺²⁵¹
					18671 ⁻³⁷⁰	16150 ⁻⁶⁹	22147 ⁻²⁵¹
					18671 ⁺²¹⁷	16150 ⁺²²	22147 ⁺²⁵¹
					19057 ⁻¹⁴⁵	15571 ⁻⁵³	21833 ⁻¹⁴⁶
					19057 ⁺¹³⁶	15571 ⁺⁵³	21833 ⁺⁹¹
					24732 ⁻⁸²	21378 ⁻⁷³	25356 ⁻⁹¹
					24732 ⁺⁷⁸	21378 ⁺⁹²	25356 ⁺¹⁰⁰

Continued on next page

Table B.2. Measured velocities of Fe II, Si II and Ca II for the Ic-BL supernovae analysed here, continued.

Event name	SG filter width	z	Obs. date [UT]	ΔT_{rest} [days]	$v_{Fe II}$ [km/s]	$v_{Si II}$ [km/s]	$v_{Ca II}$ [km/s]
PTF12gzk	23	0.01377	2012-08-09 02:58:30.00	16.60		17294 ⁻⁹⁴	21850 ⁻¹⁶⁸
PTF12gzk	25	0.01377	2012-09-10 03:42:01.00	48.19	15488 ⁻⁷⁸	7472 ⁻¹⁸⁸	18009 ⁻²⁵⁷
PTF12gzk	25	0.01377	2012-09-10 04:07:35.00	48.21	15939 ⁺²⁸⁸	7581 ⁺³²⁸	19359 ⁺³⁵³
PTF12gzk	25	0.01377	2012-09-16 03:53:05.00	54.12	15245 ⁻¹¹⁰	7642 ⁻⁸⁶	17608 ⁻²¹⁶
PTF12gzk	89	0.01377	2012-08-12 08:31:12.00	19.78	17979 ⁺¹⁰⁷	15295 ⁻³⁷	21932 ⁻⁷⁴
PTF12gzk	147	0.01377	2012-09-07 13:30:20.00	45.63	15920 ⁺¹²⁶	7586 ⁻¹⁴⁵	18378 ⁻²⁷⁵
PTF12gzk	87	0.01377	2012-08-23 10:30:43.00	30.72	16306 ⁻³¹⁰	9611 ⁺⁴³	19488 ⁻¹³⁶
2012ap	33	0.01224	2012-03-04 01:55:12.00	25.06		8425 ⁻²⁶⁷	14670 ⁻⁴⁴⁴
2012ap	81	0.01224	2012-03-15 05:31:12.00	36.08	17949 ⁻³⁰³	8968 ⁻⁹⁵⁹	15824 ⁻²⁵⁴
2012ap	55	0.01224	2012-03-03 00:43:12.00	24.03			14914 ⁻⁴¹
2012ap	101	0.01224	2012-02-21 06:28:48.00	13.40	19281 ⁻¹⁷³	15393 ⁻¹⁶⁷	19174 ⁻¹⁶¹
2012ap	33	0.01224	2012-02-26 02:24:00.00	18.17	18449 ⁺²⁰⁴	12005 ⁺¹⁴⁵	17212 ⁺⁵²
2012ap	77	0.01224	2012-02-14 18:57:36.00	6.99	20275 ⁺²⁹⁰	19522 ⁺²⁵	
2012ap	83	0.01224	2012-02-23 04:19:12.00	15.28	20275 ⁻³⁰⁶	19522 ⁺³⁰¹	
2012ap	35	0.01224	2012-02-20 19:55:12.00	12.96	18769 ⁺³⁷⁸	14439 ⁻¹⁸³	18016 ⁻¹²³
2012ap	77	0.01224	2012-02-18 19:12:00.00	10.96	19115 ⁻²²²	16598 ⁺¹⁵⁸	18030 ⁻¹⁴⁸
2012ap	41	0.01224	2012-02-27 02:38:24.00	19.17	19655 ⁻¹⁵⁶	12361 ⁺¹¹⁹	17964 ⁻¹⁸²
2012ap	77	0.01224	2012-02-16 18:43:12.00	8.96	18852 ⁺¹⁶⁶	17582 ⁺³⁹³	18220 ⁺²⁵³
PTF12as	83	0.033	2012-01-30 00:00:00.00	34.36	20297 ⁻²¹³	16218 ⁺²⁷⁸	12328 ⁻⁸³¹
PTF12as	29	0.033	2012-01-02 12:57:36.00	7.77	20859 ⁺²²²	20897 ⁺⁵⁴	32078 ⁻¹¹⁵⁴
2012aa	81	0.0799	2012-02-23 12:04:19.00	54.64	20859 ⁻²⁷⁶⁷	11236 ⁻⁴⁵⁷	
2012aa	85	0.0799	2012-02-02 11:34:04.00	35.17	17014 ⁺¹³⁴⁰	9135 ⁺³⁹⁶	
2012aa	121	0.0799	2012-03-15 15:20:09.00	74.21	16426 ⁻⁶⁰³	12018 ⁻⁵²⁰	
2013bn	101	0.054	2013-04-13 00:00:00.00	8.58	15967 ⁺⁸²⁰	11223 ⁻¹³⁵¹	23411 ⁻⁶⁸⁴
2013bn	87	0.054	2013-04-19 10:26:24.00	14.68	18815 ⁻¹⁸⁵¹	15786 ⁺¹¹⁸⁰	
2013bn	43	0.054	2013-05-02 00:00:00.00	26.60	20550 ⁺¹⁸⁰⁹	10009 ⁺²⁹⁹	
2013bn	121	0.054	2013-05-02 05:02:24.00	26.80	21038 ⁻⁹³²	8862 ⁻⁴⁵⁷	16862 ⁻⁹⁴³
iPTF13ebw	147	0.069	2013-12-04 11:49:36.00	17.57	18276 ⁺¹⁵⁰⁹	10658 ⁻⁶⁶⁵	14683 ⁻¹²⁰¹
iPTF13ebw	151	0.069	2013-12-04 11:45:36.00	17.57	27568 ⁻⁸⁴⁰	13498 ⁻⁶¹⁹	
iPTF13ebw	101	0.069	2013-12-03 13:55:12.00	16.72	25197 ⁺⁷⁵³		
iPTF13ebw	101	0.069	2014-01-01 00:00:00.00	43.30	27654 ⁻⁷⁷⁷		9449 ⁻⁴⁹⁶³
iPTF13ebw	201	0.069	2013-11-29 00:00:00.00	12.43	21979 ⁺¹⁰¹⁰	16157 ⁻⁵¹¹	
OGLE-2013-SN-134	25	0.039	2013-12-25 07:47:02.00	16.37	31363 ⁺¹¹¹⁹	6805 ⁻⁶⁴³	14145 ⁻³⁶³
LSQ14bef	51	0.05	2014-04-24 08:58:00.00	4.17	10902 ⁻⁴⁸¹	18107 ⁻¹³⁹²	
2014ad	159	0.005	2014-03-27 00:00:00.00	18.41	25225 ⁻²²⁹²	22296 ⁺¹⁴³⁶	
2014ad	151	0.005	2014-03-14 00:00:00.00	5.47			
2014ad	147	0.005	2014-05-01 00:00:00.00	53.23	46884 ⁻²⁰¹	17648 ⁻⁷⁴	18429 ⁻¹¹⁵
2014ad	147	0.005	2014-05-12 00:00:00.00	64.18	20497 ⁻¹⁸¹	18224 ⁻¹²³	17981 ⁻⁸³
2014ad	159	0.005	2014-03-20 00:00:00.00	11.44	20588 ⁺¹⁷⁹	26638 ⁺¹⁴¹	
2014ad	151	0.005	2014-03-15 00:00:00.00	6.47	35116 ⁺²¹⁹		
2014ad	25	0.005	2014-04-30 04:45:56.00	52.44	47569 ⁻³⁷⁸	15767 ⁻⁶⁸³	
2014ad	201	0.005	2014-04-20 00:00:00.00	42.29	24401 ⁺³⁷²	18545 ⁻²⁷¹	
2014ad	157	0.005	2014-03-21 00:00:00.00	12.44	22855 ⁻⁸⁸⁹	25953 ⁻²¹¹	
2014ad	81	0.005	2014-03-19 00:00:00.00	10.45	34128 ⁻²⁷⁰	26892 ⁻⁴⁶¹	
2014ad	159	0.005	2014-03-18 00:00:00.00	9.45	36774 ⁺²⁷⁰	28160 ⁻¹⁴¹	
2014ad	25	0.005	2014-04-21 03:44:33.00	43.44	37796 ⁺⁴⁴²	15639 ⁻²⁰¹	

Continued on next page

Table B.2. Measured velocities of Fe II, Si II and Ca II for the Ic-BL supernovae analysed here, continued.

Event name	SG filter width	z	Obs. date [UT]	ΔT_{rest} [days]	$v_{Fe II}$ [km/s]	$v_{Si II}$ [km/s]	$v_{Ca II}$ [km/s]
2014ad	147	0.005	2014-04-16 00:00:00.00	38.31	20846 ⁻³⁹⁶ ₊₂₉₃	18389 ⁻⁴⁰⁹ ₊₃₁₆	22167 ⁻¹³⁸ ₊₁₅₀
2014ad	23	0.005	2014-04-21 04:00:23.00	43.45		15386 ⁻¹⁷⁰ ₊₁₇₀	
2014ad	159	0.005	2014-03-19 00:00:00.00	10.45	37296 ⁻¹³⁰ ₊₁₂₆	26067 ⁻¹⁹⁴ ₊₁₉₁	
2014ad	121	0.005	2014-03-22 00:00:00.00	13.43	32763 ⁻²³⁹ ₊₁₇₆	25543 ⁻²³⁵ ₊₂₁₇	
2014ad	159	0.005	2014-04-18 00:00:00.00	40.30	25994 ⁻¹⁶⁸ ₊₂₁₃	18293 ⁻¹⁰⁹ ₊₁₀₀	
2014ad	151	0.005	2014-03-17 00:00:00.00	8.46	46582 ⁻⁸⁰⁴ ₋₈₄₂		
2014ad	153	0.005	2014-03-16 00:00:00.00	7.46	46696 ⁻³⁴⁸ ₋₃₁₅		
2014ad	109	0.005	2014-03-25 00:00:00.00	16.42	32285 ⁻⁶⁸³ ₊₅₀₈	23633 ⁻²¹² ₊₁₈₄	
2014ad	159	0.005	2014-03-30 00:00:00.00	21.39		21181 ⁻²⁸⁸ ₊₂₉₃	
2014ad	139	0.005	2014-05-17 00:00:00.00	69.15	20385 ⁻²⁹⁰ ₊₃₁₉	16881 ⁻²²⁶ ₊₂₀₄	17548 ⁻¹⁰⁴ ₊₁₀₈
2014ad	159	0.005	2014-03-28 00:00:00.00	19.40		21924 ⁻²⁰⁹ ₊₂₁₆	
2014ad	147	0.005	2014-05-23 00:00:00.00	75.12	20212 ⁻²⁹² ₊₂₈₂	17308 ⁻⁸² ₋₈₂	17563 ⁻⁷⁷ ₊₈₀
iPTF14dby	129	0.074	2014-06-29 09:36:00.00	9.14	24168 ⁻¹⁷⁷⁹ ₊₃₂₅₉	13487 ⁻⁹²³ ₊₂₃₉₇	
iPTF14dby	101	0.074	2014-08-30 06:14:24.00	66.74	23402 ⁻¹⁸⁸¹ ₊₂₃₀₀	11924 ⁻⁸²⁷ ₊₆₆₃	9281 ⁻⁵⁷⁸ ₊₅₇₄
iPTF14gaq	181	0.0826	2014-10-25 05:02:24.00	32.79	19612 ⁻⁵⁴¹ ₊₄₈₀	14042 ⁻⁴⁶⁸ ₊₁₁₁₁	19735 ⁻⁴⁴³ ₊₇₅₁
iPTF14gaq	135	0.0826	2014-10-01 00:00:00.00	10.43	28176 ⁻¹⁴⁰³ ₊₁₁₀₉	14465 ⁻⁹⁹³ ₊₇₇₅	
2014cp	71	0.016164	2014-07-08 18:42:58.00	15.53	19281 ⁻³⁴⁶² ₊₃₃₄		
2014cp	83	0.016164	2014-07-08 18:42:58.00	15.53		7654 ⁻²⁹¹ ₊₂₉₇	20573 ⁻⁴¹³ ₊₂₇₄
2014cp	71	0.016164	2014-08-05 15:32:56.00	42.95	19236 ⁻²⁹⁰ ₊₃₀₇		
2014cp	83	0.016164	2014-08-05 15:32:56.00	42.95		7903 ⁻⁴⁴⁴ ₊₅₂₄	16049 ⁻⁴⁷⁸ ₊₉₄₅
iPTF15eov	201	0.0535	2016-01-05 10:33:36.00	32.48	19343 ⁻⁹³⁰ ₊₉₄₄	13586 ⁻³¹⁰⁸ ₊₁₂₂₃	17722 ⁻⁶⁸² ₊₅₃₈
iPTF15eov	201	0.0535	2016-03-05 06:43:12.00	89.28	24734 ⁻²⁵⁷⁶ ₊₂₀₂₇	7965 ⁻¹⁷¹⁷ ₊₉₂₆	13598 ⁻²²⁶⁶ ₊₆₉₄
iPTF15eov	201	0.0535	2016-02-14 07:55:12.00	70.35	25301 ⁻²⁷⁴¹ ₊₂₇₂₈	8138 ⁻¹³⁶³ ₊₈₁₇	17616 ⁻⁷¹⁷ ₊₆₉₅
iPTF15eov	205	0.0535	2016-01-08 00:00:00.00	34.91	19278 ⁻²³⁶ ₊₂₇₇	12205 ⁻⁴¹⁵ ₊₃₈₅	18456 ⁻²⁰³ ₊₁₆₆
iPTF15eov	31	0.0535	2016-02-18 05:31:12.00	74.05		5634 ⁻⁹⁹⁰ ₊₁₄₄₀	14957 ⁻⁴⁰⁷ ₊₅₅₉
iPTF15eov	81	0.0535	2016-01-29 09:36:00.00	55.23	21497 ⁻¹⁰⁸⁶ ₊₁₁₆₃	9825 ⁻¹⁴²⁸ ₊₁₄₂₈	18092 ⁻⁶³³ ₊₄₅₄
iPTF15eov	151	0.0535	2015-12-08 12:14:24.00	5.97			
iPTF15eov	97	0.0535	2015-12-09 10:04:48.00	6.83			
iPTF15eov	97	0.0535	2016-02-06 06:14:24.00	62.69	21064 ⁻³⁹⁶ ₊₄₃₅	7014 ⁻³¹⁹ ₊₂₈₀	18300 ⁻³⁶⁶ ₊₃₇₃
iPTF15dqg	50	0.065	2015-11-18 02:10:18.00	14.89	18721 ⁻⁹⁴⁶ ₊₇₁₅	14846 ⁻⁴¹⁹ ₊₃₇₆	18720 ⁻⁷³⁶ ₊₇₉₉
iPTF15dqg	81	0.065	2015-12-06 00:00:00.00	31.71	12663 ⁻¹³⁹ ₊₁₂₈	8762 ⁻³⁹⁹ ₊₄₅₂	15911 ⁻²⁹² ₊₂₄₈
iPTF15dqg	65	0.065	2015-12-12 19:26:24.00	38.10	11449 ⁻³⁵⁷ ₊₃₆₂	7497 ⁻¹⁸⁸ ₊₁₉₅	16134 ⁻²⁹⁴ ₊₃₀₇
iPTF15dld	25	0.047	2015-11-08 02:57:34.00	34.50	6964 ⁻¹¹⁷⁴ ₊₉₄₀	7443 ⁻⁷¹⁶ ₊₅₇₈	
iPTF15dld	25	0.047	2015-11-08 03:43:08.00	34.53	4421 ⁻³⁵⁸ ₊₅₁₇		
2016P	23	0.0146	2016-02-05 08:36:14.00	20.07		3572 ⁻²⁹⁴ ₊₂₂₅	10865 ⁻³⁵³ ₊₂₆₉
2016P	23	0.0146	2016-02-16 08:36:05.00	30.91			11105 ⁻⁹¹¹ ₊₇₈₉
2016P	25	0.0146	2016-02-25 07:16:48.00	39.72	22031 ⁻⁵³² ₊₄₇₉		
2016P	23	0.0146	2016-02-25 07:47:38.00	39.74			10347 ⁻¹⁵⁶⁶ ₊₄₃₁
2016P	23	0.0146	2016-02-25 08:18:12.00	39.77			12050 ⁻³⁴⁰ ₊₃₈₂
2016P	22	0.0146	2016-01-23 05:34:03.00	7.13	18894 ⁻¹¹⁹² ₊₉₄₃		
2016P	23	0.0146	2016-01-28 07:39:42.00	12.14		8343 ⁻¹³⁴ ₊₁₇₄	18963 ⁻¹¹⁷ ₊₁₀₈
2016P	30	0.0146	2016-01-28 07:13:51.00	12.12	17447 ⁻⁶¹⁶ ₊₅₉₀	7817 ⁻²³⁵ ₊₂₂₀	
2016P	22	0.0146	2016-02-12 03:13:22.00	26.74	21016 ⁻¹⁴³² ₊₂₈₈₃		
2016P	49	0.0146	2016-01-19 22:36:30.00	3.89	19977 ⁻¹¹⁸³ ₊₁₁₈₁		
2016P	11	0.0146	2016-01-26 06:58:45.00	10.14	18010 ⁻⁸¹¹ ₊₅₄₅	8294 ⁻³²⁴ ₊₃₁₅	
2016P	23	0.0146	2016-02-16 08:05:31.00	30.89			11128 ⁻²⁹⁷ ₊₂₅₃

Continued on next page

Table B.2. Measured velocities of Fe II, Si II and Ca II for the Ic-BL supernovae analysed here, continued.

Event name	SG filter width	z	Obs. date [UT]	ΔT_{rest} [days]	$v_{Fe II}$ [km/s]	$v_{Si II}$ [km/s]	$v_{Ca II}$ [km/s]
2016P	25	0.0146	2016-02-05 08:10:24.00	20.05	19349 ⁻²²⁷ ₊₂₀₅	3830 ⁻²⁰² ₊₂₈₈	
2016P	51	0.0146	2016-02-25 06:46:14.00	39.70	20086 ⁻¹⁷⁴⁹ ₊₉₀		
2016P	15	0.0146	2016-02-05 03:20:45.00	19.85	20708 ⁻¹¹⁵⁰ ₊₂₄₀₂	3249 ⁻⁸⁷⁹ ₊₆₅₄	
2016P	25	0.0146	2016-02-16 07:34:41.00	30.87	21116 ⁻³²⁰ ₊₃₃₉		
2016P	22	0.0146	2016-01-21 03:27:41.00	5.07	18113 ⁻³⁵¹⁹ ₊₁₁₂₄		
2016P	25	0.0146	2016-02-16 07:04:07.00	30.84	18670 ⁻⁶²⁹ ₊₄₀₇		
2016coi	11	0.0036	2016-05-29 03:09:04.00	5.21		21399 ⁻²⁴⁷ ₊₂₄₅	
2016coi	21	0.0036	2016-08-09 00:20:07.00	76.84	15965 ⁻⁹⁷ ₊₁₁₀		15696 ⁻⁸⁵ ₊₁₁₀
2016coi	11	0.0036	2016-06-19 01:50:58.00	26.08	18055 ⁻⁵⁷³ ₊₃₆₆	9753 ⁻¹⁰⁹ ₊₉₇	
2016coi	67	0.0036	2016-06-03 11:07:34.00	10.53	25955 ⁻³⁵⁵ ₊₅₃₆	18786 ⁻¹⁵⁶ ₊₁₅₂	
2016coi	11	0.0036	2016-06-19 03:31:40.00	26.15	18582 ⁻³²⁵ ₊₄₁₂	9745 ⁻⁶⁶ ₊₂₁	
2016coi	15	0.0036	2016-06-01 02:50:59.00	8.19	26241 ⁻⁵³⁸ ₊₅₃₁	19662 ⁻⁴⁰⁹ ₊₄₀₂	
2016coi	67	0.0036	2016-06-04 10:17:28.00	11.49	25632 ⁻⁵²¹ ₊₁₄₂₃	18130 ⁻¹⁶⁶ ₊₁₅₈	
2016coi	11	0.0036	2016-07-06 03:28:05.00	43.09	16712 ⁻⁴⁵⁵ ₊₆₁₇	5978 ⁻¹⁰⁴ ₊₁₅₆	
2016coi	11	0.0036	2016-05-28 05:03:59.00	4.30		21771 ⁻⁵⁸⁵ ₊₈₃₇	
2016coi	49	0.0036	2016-05-31 21:09:22.00	7.95	25788 ⁻⁵⁸³ ₊₅₆₇	20383 ⁻²²⁵ ₊₂₁₁	
2016coi	31	0.0036	2016-06-15 16:10:59.00	22.69		13647 ⁻²³⁵ ₊₂₂₅	
2016coi	45	0.0036	2016-05-29 03:08:52.00	5.21	28596 ⁻²⁵⁸ ₊₂₄₄	20978 ⁻¹⁷³ ₊₁₆₉	
2016coi	11	0.0036	2016-06-15 02:14:21.00	22.11	18533 ⁻²⁹⁹ ₊₃₆₇	13254 ⁻¹³⁶ ₊₁₉₄	
2016coi	351	0.0036	2016-06-14 10:33:49.00	21.46	18175 ⁻⁴⁰ ₊₄₂	13376 ⁻⁵² ₊₅₂	19106 ⁻¹¹⁵ ₊₅₈
2016coi	11	0.0036	2016-06-01 02:24:52.00	8.17	26830 ⁻⁴⁹⁶ ₊₁₀₃₂	19998 ⁻⁸⁸ ₊₁₁₂	
2016coi	53	0.0036	2016-07-07 01:41:09.00	44.01	16235 ⁻³⁷⁴ ₊₁₁₉	6949 ⁻²⁴¹ ₊₂₄₄	
2016coi	22	0.0036	2016-08-02 16:27:17.00	70.53	16044 ⁻¹¹⁹ ₊₁₂₇	7169 ⁻¹⁰⁷ ₊₁₁₂	
2016coi	11	0.0036	2016-05-28 04:42:53.00	4.28		21719 ⁻³⁵⁷ ₊₄₀₈	
2016coi	67	0.0036	2016-06-02 09:39:02.00	9.47	27217 ⁻²²⁵ ₊₂₂₈	19174 ⁻¹²⁴ ₊₁₄₄	
2016coi	11	0.0036	2016-07-17 03:29:48.00	54.05	15882 ⁻²⁵³ ₊₄₀₃	5645 ⁻¹⁷⁸ ₊₄₁	
2016coi	11	0.0036	2016-06-18 02:48:23.00	25.13	17635 ⁻²⁹⁹ ₊₃₀₄	10703 ⁻¹⁵⁷ ₊₁₁₂	
2016coi	87	0.0036	2016-07-15 17:27:43.00	52.64		6741 ⁻²⁹² ₊₂₉₃	16199 ⁻³⁷⁶ ₊₁₁₀₅
2016coi	97	0.0036	2016-06-18 12:57:21.00	25.55	17599 ⁻²⁴⁴ ₊₂₄₆	10460 ⁻⁷⁵ ₊₇₁	17130 ⁻¹⁹⁵ ₊₁₆₇
2016coi	101	0.0036	2016-06-02 10:20:23.00	9.50	26225 ⁻³⁸³ ₊₄₀₀	19113 ⁻¹⁵² ₊₁₅₄	
2016coi	51	0.0036	2016-07-14 14:09:53.00	51.50	16309 ⁻¹³⁶ ₊₁₅₁	6688 ⁻⁷⁷ ₊₈₉	15662 ⁻¹⁶² ₊₁₆₃
2016coi	11	0.0036	2016-07-12 01:53:47.00	49.00	16190 ⁻³⁰² ₊₂₉₆	6306 ⁻¹¹¹ ₊₁₂₁	
2016coi	11	0.0036	2016-07-12 00:21:50.00	48.94	15490 ⁻⁵⁵² ₊₇₉₂	6025 ⁻²⁶¹ ₊₂₆₁	
2016coi	11	0.0036	2016-07-18 00:35:41.00	54.93	15887 ⁻²⁷⁶ ₊₃₁₆	6293 ⁻¹¹¹ ₊₁₁₁	
2016coi	11	0.0036	2016-06-24 03:33:04.00	31.14	16043 ⁻⁸³⁵ ₊₁₇₆	8181 ⁻⁷⁷ ₊₇₇	
2016coi	81	0.0036	2016-06-02 14:14:13.00	9.66	27375 ⁻²⁵⁴ ₊₂₄₅	19087 ⁻¹¹⁹ ₊₁₂₂	22837 ⁻⁸²² ₊₃₀₆
2016coi	22	0.0036	2016-08-01 03:23:51.00	68.99	16171 ⁻³⁷ ₊₆₁	6966 ⁻⁷⁸ ₊₇₅	16407 ⁻¹³¹ ₊₂₉₂₈
2016coi	67	0.0036	2016-07-10 10:12:04.00	47.35	16148 ⁻²⁰⁸ ₊₂₁₆	6561 ⁻⁹⁰ ₊₉₆	
2016coi	31	0.0036	2016-07-10 06:52:28.00	47.22	16228 ⁻⁷³ ₊₇₃	6816 ⁻⁴⁰ ₊₄₀	15028 ⁻⁸⁴ ₊₅₇
2016coi	15	0.0036	2016-07-19 03:22:40.00	56.04	16179 ⁻⁸²⁸ ₊₆₈₅	5252 ⁻³⁰⁶ ₊₂₉₂	
2016coi	49	0.0036	2016-06-02 20:53:21.00	9.93	24489 ⁻⁵⁹³ ₊₇₁₀	18972 ⁻¹⁹¹ ₊₁₉₄	22981 ⁻³⁶⁶ ₊₃₄₂
2016coi	23	0.0036	2016-06-24 17:52:46.00	31.73	16826 ⁻⁴⁵² ₊₃₃₉	8330 ⁻⁵² ₊₇₆	17298 ⁻¹³³ ₊₁₀₁
2016coi	11	0.0036	2016-06-03 04:11:52.00	10.24	23009 ⁻¹³⁵⁷ ₊₄₃₄	19048 ⁻¹³⁹ ₊₂₁₅	
2016coi	7	0.0036	2016-05-29 03:45:00.00	5.24	27521 ⁻⁵⁶⁴ ₊₆₀₉	20688 ⁻¹⁵³ ₊₁₇₄	
2016coi	51	0.0036	2016-07-05 14:22:37.00	42.55	16777 ⁻²²⁵ ₊₂₃₆	6935 ⁻⁶² ₊₅₅	15760 ⁻⁹⁶ ₊₉₇
2016coi	11	0.0036	2016-07-02 04:05:45.00	39.13	16535 ⁻¹⁹² ₊₂₄₅	6600 ⁻⁸⁸ ₊₁₀₄	

Continued on next page

Table B.2. Measured velocities of Fe II, Si II and Ca II for the Ic-BL supernovae analysed here, continued.

Event name	SG filter width	z	Obs. date [UT]	ΔT_{rest} [days]	$v_{Fe\ II}$ [km/s]	$v_{Si\ II}$ [km/s]	$v_{Ca\ II}$ [km/s]
2016coi	11	0.0036	2016-06-22 01:09:31.00	29.04	17540 ⁻³⁸⁸	8642 ⁻¹⁴⁶	
2016coi	11	0.0036	2016-06-10 03:42:17.00	17.19	19228 ⁺³⁷⁹	15598 ⁺²²⁵	
2016coi	11	0.0036	2016-06-22 01:16:35.00	29.05	19240 ⁻⁵¹⁹	8802 ⁻⁹¹	
2016coi	61	0.0036	2016-07-01 14:21:12.00	38.56	16458 ⁺³⁹⁶	7176 ⁺⁸⁷	15782 ⁻⁷⁰
2016coi	47	0.0036	2016-06-13 03:56:21.00	20.19	18520 ⁻⁹²⁵	14337 ⁺⁶⁵	20205 ⁺⁹⁴
2016coi	22	0.0036	2016-08-02 15:40:10.00	70.50	16525 ⁺²⁶⁶	7365 ⁺¹⁰⁴	15976 ⁺⁹¹
2016coi	31	0.0036	2016-08-03 12:57:34.00	71.38	15569 ⁺⁶³	7129 ⁺⁷⁸	14727 ⁻⁶⁶
2016coi	67	0.0036	2016-06-08 10:27:52.00	15.48	20476 ⁻¹⁷⁴	16157 ⁺⁸⁴	
2016coi	51	0.0036	2016-06-27 12:24:52.00	34.49	16308 ⁺²⁶⁰	7787 ⁻²⁴¹	15705 ⁻²²⁸
2016coi	97	0.0036	2016-07-22 13:57:39.00	59.47	16308 ⁺⁶⁸⁰	6594 ⁺¹²⁸	14408 ⁺¹³⁸
2016coi	101	0.0036	2016-05-31 10:00:43.00	7.49	27342 ⁻³⁸²	19882 ⁺¹⁶⁷	
2016coi	11	0.0036	2016-06-09 03:35:32.00	16.19	19789 ⁺⁸⁰²	16100 ⁺¹³³	
2016coi	67	0.0036	2016-06-09 11:05:25.00	16.50	19734 ⁻⁴⁶¹	16055 ⁺¹⁵⁴	
2016coi	11	0.0036	2016-07-24 03:00:26.00	61.01	15085 ⁺³⁸²	5155 ⁺¹²⁴	
2016coi	11	0.0036	2016-06-12 03:25:06.00	19.17	18883 ⁻⁴⁷¹	15134 ⁺²¹¹	
2016coi	47	0.0036	2016-06-07 04:54:31.00	14.25	20966 ⁺⁴⁹²	16911 ⁺¹⁴²	22001 ⁻¹¹⁰
2016coi	51	0.0036	2016-06-07 13:38:20.00	14.62	20293 ⁻¹⁰³	16516 ⁺⁶¹	22202 ⁺⁸⁶
2016coi	33	0.0036	2016-06-23 01:04:00.00	30.04	17276 ⁺¹⁰⁷	8600 ⁻¹⁰⁰	15565 ⁻³¹¹
2016coi	11	0.0036	2016-06-26 00:39:19.00	33.01	17813 ⁺⁴⁴⁹	7670 ⁺⁵⁵	
2016coi	67	0.0036	2016-07-05 10:43:34.00	42.39	16304 ⁻¹⁵⁰	6718 ⁺⁴⁹	
2016coi	11	0.0036	2016-06-14 02:18:25.00	21.12	17985 ⁺¹⁸⁵	13629 ⁺⁵²	
2016coi	6	0.0036	2016-06-14 01:52:45.00	21.10	18513 ⁻¹⁶⁷	14627 ⁺¹⁵⁹	
2016coi	11	0.0036	2016-07-05 04:50:06.00	42.15	16749 ⁺¹⁰²	6106 ⁺²⁹²	
2016coi	67	0.0036	2016-06-05 10:59:33.00	12.51	23905 ⁻⁴⁴⁰	17941 ⁺¹⁸²	
2016coi	11	0.0036	2016-06-10 04:48:36.00	17.24	20309 ⁻⁴¹⁵	15984 ⁺¹⁵⁶	
2016coi	11	0.0036	2016-06-23 02:57:05.00	30.11	17655 ⁻¹⁶⁷³	8414 ⁺¹⁵⁰	
2016coi	45	0.0036	2016-05-28 03:37:05.00	4.24	17655 ⁺⁹⁹³	21485 ⁻⁷⁸	
2016coi	33	0.0036	2016-06-18 00:20:38.00	25.02	17396 ⁻⁴²¹	11065 ⁺⁸⁶	16048 ⁻⁹⁴
2016coi	81	0.0036	2016-06-13 16:16:05.00	20.70	18498 ⁻⁵³³	12321 ⁺³⁹⁸	16739 ⁺⁷²
2016coi	67	0.0036	2016-06-06 10:43:07.00	13.50	22027 ⁺⁴⁹⁴	17420 ⁺³⁶⁴	
2016coi	11	0.0036	2016-07-26 23:33:16.00	63.85	15690 ⁻⁶¹²	6335 ⁺¹²³	
2016coi	11	0.0036	2016-06-12 04:21:05.00	19.21	19528 ⁺⁵²⁸	14592 ⁺²⁴¹	
2016coi	25	0.0036	2016-07-21 02:35:04.00	58.00	16303 ⁻²¹⁵	6421 ⁺¹⁰⁶	15626 ⁻⁷¹
2016coi	21	0.0036	2016-07-04 00:47:14.00	40.99	16487 ⁺⁹²	7172 ⁺⁸⁴	15731 ⁺⁶⁶
2016ilj	25	0.039711	2016-11-28 23:16:48.00	19.45	28050 ⁻⁹¹	17884 ⁻⁶³	25188 ⁺¹²¹
2016ilj	5	0.039711	2016-11-25 00:00:00.00	15.63	31437 ⁺⁸¹	18174 ⁺³⁸²	28834 ⁺⁶⁸³
2016ilj	5	0.039711	2016-11-30 00:00:00.00	20.44	15704 ⁻⁵⁰²	15704 ⁺⁷⁸³	21276 ⁺⁷³¹
2016gox	131	0.042	2016-10-06 00:00:00.00	24.87	12394 ⁺⁹²⁴	12394 ⁺³⁶⁵	24750 ⁺²⁶⁰
2016gox	133	0.042	2016-10-01 00:00:00.00	20.07	26950 ⁻¹³⁰²	14591 ⁺⁶³¹	29281 ⁺¹⁰²¹
2016gox	90	0.042	2016-10-15 02:38:24.00	33.61	29411 ⁺¹⁹⁴⁴	10289 ⁺⁹⁰⁹	24934 ⁺⁸¹⁵
2017dgk	25	0.065	2017-04-29 00:36:04.00	6.65	18318 ⁻⁶⁹³⁶	16505 ⁻¹¹²²	18669 ⁻⁵⁹⁹
2017dgk	25	0.065	2017-04-24 02:29:45.00	2.03	21474 ⁺³⁷⁷⁸	17863 ⁺²⁴¹⁷	16178 ⁺⁶⁷⁹
2017cw	127	0.093	2017-02-27 10:33:36.00	54.47	18512 ⁻¹⁹⁵	13051 ⁻¹⁷⁶	20647 ⁻¹¹⁹⁸
2017cw	133	0.093	2017-01-07 00:00:00.00	7.41	27395 ⁺²⁵⁶	17480 ⁺¹⁴⁴	
2017cw	101	0.093	2017-02-01 08:38:24.00	30.61	20218 ⁺⁴³³	12694 ⁺²⁷⁹	
2017dcc	25	0.0245	2017-04-22 06:41:45.00	9.55	15795 ⁺⁷¹⁷	10081 ⁺²⁵⁷	20973 ⁻³⁷⁸

Continued on next page

Table B.2. Measured velocities of Fe II, Si II and Ca II for the Ic-BL supernovae analysed here, continued.

Event name	SG filter width	z	Obs. date [UT]	ΔT_{rest} [days]	$v_{Fe II}$ [km/s]	$v_{Si II}$ [km/s]	$v_{Ca II}$ [km/s]
2017dcc	41	0.0245	2017-04-29 02:35:08.00	16.22		7402 ⁻²⁴¹ ₊₂₀₉	14503 ⁻⁹⁷⁷ ₊₈₁₇
2017dcc	20	0.0245	2017-04-23 07:02:15.00	10.54	15091 ⁻²⁷¹ ₊₂₇₀	10469 ⁻²⁵⁸ ₊₁₈₈	
2017dcc	41	0.0245	2017-04-23 07:28:02.00	10.56		10379 ⁻²⁰⁵ ₊₁₇₉₀	20018 ⁻⁸⁸² ₊₁₅₅₁
2017dcc	20	0.0245	2017-05-01 05:11:29.00	18.28	13881 ⁻⁸⁴⁵ ₊₅₄₆	6549 ⁻¹⁰⁸¹ ₊₄₈₁	
2017dcc	25	0.0245	2017-04-29 02:09:16.00	16.20	13966 ⁻⁴⁸¹ ₊₄₈₂	8132 ⁻³⁵⁸ ₊₆₅₆	
2017dcc	23	0.0245	2017-05-01 05:37:20.00	18.30		8388 ⁻³⁹⁹ ₊₅₉₈	15286 ⁻³⁴⁸ ₊₃₈₀
2017dio	47	0.037	2017-05-02 00:00:00.00	17.12	5267 ⁻⁴²⁵ ₊₄₃₉		12096 ⁻¹⁰⁹⁵ ₊₄₀₂
2017dio	41	0.037	2017-05-01 00:00:00.00	16.15	4915 ⁻¹⁶²⁴ ₊₈₅₉	5427 ⁻¹⁰⁴³ ₊₁₁₂₁	
2017dio	25	0.037	2017-04-30 00:00:00.00	15.19	5219 ⁻³⁸² ₊₁₃₇₀		
2017dio	22	0.037	2017-05-13 00:00:00.00	27.72	1007 ⁻¹¹⁸¹ ₊₂₄₅₂		
2017ifh	21	0.039	2017-12-01 02:22:24.00	30.88	10682 ⁻³⁷⁴³ ₊₁₆₄₃	6235 ⁻¹⁰⁸⁴ ₊₉₁₄	
2017ifh	22	0.039	2017-11-19 00:08:37.00	19.24	21455 ⁻¹⁶⁴³ ₊₁₀₇₉		
2017ifh	22	0.039	2017-12-15 00:10:38.00	44.27	6834 ⁻¹⁷⁰³ ₊₁₅₂₉		
2017ifh	177	0.039	2017-11-17 15:32:00.00	17.94	23085 ⁻⁷⁰¹ ₊₇₂₂	14194 ⁻¹⁰⁰² ₊₁₆₈₅	
2017fwm	51	0.016	2017-08-16 23:44:52.00	20.88		2804 ⁻¹⁵⁵² ₊₁₄₃₁	17057 ⁻⁸³⁵ ₊₉₀₁
2017fwm	25	0.016	2017-08-22 02:34:44.00	25.92		3878 ⁻⁷⁹⁹ ₊₁₁₁₃	17126 ⁻⁷⁰² ₊₅₈₁
2017fwm	25	0.016	2017-08-28 02:35:53.00	31.82		2072 ⁻⁹⁴⁵ ₊₇₅₀	16237 ⁻²³¹³ ₊₁₁₄₂
2017fwm	50	0.016	2017-09-14 01:33:07.00	48.51		2923 ⁻¹⁴⁷⁹ ₊₃₂₁₅	14257 ⁻²³⁷⁶ ₊₁₂₆₂
2017ens	50	0.1086	2018-01-14 07:29:01.00	202.52	20219 ⁻²⁵⁶⁵ ₊₁₆₃₈		
2018giu	23	0.026	2018-10-18 01:15:04.00	33.29		4418 ⁻³⁰⁰ ₊₃₄₃	13359 ⁻³⁸⁶ ₊₅₂₃
2018giu	41	0.026	2018-09-17 03:41:09.00	3.18	17777 ⁻¹⁰⁴² ₊₁₆₄₂	8790 ⁻⁵⁰² ₊₆₃₈	
2018giu	23	0.026	2018-11-01 00:54:34.00	46.93			12209 ⁻⁶⁹⁷ ₊₆₃₂
2018giu	23	0.026	2018-10-03 02:28:17.00	18.72		10225 ⁻¹⁹⁶ ₊₂₂₃	15667 ⁻³³² ₊₁₅₈₀
2018giu	25	0.026	2018-10-03 02:02:28.00	18.71	11899 ⁻¹⁶⁵ ₊₁₄₄	9830 ⁻²⁰⁷ ₊₁₉₉	
2018giu	25	0.026	2018-10-18 00:44:14.00	33.27	10310 ⁻³⁷⁵ ₊₃₈₅	4282 ⁻²⁷⁵ ₊₃₀₆	
2018giu	25	0.05	2018-09-18 07:55:56.00	4.58	21414 ⁻³⁶⁶ ₊₄₉₁	22883 ⁻⁴⁰³ ₊₄₁₈	
2018kqr	109	0.045	2018-12-14 08:15:46.00	7.50	17761 ⁻⁴⁵⁸ ₊₄₈₅	15162 ⁻⁶⁵⁶ ₊₄₉₀	17656 ⁻¹⁶¹⁹ ₊₁₀₆₉
2018kqr	109	0.045	2018-12-27 00:00:00.00	19.61	17521 ⁻⁸⁸⁴ ₊₁₅₃₁	8306 ⁻⁶³⁹ ₊₇₅₃	19431 ⁻¹³¹⁰ ₊₁₇₇₄
2018gsk	23	0.0116	2018-10-18 06:41:37.00	32.27		14292 ⁻¹⁰⁷ ₊₈₉	10813 ⁻⁶⁵² ₊₂₉₃
2018gsk	23	0.0116	2018-10-10 07:17:45.00	24.39			11141 ⁻³⁸² ₊₃₆₈
2018gsk	25	0.0116	2018-10-10 06:51:54.00	24.37	5419 ⁻²³⁸ ₊₂₄₀	9529 ⁻⁷⁰⁶ ₊₆₈₇	
2018gsk	23	0.0116	2018-11-01 07:48:52.00	46.15		13637 ⁻⁹¹ ₊₂₂₃	9399 ⁻⁸⁶³ ₊₅₂₀
2018gsk	23	0.0116	2018-10-18 07:24:53.00	32.30		14102 ⁻⁷² ₊₄₀	10146 ⁻⁴³⁰ ₊₄₉₇
2018gsk	25	0.0116	2018-10-31 07:45:04.00	45.16	5054 ⁻²⁹⁷ ₊₂₇₁	13212 ⁻¹⁸⁷ ₊₂₁₀	
2018gsk	11	0.0116	2018-09-23 05:37:55.00	7.51	7844 ⁻⁸⁰⁹ ₊₁₁₈₆	9224 ⁻¹⁰⁶¹ ₊₁₂₀₆	
2018gsk	35	0.0116	2018-11-16 06:13:26.00	60.92	4473 ⁻⁹¹⁹ ₊₇₁₄	11835 ⁻⁴⁸⁶ ₊₄₂₄	7316 ⁻¹⁹⁹³ ₊₉₃₄
2018gsk	25	0.0116	2018-10-18 05:32:07.00	32.22	5318 ⁻¹⁵⁹ ₊₁₈₆	13844 ⁻¹⁵² ₊₁₅₇	
2018gsk	15	0.0116	2018-10-18 06:05:37.00	32.24	5283 ⁻¹⁸² ₊₁₉₉	14193 ⁻¹⁴³ ₊₂₀₀	
2018gsk	25	0.0116	2018-10-03 07:29:43.00	17.47	5721 ⁻²³³ ₊₂₂₀	3516 ⁻⁴⁵³ ₊₁₉₇	11589 ⁻⁶⁹⁰ ₊₁₁₈₃
2018cbz	21	0.0223	2018-06-09 21:17:56.00	11.27	11766 ⁻²⁰⁰³ ₊₁₃₈₂	14406 ⁻⁹²¹ ₊₆₇₆	
2018cbz	15	0.0223	2018-06-19 22:09:19.00	21.08		8085 ⁻⁸⁹⁹ ₊₁₀₀₅	
2018cbz	22	0.0223	2018-06-15 21:20:57.00	17.14	13613 ⁻¹⁶³⁷ ₊₁₃₄₇	11893 ⁻⁸⁸⁴ ₊₆₅₇	
2018cbz	15	0.0223	2018-06-07 22:15:46.00	9.35	16803 ⁻⁷⁷¹ ₊₆₀₀	14973 ⁻³⁸⁶ ₊₅₁₈	
2018cbz	15	0.0223	2018-06-11 21:23:50.00	13.23	16124 ⁻⁴²² ₊₄₂₆	14153 ⁻¹⁹⁹ ₊₂₁₆	
2018gep	71	0.033	2018-09-19 05:42:17.00	9.81	19889 ⁻¹⁹¹ ₊₁₆₆	21826 ⁻²⁷⁷ ₊₂₇₇	
2020abdw	51	0.0327790007	2020-12-08 01:46:18.00	16.29	9272 ⁻¹⁰⁴⁷ ₊₈₇₉	9793 ⁻²⁵⁹¹ ₊₈₄₅	14816 ⁻⁶⁶⁴ ₊₁₃₂₄

Continued on next page

Table B.2. Measured velocities of Fe II, Si II and Ca II for the Ic-BL supernovae analysed here, continued.

Event name	SG filter width	z	Obs. date [UT]	ΔT_{rest} [days]	$v_{\text{Fe II}}$ [km/s]	$v_{\text{Si II}}$ [km/s]	$v_{\text{Ca II}}$ [km/s]
2020abdw	63	0.0327790007	2020-12-14 03:43:12.00	22.18	7005^{+290}_{-250}	7066^{+732}_{-588}	12938^{+421}_{-411}
2020abdw	15	0.0327790007	2020-12-16 03:25:05.00	24.10	12092^{+2141}_{-2431}	9003^{+3628}_{-2505}	12670^{+430}_{-283}
2022crr	67	0.0188	2022-02-24 08:19:00.00	15.79	22793^{+364}_{-447}	20614^{+312}_{-304}	42257^{+508}_{-1383}

Table B.3. Measured velocities of Fe II, Si II and Ca II for the GRB-SNe analysed here. Each line in the table represents one observation. The name of the event, SG filter width, redshift (z), observation date of the spectrum and rest-frame time relative to the explosion date (ΔT_{rest}) are all given. The velocities (and uncertainties) of the Fe II (v_{FeII}), Si II (v_{SiII}) and Ca II (v_{CaII}) features are reported for each observation. In some cases, no velocity is reported for a feature, for example because the wavelength range of the feature in question was not covered by the spectrum.

Event name	SG filter width	z	Obs. date [UT]	ΔT_{rest} [days]	v_{FeII} [km/s]	v_{SiII} [km/s]	v_{CaII} [km/s]
GRB980425-SN1998bw	51	0.008499	1998-09-12 00:00:00.00	137.92	23934 ⁻¹⁴⁶ ₊₁₃₀	14966 ⁻¹⁴⁶ ₊₁₇₀	17912 ⁻¹¹⁶ ₊₁₂₅
GRB980425-SN1998bw	47	0.008499	1998-05-03 09:30:00.00	7.42	39762 ⁻³²⁴ ₊₂₈₇	24954 ⁻²²⁹ ₊₂₅₀	
GRB980425-SN1998bw	40	0.008499	1998-06-08 00:00:00.00	42.73	28326 ⁻³²⁰ ₊₃₇₇	6580 ⁻⁹⁸⁹ ₊₃₄₀	
GRB980425-SN1998bw	21	0.008499	1998-05-29 00:00:00.00	32.81	28411 ⁻⁷⁰ ₊₉₄	8139 ⁻¹⁰³⁷ ₊₄₇₈	16447 ⁻¹⁹⁰ ₊₁₅₅
GRB980425-SN1998bw	47	0.008499	1998-05-07 00:00:00.00	11.00	35464 ⁻¹⁷⁶⁶ ₊₁₇₄₉	24363 ⁻²³³ ₊₂₂₉	
GRB980425-SN1998bw	71	0.008499	1998-06-24 05:45:00.00	58.83	25970 ⁻¹⁵⁷ ₊₁₆₃	7785 ⁻²⁴⁴ ₊₂₂₅	16166 ⁻¹⁸⁹ ₊₁₈₉
GRB980425-SN1998bw	57	0.008499	1998-05-08 00:00:00.00	11.99	28501 ⁻¹¹⁸⁷ ₊₁₁₀₃	24838 ⁻¹⁶³ ₊₁₉₇	
GRB980425-SN1998bw	31	0.008499	1998-05-04 00:00:00.00	8.02	38268 ⁻¹⁸⁶ ₊₁₆₆	28085 ⁻⁹¹⁰ ₊₁₀₀₅	
GRB980425-SN1998bw	59	0.008499	1998-05-09 00:00:00.00	12.98	31467 ⁻⁴⁵⁷ ₊₅₆₄	24084 ⁻²⁵⁴ ₊₂₈₃	
GRB980425-SN1998bw	25	0.008499	1998-07-22 00:00:00.00	86.36	26408 ⁻⁴⁹⁷ ₊₇₅₃	13441 ⁻²⁷¹ ₊₂₆₁	14949 ⁻⁸¹⁸ ₊₄₀₃
GRB980425-SN1998bw	29	0.008499	1998-05-01 00:00:00.00	5.05			11286 ⁻²⁸³ ₊₅₆₀
GRB980425-SN1998bw	57	0.008499	1998-05-11 00:00:00.00	14.96	30203 ⁻³²⁸ ₊₃₇₉	22748 ⁻⁴⁰⁸ ₊₄₈₃	
GRB980425-SN1998bw	31	0.008499	1998-05-19 00:00:00.00	22.90	28115 ⁻³²³ ₊₃₅₄	12054 ⁻³²⁴ ₊₁₉₄	
GRB980425-SN1998bw	31	0.008499	1998-05-21 00:00:00.00	24.88	27733 ⁻²²⁷ ₊₂₂₇	12303 ⁻²⁵⁴ ₊₂₅₄	16741 ⁻⁵⁰⁶ ₊₆₅₂
GRB980425-SN1998bw	31	0.008499	1998-05-22 00:00:00.00	25.87	27850 ⁻²²⁷ ₊₂₅₀	12264 ⁻²⁴⁴ ₊₃₉₃	16470 ⁻³⁰² ₊₆₀₉
GRB980425-SN1998bw	31	0.008499	1998-07-01 04:15:00.00	65.71	25733 ⁻²⁵² ₊₂₉₁	8345 ⁻⁹⁵⁷ ₊₁₁₇₅	15867 ⁻⁵⁹² ₊₅₀₈
GRB980425-SN1998bw	41	0.008499	1998-05-23 00:00:00.00	26.86	28755 ⁻¹¹³ ₊₁₀₅	9488 ⁻³⁴⁷ ₊₃₆₂	16584 ⁻¹⁴⁰ ₊₁₄₅
GRB980425-SN1998bw	47	0.008499	1998-06-01 00:00:00.00	35.79	27682 ⁻¹⁶⁴ ₊₁₇₂	8772 ⁻⁹⁷³ ₊₇₂₀	16446 ⁻⁴⁵⁵ ₊₄₄₃
GRB980425-SN1998bw	47	0.008499	1998-05-16 00:00:00.00	19.92	28336 ⁻¹⁴⁶ ₊₁₄₈	13654 ⁻⁹⁵ ₊₁₁₁	14654 ⁻⁰ ₊₀
GRB980425-SN1998bw	49	0.008499	1998-07-13 00:00:00.00	77.43	25258 ⁻³¹⁶ ₊₅₁₀	12849 ⁻⁴²³ ₊₈₉₈	15881 ⁻⁸¹⁶ ₊₈₉₈
GRB980425-SN1998bw	47	0.008499	1998-05-14 00:00:00.00	17.94	28853 ⁻¹⁷¹ ₊₁₄₉	14598 ⁻¹⁹¹ ₊₂₀₇	37603 ⁻¹²⁷⁴ ₊₉₉₁
GRB980425-SN1998bw	57	0.008499	1998-05-13 09:30:00.00	17.34	28653 ⁻²⁷⁹ ₊₂₉₃	15170 ⁻¹²⁹ ₊₁₁₈	40869 ⁻³⁴⁶ ₊₆₂₂₅
GRB030329-SN2003dh	49	0.1685	2003-05-02 01:12:00.00	28.73	29191 ⁻²⁴⁴ ₊₃₈₈	7446 ⁻¹⁷⁸ ₊₁₇₅	
GRB030329-SN2003dh	45	0.1685	2003-04-09 03:50:24.00	9.14	31483 ⁻⁶⁴ ₊₅₇	33296 ⁻¹⁶⁵ ₊₁₉₀	
GRB030329-SN2003dh	81	0.1685	2003-05-08 00:00:00.00	33.82	28073 ⁻²²⁰ ₊₂₀₀	12475 ⁻³⁵⁸ ₊₃₉₀	11642 ⁻²⁹⁷ ₊₁₉₉
GRB030329-SN2003dh	55	0.1685	2003-04-08 03:36:00.00	8.27	34666 ⁻¹⁷⁷ ₊₂₀₃	30149 ⁻¹²³¹ ₊₈₈₅	
GRB030329-SN2003dh	49	0.1685	2003-05-04 00:14:24.00	30.40	29097 ⁻¹⁸⁷ ₊₄₄₃	11917 ⁻²⁰³ ₊₂₉₈	
GRB030329-SN2003dh	55	0.1685	2003-04-10 03:21:36.00	9.98	36343 ⁻⁶⁴⁷ ₊₆₇		
GRB030329-SN2003dh	41	0.1685	2003-04-24 04:33:36.00	22.00	24833 ⁻¹⁰⁵ ₊₉₇	16071 ⁻⁶⁶ ₊₆₁	
GRB030329-SN2003dh	37	0.1685	2003-04-06 03:36:00.00	6.56	37440 ⁻⁶²⁶ ₊₆₂₉	44442 ⁻¹¹⁵ ₊₁₁₀	
GRB030329-SN2003dh	55	0.1685	2003-04-07 06:14:24.00	7.51	40924 ⁻²⁶⁶ ₊₃₂₇		
GRB030329-SN2003dh	81	0.1685	2003-06-22 06:43:12.00	72.57	25182 ⁻²⁴⁵ ₊₂₉₇	13895 ⁻¹⁵¹ ₊₁₅₂	
GRB030329-SN2003dh	81	0.1685	2003-05-24 09:07:12.00	47.84	24282 ⁻²⁰¹ ₊₁₇₉	12316 ⁻⁴²⁵ ₊₃₄₅	
GRB060218-SN2006aj	101	0.033023	2006-03-03 03:21:36.00	12.58	20284 ⁻⁶⁴⁹ ₊₁₂₁₇	18874 ⁻⁴²⁸ ₊₅₁₃	
GRB060218-SN2006aj	81	0.033023	2006-03-02 03:07:12.00	11.60	22874 ⁻⁴⁶³ ₊₄₆₀	20742 ⁻⁴⁸⁹ ₊₁₀₃₉	
GRB060218-SN2006aj	121	0.033023	2006-03-02 03:36:00.00	11.62	19845 ⁻¹³⁵¹ ₊₁₃₈₈	19383 ⁻⁸⁵² ₊₈₀₆	
GRB060218-SN2006aj	47	0.033023	2006-03-03 00:14:24.00	12.45	21131 ⁻⁷⁹⁷ ₊₁₆₆	19081 ⁻⁷⁰⁹ ₊₁₆₆	23068 ⁻²³⁸ ₊₄₈₄
GRB060218-SN2006aj	201	0.033023	2006-02-26 00:00:00.00	7.60	25539 ⁻⁴²⁶ ₊₄₅₅	20185 ⁻⁷⁰⁹ ₊₉₉₆	23478 ⁻⁸⁵⁶ ₊₆₂₅
GRB060218-SN2006aj	67	0.033023	2006-03-03 03:36:00.00	12.59	22328 ⁻⁶⁴⁴ ₊₄₉₅	17857 ⁻⁵⁰³ ₊₄₃₈	20825 ⁻⁸²⁶ ₊₄₅₆
GRB060218-SN2006aj	121	0.033023	2006-02-23 03:07:12.00	4.82	29023 ⁻²⁸¹⁶ ₊₂₂₀₅		
GRB060218-SN2006aj	41	0.033023	2006-03-04 00:12:58.00	13.42		18271 ⁻¹⁷⁹ ₊₁₈₀	22912 ⁻³²⁶ ₊₂₁₀₇
GRB060218-SN2006aj	67	0.033023	2006-02-23 02:24:00.00	4.79	26823 ⁻⁵⁴⁶ ₊₅₇₀		
GRB060218-SN2006aj	47	0.033023	2006-03-05 00:38:53.00	14.40		17753 ⁻²³⁷ ₊₂₃₀	22828 ⁻⁵⁰⁶ ₊₂₇₆₁
GRB060218-SN2006aj	47	0.033023	2006-03-06 00:20:10.00	15.36		17327 ⁻²¹³ ₊₂₂₄	20576 ⁻²⁶¹³ ₊₅₀₈

Continued on next page

Table B.3. Measured velocities of Fe II, Si II and Ca II for the GRB-SNe analysed for this work, continued.

Event name	SG filter width	z	Obs. date [UT]	ΔT_{rest} [days]	$v_{Fe II}$ [km/s]	$v_{Si II}$ [km/s]	$v_{Ca II}$ [km/s]
GRB060218-SN2006aj	101	0.033023	2006-03-08 00:10:05.00	17.29		15697 ⁻¹⁹³ ₊₁₅₅	21642 ⁻¹³¹ ₊₁₂₉
GRB060218-SN2006aj	133	0.033023	2006-02-22 00:00:00.00	3.73	23930 ⁻⁶⁶⁹ ₊₁₅₁₃		
GRB060218-SN2006aj	71	0.033023	2006-03-09 00:18:43.00	18.26		14936 ⁻³²¹ ₊₂₈₆	21976 ⁻⁴³⁹ ₊₅₀₈
GRB060218-SN2006aj	47	0.033023	2006-03-10 00:18:43.00	19.23		13468 ⁻²⁴² ₊₁₉₆	20107 ⁻⁶⁵⁴ ₊₃₈₂
GRB060218-SN2006aj	81	0.033023	2006-02-21 00:00:00.00	2.76	32313 ⁻⁵⁸⁵ ₊₈₆₉		
GRB060218-SN2006aj	125	0.033023	2006-02-24 03:50:24.00	5.82	23521 ⁻⁶³¹ ₊₆₄₃		
GRB060218-SN2006aj	47	0.033023	2006-03-02 00:10:05.00	11.48	23362 ⁻¹⁰⁵ ₊₁₂₅	19728 ⁻¹⁵⁸ ₊₁₆₇	23143 ⁻²⁶⁴ ₊₇₂₉
GRB060218-SN2006aj	35	0.033023	2006-03-01 00:12:58.00	10.51	23956 ⁻¹⁵¹ ₊₁₈₉	20368 ⁻³⁶⁷ ₊₃₅₅	23428 ⁻¹²⁹ ₊₁₅₂
GRB060218-SN2006aj	101	0.033023	2006-02-27 02:52:48.00	8.68	24549 ⁻¹³¹⁴ ₊₂₀₀₃	20016 ⁻⁶²⁵ ₊₅₁₅	
GRB060218-SN2006aj	67	0.033023	2006-02-28 03:36:00.00	9.68	21833 ⁻⁷⁰⁷ ₊₁₀₈₄	18998 ⁻⁵¹³ ₊₄₅₅	
GRB060218-SN2006aj	201	0.033023	2006-02-25 00:00:00.00	6.63	24980 ⁻³⁴² ₊₄₀₆		
GRB060218-SN2006aj	47	0.033023	2006-02-28 00:36:00.00	9.56	23827 ⁻⁴²⁴ ₊₄₂₉	20686 ⁻²⁶⁰ ₊₄₂₈	23177 ⁻³⁶¹ ₊₅₇₁
GRB060218-SN2006aj	47	0.033023	2006-02-27 00:33:07.00	8.59	24476 ⁻²³⁰ ₊₂₆₃	21035 ⁻³⁴⁵ ₊₃₄₅	24037 ⁻⁵⁷¹ ₊₁₄₁
GRB101219B-SN2010ma	61	0.55185	2011-01-05 02:09:36.00	10.57	33596 ⁻¹⁷⁸⁴ ₊₄₅₅₆	11493 ⁻²¹⁵³ ₊₄₂₆₉	
GRB101219B-SN2010ma	31	0.55185	2010-12-20 00:00:00	0.20	28985 ⁻⁹⁴⁶ ₊₁₀₂₈		
GRB101219B-SN2010ma	51	0.55185	2011-01-25 13:12:00.00	23.75		13980 ⁻³⁷⁰ ₊₄₀₀	
GRB100316D-SN2010bh	55	0.0593	2010-03-26 00:00:00.00	8.94	41038 ⁻⁴⁵² ₊₄₈₂		43349 ⁻⁶²² ₊₄₉₂
GRB100316D-SN2010bh	31	0.0593	2010-04-01 00:00:00.00	14.60	35722 ⁻⁹⁷⁷ ₊₇₂₄	32478 ⁻⁴⁴⁸ ₊₄₄₀	39142 ⁻²⁷⁴ ₊₂₉₇
GRB100316D-SN2010bh	31	0.0593	2010-03-30 00:00:00.00	12.71	36034 ⁻⁵¹⁸ ₊₇₅₆	33385 ⁻⁶³⁸ ₊₅₀₄	40204 ⁻³⁵⁷ ₊₇₀₆
GRB100316D-SN2010bh	51	0.0593	2010-04-05 00:00:00.00	18.38	35268 ⁻¹⁵¹⁰ ₊₁₀₄₄	30143 ⁻⁸³⁸ ₊₁₃₅₁	37781 ⁻⁵²⁹ ₊₄₃₁
GRB100316D-SN2010bh	25	0.0593	2010-03-28 00:00:00.00	10.83	38281 ⁻¹³⁵² ₊₈₁₁	33621 ⁻¹⁸⁶² ₊₂₁₆₃	41287 ⁻⁴³¹ ₊₃₉₆
GRB100316D-SN2010bh	55	0.0593	2010-03-25 00:00:00.00	7.99	41894 ⁻⁶⁷⁵ ₊₇₁₉		43385 ⁻³⁶⁵ ₊₃₅₅
GRB100316D-SN2010bh	31	0.0593	2010-03-24 00:00:00.00	7.05	42458 ⁻⁷¹⁹ ₊₈₁₄	34321 ⁻²⁰⁷⁴ ₊₁₃₇₁	
GRB100316D-SN2010bh	51	0.0593	2010-04-03 00:00:00.00	16.49	38097 ⁻¹⁰⁰⁹ ₊₁₅₄₁	31805 ⁻⁶⁴⁸ ₊₁₃₆₁	38874 ⁻³⁹⁸ ₊₅₇₂
GRB100316D-SN2010bh	101	0.0593	2010-04-08 00:00:00.00	21.21	31338 ⁻¹³⁹³ ₊₁₁₉₂	26809 ⁻⁸⁴⁰ ₊₆₈₉	32972 ⁻¹⁷²⁸ ₊₇₄₇
GRB100316D-SN2010bh	31	0.0593	2010-04-18 00:00:00.00	30.65	17836 ⁻¹³⁹² ₊₁₄₆₆	27027 ⁻³⁵¹¹ ₊₄₁₆₇	33668 ⁻¹⁷⁶⁹ ₊₁₅₁₀
GRB120422A-SN2012bz	501	0.283	2012-05-10 23:54:14.00	14.57	25941 ⁻³³³⁴ ₊₂₆₈₁		
GRB120422A-SN2012bz	901	0.283	2012-05-01 01:27:50.00	6.83	33682 ⁻⁵⁵⁷² ₊₂₇₅₉		
GRB120422A-SN2012bz	451	0.283	2012-05-16 23:58:33.00	19.25	21991 ⁻¹³⁴⁶ ₊₁₈₀₆	19902 ⁻⁸⁰² ₊₁₀₆₂	
GRB120422A-SN2012bz	151	0.283	2012-05-03 00:00:00.00	8.34	24782 ⁻³¹⁵⁰ ₊₃₉₁₄	19696 ⁻¹⁰⁹⁴ ₊₁₇₆₃	
GRB120422A-SN2012bz	901	0.283	2012-05-29 00:36:00.00	28.62	6151 ⁻³⁹²⁸ ₊₁₃₃₅	9713 ⁻¹⁸⁸² ₊₂₇₇₃	
GRB120422A-SN2012bz	125	0.283	2012-04-27 06:10:04.00	3.86	36123 ⁻²⁸³³ ₊₃₂₉₂		
GRB130702A-SN2013dx	121	0.15	2013-07-11 00:00:00.00	7.82	27483 ⁻⁴⁵⁴ ₊₄₂₁	20043 ⁻¹³⁷⁵ ₊₁₀₉₁	23423 ⁻⁶⁵⁶ ₊₁₀₀₂
GRB130702A-SN2013dx	401	0.15	2013-07-05 00:00:00.00	2.61	28546 ⁻⁶⁵⁴ ₊₆₁₁		29711 ⁻⁶⁷⁶ ₊₆₃₅
GRB130702A-SN2013dx	351	0.15	2013-07-04 03:50:24.00	1.88	34574 ⁻¹²¹¹ ₊₂₁₆₁	31291 ⁻¹³³² ₊₂₆₃₈	
GRB130702A-SN2013dx	103	0.15	2013-07-03 00:00:00.00	0.87	42936 ⁻⁹⁸⁰ ₊₁₂₄₈	35214 ⁻¹¹⁸² ₊₁₉₇₃	
GRB130702A-SN2013dx	67	0.15	2013-07-30 00:00:00.00	24.34	17142 ⁻⁷⁴² ₊₇₁₄	6593 ⁻¹⁸¹⁵ ₊₈₂₂	
GRB130702A-SN2013dx	101	0.15	2013-07-22 00:00:00.00	17.39	21075 ⁻³²³⁴ ₊₂₀₀₆	13722 ⁻⁷⁸² ₊₈₂₂	19274 ⁻³¹⁴⁹ ₊₃₂₁₇
GRB130702A-SN2013dx	43	0.15	2013-07-11 00:00:00.00	7.82	23638 ⁻¹⁴⁶⁸ ₊₉₉₃		
GRB130702A-SN2013dx	71	0.15	2013-07-09 00:00:00.00	6.08	26295 ⁻²⁴³⁷ ₊₂₉₂₁		
GRB130702A-SN2013dx	251	0.15	2013-08-02 00:00:00.00	26.95	18444 ⁻⁷⁸⁵ ₊₈₆₂	8876 ⁻⁵⁸⁶ ₊₅₄₁	20025 ⁻²⁴⁸ ₊₈₀₉
GRB130702A-SN2013dx	51	0.15	2013-07-20 00:00:00.00	15.65	15612 ⁻⁹²³ ₊₆₇₃	15553 ⁻⁵⁷⁵ ₊₇₆₇	
GRB130702A-SN2013dx	81	0.15	2013-07-20 00:00:00.00	15.65	17561 ⁻¹³¹² ₊₁₈₆₄	16023 ⁻¹⁰¹⁷ ₊₁₃₂₁	21364 ⁻¹⁴⁶³ ₊₂₇₃₄
GRB130702A-SN2013dx	61	0.15	2013-08-03 00:00:00.00	27.82	14780 ⁻¹⁴⁴⁸ ₊₉₃₄	8197 ⁻⁵²⁰¹ ₊₁₈₂₉	21083 ⁻⁷⁶⁴ ₊₆₈₀
GRB130702A-SN2013dx	81	0.15	2013-07-17 00:00:00.00	13.04	17784 ⁻¹¹⁴⁹ ₊₉₃₃	15523 ⁻¹⁶⁵³ ₊₁₄₄₃	
GRB130702A-SN2013dx	43	0.15	2013-07-13 00:00:00.00	9.56	21490 ⁻¹⁰⁶² ₊₇₃₂	17123 ⁻⁶²⁸ ₊₅₃₇	

Continued on next page

Table B.3. Measured velocities of Fe II, Si II and Ca II for the GRB-SNe analysed for this work, continued.

Event name	SG filter width	z	Obs. date [UT]	ΔT_{rest} [days]	v_{FeII} [km/s]	v_{SiII} [km/s]	v_{CaII} [km/s]
GRB130702A-SN2013dx	91	0.15	2013-08-06 00:00:00.00	30.43	16909 ⁻¹⁰⁷¹ ₊₈₉₉	5005 ⁻⁴⁰⁹⁴ ₊₁₆₀₂	18826 ⁻⁹²⁴ ₊₁₉₁₉
GRB130702A-SN2013dx	43	0.15	2013-07-16 00:00:00.00	12.17	16314 ⁻¹⁰⁵³ ₊₆₈₂	16033 ⁻⁶⁴⁰ ₊₅₀₃	24096 ⁻²⁷⁴² ₊₂₃₁₉
GRB130702A-SN2013dx	71	0.15	2013-07-16 00:00:00.00	12.17	20264 ⁻¹⁷⁹² ₊₁₉₆₈	15161 ⁻⁴⁰⁷⁴ ₊₂₅₂₂	
GRB130702A-SN2013dx	141	0.15	2013-07-08 05:31:12.00	5.41	27162 ⁻²⁸⁰⁸ ₊₂₄₁₅	21551 ⁻¹⁴²⁵ ₊₁₇₀₇	23272 ⁻⁵³⁰ ₊₅₁₅
GRB130702A-SN2013dx	37	0.15	2013-07-14 00:00:00.00	10.43	18254 ⁻¹⁰⁷⁷ ₊₁₁₃₁	15772 ⁻⁵⁴⁷ ₊₅₉₉	
GRB130702A-SN2013dx	61	0.15	2013-07-27 00:00:00.00	21.74	17969 ⁻²⁵⁶⁵ ₊₈₇₁	11709 ⁻³⁶⁴ ₊₅₇₇	20259 ⁻⁴²⁴ ₊₇₅₆
GRB130702A-SN2013dx	51	0.15	2013-07-09 00:00:00.00	6.08	29207 ⁻¹⁰¹³ ₊₁₀₂₇		
GRB130702A-SN2013dx	201	0.15	2013-08-02 00:00:00.00	26.95	20987 ⁻⁸¹² ₊₁₆₃₉	4688 ⁻¹⁰⁴⁸ ₊₁₀₆₄	20972 ⁻¹²⁷⁷ ₊₈₂₅
GRB130702A-SN2013dx	71	0.15	2013-08-10 00:00:00.00	33.91	23169 ⁻⁴²⁸ ₊₅₁₇	3017 ⁻¹²³² ₊₁₅₄₅	
GRB161219B-SN2016jca	51	0.1475	2017-01-04 04:55:30.00	13.44	27080 ⁻⁶⁷⁷ ₊₇₁₁	25481 ⁻⁸⁹⁶ ₊₁₁₁₀	
GRB161219B-SN2016jca	101	0.1475	2016-12-25 03:00:00.00	4.65	46570 ⁻⁸⁶⁶ ₊₆₉₀		
GRB161219B-SN2016jca	25	0.1475	2017-01-04 05:47:24.00	13.47	25968 ⁻³⁰³¹ ₊₁₀₂₇		
GRB171205A-SN2017iuk	21	0.0368	2017-12-29 05:22:02.00	23.07	12796 ⁻¹⁰⁹⁷ ₊₉₉₀	5424 ⁻¹¹⁹⁶ ₊₆₉₇	
GRB171205A-SN2017iuk	51	0.0368	2018-02-21 08:24:25.00	75.27	7647 ⁻¹⁸⁷⁷ ₊₁₄₁₈		14383 ⁻¹⁰⁵³ ₊₁₀₄₉
GRB171205A-SN2017iuk	51	0.0368	2018-02-21 07:32:04.00	75.24	4877 ⁻¹⁴⁰⁷ ₊₁₂₈₉		18336 ⁻¹¹⁸⁰ ₊₂₄₆₇
GRB171205A-SN2017iuk	61	0.0368	2018-02-21 06:40:03.00	75.20	7862 ⁻²⁵³⁷ ₊₁₆₅₄		15375 ⁻²⁰⁹⁷ ₊₅₀₁₉
GRB171205A-SN2017iuk	35	0.0368	2017-12-12 06:25:19.00	6.71	29945 ⁻²¹¹⁹ ₊₃₀₁₉		
GRB171205A-SN2017iuk	51	0.0368	2017-12-12 07:00:57.00	6.74			31804 ⁻¹¹¹⁵ ₊₁₈₂₅
GRB171205A-SN2017iuk	51	0.0368	2017-12-13 06:27:34.00	7.68	26702 ⁻²⁵⁹¹ ₊₁₄₁₄		
GRB171205A-SN2017iuk	23	0.0368	2017-12-13 07:07:08.00	7.71		11799 ⁻⁵⁵⁰ ₊₈₄₃	
GRB171205A-SN2017iuk	51	0.0368	2018-01-06 05:45:17.00	30.80	10328 ⁻¹⁴⁷⁰ ₊₁₀₁₇	2257 ⁻⁴⁸³ ₊₄₅₃	
GRB171205A-SN2017iuk	25	0.0368	2018-01-06 04:55:26.00	30.77	12508 ⁻⁴³⁵ ₊₃₈₅	1802 ⁻¹⁷⁸⁸ ₊₁₆₃₅	
GRB171205A-SN2017iuk	23	0.0368	2017-12-27 06:09:12.00	21.17		8912 ⁻²¹⁴ ₊₂₀₀	17917 ⁻⁹⁶⁶ ₊₄₀₂
GRB171205A-SN2017iuk	23	0.0368	2017-12-15 06:55:43.00	9.63		12503 ⁻⁴⁴² ₊₃₉₆	28981 ⁻⁹⁰⁶ ₊₄₄₂
GRB171205A-SN2017iuk	31	0.0368	2018-01-05 06:11:50.00	29.85		2097 ⁻¹⁴⁵² ₊₁₃₁₄	14620 ⁻²⁶⁷³ ₊₄₅₁
GRB171205A-SN2017iuk	25	0.0368	2017-12-15 06:19:35.00	9.60	22624 ⁻⁹¹⁴ ₊₅₈₀	12370 ⁻⁶²⁶ ₊₁₅₄₇	
GRB171205A-SN2017iuk	25	0.0368	2017-12-17 06:25:26.00	11.54	21436 ⁻⁷⁵⁶ ₊₁₀₄₆	12376 ⁻⁵⁴⁶ ₊₅₆₆	
GRB171205A-SN2017iuk	40	0.0368	2017-12-29 06:13:23.00	23.10		7131 ⁻¹⁰⁵⁹ ₊₈₃₇	17790 ⁻⁷⁶² ₊₈₁₆
GRB171205A-SN2017iuk	25	0.0368	2017-12-27 05:18:15.00	21.14	14221 ⁻⁹¹³ ₊₁₂₉₁	8342 ⁻⁵⁴⁴ ₊₁₉₃₅	
GRB171205A-SN2017iuk	31	0.0368	2017-12-30 05:47:05.00	24.05	11894 ⁻⁹³⁶ ₊₁₃₂₇	5928 ⁻¹⁴⁰⁰ ₊₆₉₈	
GRB171205A-SN2017iuk	41	0.0368	2017-12-26 06:07:59.00	20.21	13704 ⁻⁹⁹⁸ ₊₁₀₆₇	9230 ⁻⁷²⁷ ₊₈₉₇	
GRB171205A-SN2017iuk	51	0.0368	2017-12-30 06:37:58.00	24.08		6767 ⁻⁶⁵⁸ ₊₆₆₅	18386 ⁻⁵⁴⁵ ₊₁₁₅
GRB171205A-SN2017iuk	40	0.0368	2017-12-26 06:44:04.00	20.23		9308 ⁻²⁷³ ₊₃₄₃	18977 ⁻⁴⁶⁷ ₊₄₈₄
GRB171205A-SN2017iuk	51	0.0368	2018-01-05 05:12:59.00	29.81		4092 ⁻⁷⁹⁵ ₊₇₉₃	14556 ⁻¹⁹¹⁶ ₊₈₃₉
GRB171010A-SN2017htp	8	0.328	2017-11-01 03:00:00	16.06	28601 ⁻²⁷⁴⁰ ₊₃₈₇₄		
GRB180728A-SN2018fip	1200	0.117	2018-08-21 02:04:46.361	20.91		6959 ⁻⁴³⁴ ₊₄₉₆	8015 ⁻⁴⁴³ ₊₃₆₇
GRB180728A-SN2018fip	30	0.117	2018-08-21 01:52:19	20.90		6363 ⁻³⁰⁸ ₊₃₇₆	11818 ⁻⁴²¹ ₊₄₁₂
GRB180728A-SN2018fip	30	0.117	2018-07-28 17:29:38.000	0.00		6490 ⁻²²⁸ ₊₂₄₅	11757 ⁻⁴²¹ ₊₄₃₉
GRB180728A-SN2018fip	600	0.117	2018-09-08 01:30:40.040	37.00	21477 ⁻³¹⁸ ₊₃₇₂		
SN2020bvc	61	0.025235	2020-03-02 04:04:48	26.82	20150 ⁻⁶³⁶ ₊₆₀₂	10321 ⁻³³⁰ ₊₃₂₀	20550 ⁻⁵⁸³ ₊₆₃₄
SN2020bvc	81	0.025235	2020-03-22 13:40:48	46.72	17786 ⁻³⁴⁶ ₊₃₄₇	9615 ⁻²⁵⁴ ₊₂₃₅	18689 ⁻¹⁰⁴² ₊₇₆₈
SN2020bvc	105	0.025235	2020-02-12 11:16:48	8.58	26242 ⁻³⁹⁴ ₊₃₅₃	21993 ⁻³⁷⁶ ₊₅₁₃	42224 ⁻²⁶⁸ ₊₂₉₀
SN2020bvc	12	0.025235	2020-02-09 08:52:48	5.56	29535 ⁻¹⁶⁶⁶ ₊₁₉₉₄	29944 ⁻³⁶²⁷ ₊₁₅₇₅	
SN2020bvc	10	0.025235	2020-02-13 08:52:48	9.46	28373 ⁻⁸⁹⁸ ₊₁₂₇₂		33533 ⁻¹⁶⁵⁵ ₊₁₃₁₂
SN2020bvc	31	0.025235	2020-02-08 05:52:18.00	4.46	34948 ⁻²⁷³¹ ₊₂₁₉₄		
SN2020bvc	12	0.025235	2020-02-21 08:52:48	17.26	28422 ⁻²⁰⁷¹ ₊₁₈₈₇	18775 ⁻⁶⁷⁵ ₊₉₀₁	24685 ⁻⁷⁰⁵ ₊₈₀₀

Continued on next page

Table B.3. Measured velocities of Fe II, Si II and Ca II for the GRB-SNe analysed for this work, continued.

Event name	SG filter width	z	Obs. date [UT]	ΔT_{rest} [days]	$v_{\text{Fe II}}$ [km/s]	$v_{\text{Si II}}$ [km/s]	$v_{\text{Ca II}}$ [km/s]
SN2020bvc	71	0.025235	2020-02-16 04:04:48	12.19	27014_{-1155}^{+1098}	20459_{-402}^{+590}	
SN2020bvc	7	0.025235	2020-02-15 08:52:48	11.41	26772_{-1126}^{+1810}	18349_{-1571}^{+1032}	27876_{-2613}^{+1271}
SN2020bvc	5	0.025235	2020-02-07 08:52:48	3.61	31514_{-631}^{+829}		
SN2020bvc	21	0.025235	2020-03-17 06:28:48	41.55	16643_{-611}^{+1090}	9796_{-1336}^{+3452}	

Table B.4. Fit results for Fe II velocity evolution in Ic-BLs and GRB-SNe. The name and type of the event, best fit type (power-law (PL) or broken power-law (BPL)) and sample that the event belongs to (*Gold, Silver, Bronze, Exclude*) are all provided. For power-law fits, the Fe II velocity at t_0+1 day (a) and the slope of the evolution (b) are listed. In cases where a broken power-law fit was used, the SN velocity at the break time (A); the slopes of the power-law segments (α_1 and α_2); rest-frame time of the break (t_b); and s , a parameter which controls the smoothness of the break; are given. In some cases a broken power-law fit was not attempted, and so there are no parameters to report.

Event name	Type	a [10^3 kms/s]	b	A [10^3 km/s]	α_1	α_2	t_b [days]	s	Best fit	Sample
GRB980425-SN1998bw	GRB-SN	52^{+4}_{-4}	$-0.18^{+0.03}_{-0.03}$	$29.4^{+0.7}_{-0.8}$	$-0.51^{+0.11}_{-0.07}$	$-0.06^{+0.02}_{-0.02}$	14^{+2}_{-2}	-20	BPL	Gold
GRB030329-SN2003dh	GRB-SN	57^{+6}_{-7}	$-0.21^{+0.04}_{-0.04}$	34^{+7}_{-5}	$-0.3^{+1.3}_{-0.1}$	$-0.2^{+1.2}_{-0.1}$	8^{+2}_{-10}	-20	PL	Silver
GRB060218-SN2006aj	GRB-SN	37^{+2}_{-3}	$-0.20^{+0.05}_{-0.03}$	21^{+1}_{-1}	$-0.27^{+3.05}_{-0.09}$	$-0.26^{+3.14}_{-0.07}$	18^{+4}_{-5}	20	PL	Gold
GRB100316D-SN2010bh	GRB-SN	100^{+20}_{-30}	$-0.41^{+0.10}_{-0.10}$	33^{+1}_{-2}	$-0.23^{+0.04}_{-0.04}$	$-1.8^{+0.6}_{-0.4}$	22^{+2}_{-2}	20	BPL	Bronze
GRB120422A-SN2012bz	GRB-SN	70^{+20}_{-40}	$-0.4^{+0.2}_{-0.1}$	22^{+3}_{-4}	$-0.5^{+3.3}_{-0.3}$	$-0.8^{+3.1}_{-0.5}$	20^{+2}_{-3}	20	PL	Silver
GRB130702A-SN2013dx	GRB-SN	40^{+3}_{-3}	$-0.27^{+0.03}_{-0.03}$	17^{+1}_{-1}	$-0.25^{+0.08}_{-0.59}$	$-0.23^{+0.09}_{-0.59}$	21^{+5}_{-3}	-20	PL	Gold
GRB161219B-SN2016jca	GRB-SN	100^{+10}_{-20}	$-0.52^{+0.03}_{-0.06}$						PL	Silver
GRB171205A-SN2017iuk	GRB-SN	90^{+10}_{-10}	$-0.59^{+0.05}_{-0.05}$	28^{+9}_{-4}	$-0.55^{+0.09}_{-1.13}$	$-0.54^{+0.10}_{-1.30}$	7^{+1}_{-7}	20	PL	Gold
SN2020bvc	GRB-SN	46^{+3}_{-4}	$-0.24^{+0.03}_{-0.02}$	24^{+3}_{-4}	$-0.25^{+0.05}_{-0.04}$	$-0.25^{+0.05}_{-0.04}$	14^{+7}_{-8}	-20	PL	Gold
1997ef	Ic-BL	74^{+6}_{-6}	$-0.51^{+0.03}_{-0.03}$						PL	Gold
1997dq	Ic-BL	14^{+4}_{-6}	$-0.21^{+0.09}_{-0.08}$						PL	Bronze
1998ey	Ic-BL	120^{+30}_{-40}	$-0.9^{+0.1}_{-0.1}$						PL	Bronze
2002ap	Ic-BL	34^{+3}_{-3}	$-0.11^{+0.03}_{-0.03}$	$24.1^{+0.5}_{-0.6}$	-3^{+1}_{-1}	$0.01^{+0.02}_{-0.02}$	$5.3^{+0.2}_{-0.4}$	-5	BPL	Bronze
2002bl	Ic-BL	30^{+10}_{-50}	$-0.2^{+0.4}_{-0.2}$						PL	Bronze
2003bg	Ic-BL/IIb	48^{+5}_{-6}	$-0.56^{+0.04}_{-0.04}$						PL	Gold
2003jd	Ic-BL	35^{+3}_{-3}	$-0.29^{+0.04}_{-0.03}$						PL	Silver
2005da	Ic-BL	25^{+3}_{-4}	$0.00^{+0.06}_{-0.06}$						PL	Exclude
2007ce	Ic-BL	110^{+50}_{-50}	$-0.7^{+0.1}_{-0.2}$						PL	Silver
2007ru	Ic-BL	40^{+5}_{-6}	$-0.29^{+0.06}_{-0.05}$	24^{+2}_{-1}	$-0.28^{+0.09}_{-0.63}$	$-0.2^{+0.2}_{-0.6}$	8^{+2}_{-5}	20	PL	Gold
2007I	Ic-BL	21^{+4}_{-6}	$-0.2^{+0.1}_{-0.1}$						PL	Bronze
2007D	Ic/Ic-BL	31^{+3}_{-5}	$-0.13^{+0.06}_{-0.04}$						PL	Gold
2008ew	Ic/Ic-BL	60^{+50}_{-90}	$-0.5^{+0.3}_{-0.5}$						PL	Exclude
2009dr	Ic-BL	19^{+2}_{-3}	$-0.12^{+0.06}_{-0.05}$						PL	Bronze
2009bb	Ic-BL (pec.)	47^{+4}_{-4}	$-0.20^{+0.02}_{-0.02}$	$27.3^{+0.7}_{-0.6}$	-2^{+1}_{-1}	$-0.12^{+0.02}_{-0.02}$	$9.4^{+0.2}_{-0.5}$	-5	BPL	Gold
2009ca	Ic-BL/SLSN	22^{+4}_{-23}	$-0.18^{+0.26}_{-0.08}$						PL	Silver
2010ah	Ic-BL	90^{+60}_{-70}	$-0.9^{+0.3}_{-0.4}$						PL	Bronze
PTF10qts	Ic-BL	31^{+7}_{-13}	$-0.10^{+0.11}_{-0.09}$						PL	Exclude
PTF10gvb	Ic-BL/SLSN	30^{+10}_{-60}	$-0.2^{+0.5}_{-0.3}$						PL	Exclude
PTF12gzk	Ic/Ic-BL	47^{+2}_{-3}	$-0.29^{+0.02}_{-0.02}$	$15.8^{+0.6}_{-0.7}$	$-0.36^{+0.03}_{-0.29}$	$-0.1^{+0.3}_{-0.1}$	31^{+5}_{-5}	-20	PL	Gold
2012ap	Ic-BL (pec.)	$24.1^{+0.9}_{-1.0}$	$-0.09^{+0.01}_{-0.01}$						PL	Gold
iPTF13ebw	Ic-BL	60^{+10}_{-10}	$-0.29^{+0.06}_{-0.07}$						PL	Gold
2013bn	Ic-BL	24^{+7}_{-10}	$-0.1^{+0.1}_{-0.1}$						PL	Exclude
2014ad	Ic-BL	86^{+6}_{-7}	$-0.35^{+0.02}_{-0.03}$						PL	Gold
iPTF15dqg	Ic-BL	80^{+20}_{-30}	$-0.54^{+0.08}_{-0.08}$						PL	Gold
iPTF15eov	Ic-BL	13^{+6}_{-20}	$0.1^{+0.3}_{-0.2}$						PL	Exclude
2016P	Ic/Ic-BL	17^{+1}_{-2}	$0.06^{+0.04}_{-0.03}$						PL	Exclude
2016coi	Ic/Ic-BL	45^{+2}_{-2}	$-0.27^{+0.01}_{-0.01}$	$16.8^{+0.5}_{-0.6}$	$-0.36^{+0.02}_{-0.02}$	$-0.06^{+0.04}_{-0.05}$	28^{+4}_{-4}	-20	BPL	Gold
2017dcc	Ic-BL	25^{+5}_{-7}	$-0.21^{+0.10}_{-0.09}$						PL	Silver
2017cw	Ic-BL	42^{+5}_{-8}	$-0.21^{+0.05}_{-0.04}$						PL	Gold
2017ifh	Ic-BL	160^{+60}_{-30}	$-0.72^{+0.07}_{-0.14}$						PL	Bronze
2018gsk	Ic-BL	10^{+2}_{-2}	$-0.17^{+0.07}_{-0.06}$	$6.2^{+0.7}_{-0.8}$	$-0.2^{+1.8}_{-0.1}$	$-0.2^{+1.9}_{-0.1}$	8^{+2}_{-8}	-20	PL	Bronze
2018cbz	Ic-BL	40^{+20}_{-60}	$-0.4^{+0.4}_{-0.3}$						PL	Bronze
2018giu	Ic-BL	24^{+3}_{-4}	$-0.24^{+0.05}_{-0.05}$						PL	Gold

Continued on next page

Table B.4. Fit results for Fe II velocity evolution in Ic-BLs and GRB-SNe, continued.

Event name	Type	a [10^3 kms/s]	b	A [10^3 km/s]	α_1	α_2	t_b [days]	s	Best fit	Sample
2020abdw	Ic/Ic-BL	90^{+60}_{-70}	$-0.8^{+0.2}_{-0.3}$						PL	Exclude

Table B.5. Fit results for Si II velocity evolution in Ic-BLs and GRB-SNe. The name and type of the event, best fit type (power-law (PL) or broken power-law (BPL)) and sample that the event belongs to (*Gold, Silver, Bronze, Exclude*) are all provided. For power-law fits, the Si II velocity at t_0+1 day (a) and the slope of the evolution (b) are listed. In cases where a broken power-law fit was used, the SN velocity at the break time (A); the slopes of the power-law segments (α_1 and α_2); rest-frame time of the break (t_b); and s , a parameter which controls the smoothness of the break; are given. In some cases a broken power-law fit was not attempted, and so there are no parameters to report.

Event name	Type	a [10^3 kms/s]	b	A [10^3 km/s]	α_1	α_2	t_b [days]	s	Best fit	Sample
GRB980425-SN1998bw	GRB-SN	150^{+20}_{-30}	$-0.78^{+0.06}_{-0.06}$	29^{+4}_{-6}	$-0.7^{+0.2}_{-1.6}$	$-0.7^{+0.1}_{-1.5}$	9^{+2}_{-2}	20	PL	Gold
GRB030329-SN2003dh	GRB-SN	140^{+30}_{-30}	$-0.70^{+0.07}_{-0.09}$	40^{+10}_{-10}	$-0.6^{+0.2}_{-1.0}$	$-0.6^{+0.2}_{-1.1}$	8^{+2}_{-8}	20	PL	Gold
GRB060218-SN2006aj	GRB-SN	55^{+7}_{-8}	$-0.44^{+0.05}_{-0.05}$	$17.9^{+0.6}_{-1.1}$	$-0.27^{+0.06}_{-0.08}$	$-1.2^{+0.4}_{-0.3}$	16^{+2}_{-1}	20	BPL	Gold
GRB100316D-SN2010bh	GRB-SN	60^{+10}_{-10}	$-0.24^{+0.07}_{-0.07}$	34^{+3}_{-4}	$-0.2^{+0.08}_{-0.4}$	$-0.3^{+0.3}_{-0.4}$	13^{+5}_{-5}	20	PL	Silver
GRB120422A-SN2012bz	GRB-SN	80^{+50}_{-70}	$-0.6^{+0.3}_{-0.3}$						PL	Bronze
GRB130702A-SN2013dx	GRB-SN	46^{+8}_{-13}	$-0.48^{+0.10}_{-0.07}$	$13.7^{+0.6}_{-0.6}$	$-0.31^{+0.02}_{-0.02}$	$-2.1^{+0.6}_{-0.4}$	20^{+1}_{-1}	20	BPL	Gold
GRB171205A-SN2017iuk	GRB-SN	100^{+40}_{-50}	$-0.9^{+0.1}_{-0.2}$	12^{+2}_{-2}	$-0.1^{+0.2}_{-0.3}$	$-3.2^{+0.6}_{-0.5}$	20^{+2}_{-2}	5	BPL	Gold
SN2020bvc	GRB-SN	80^{+20}_{-20}	$-0.56^{+0.08}_{-0.07}$	24^{+7}_{-6}	$-0.5^{+0.2}_{-0.6}$	$-0.5^{+0.2}_{-0.5}$	9^{+3}_{-9}	20	PL	Gold
1997dq	Ic-BL	27^{+4}_{-6}	$-0.18^{+0.05}_{-0.04}$						PL	Bronze
1997ef	Ic-BL	180^{+20}_{-10}	$-0.99^{+0.03}_{-0.04}$	12^{+1}_{-1}	$-0.58^{+0.08}_{-0.09}$	$-2.0^{+0.2}_{-0.3}$	23^{+2}_{-2}	20	BPL	Gold
1998ey	Ic-BL	130^{+40}_{-40}	$-1.2^{+0.1}_{-0.1}$	9^{+4}_{-4}	$-1.1^{+0.9}_{-1.0}$	-1^{+1}_{-1}	12^{+4}_{-7}	20	PL	Bronze
2002bl	Ic-BL	140^{+70}_{-50}	$-0.9^{+0.1}_{-0.3}$						PL	Bronze
2002ap	Ic-BL	180^{+20}_{-10}	$-1.09^{+0.03}_{-0.03}$	14^{+2}_{-2}	$-0.8^{+0.1}_{-0.1}$	$-1.7^{+0.2}_{-0.2}$	13^{+1}_{-1}	20	PL	Gold
2003jd	Ic-BL	45^{+2}_{-3}	$-0.52^{+0.02}_{-0.02}$						PL	Silver
2003bg	Ic-BL/IIb	35^{+6}_{-9}	$-0.65^{+0.07}_{-0.06}$	$3.9^{+0.8}_{-1.5}$	$-0.8^{+0.2}_{-0.7}$	$-0.5^{+0.6}_{-0.4}$	15^{+6}_{-7}	-5	PL	Gold
2005da	Ic-BL	25^{+6}_{-8}	$-0.1^{+0.1}_{-0.1}$						PL	Exclude
2007I	Ic-BL	31^{+6}_{-9}	$-0.6^{+0.1}_{-0.1}$						PL	Bronze
2007ce	Ic-BL	160^{+50}_{-30}	$-0.84^{+0.05}_{-0.11}$						PL	Exclude
2007D	Ic/Ic-BL	20^{+4}_{-8}	$-0.13^{+0.13}_{-0.08}$						PL	Silver
2007ru	Ic-BL	52^{+8}_{-10}	$-0.44^{+0.06}_{-0.06}$	18^{+3}_{-3}	$-0.4^{+0.1}_{-0.3}$	$-0.3^{+0.2}_{-0.2}$	14^{+5}_{-7}	20	PL	Gold
2008ew	Ic/Ic-BL	11^{+6}_{-37}	$-0.1^{+0.4}_{-0.2}$						PL	Exclude
2009ca	Ic-BL/SLSN	17^{+4}_{-9}	$-0.25^{+0.15}_{-0.09}$						PL	Silver
2009bb	Ic-BL (pec.)	140^{+10}_{-20}	$-0.75^{+0.03}_{-0.03}$	26^{+4}_{-7}	$-0.73^{+0.09}_{-0.90}$	$-0.6^{+0.2}_{-0.9}$	10^{+3}_{-3}	20	PL	Gold
2010ah	Ic-BL	110^{+60}_{-60}	$-1.2^{+0.2}_{-0.3}$						PL	Bronze
PTF10gvb	Ic-BL/SLSN	90^{+60}_{-70}	$-1.1^{+0.3}_{-0.4}$						PL	Exclude
PTF10vgv	Ic-BL	30^{+10}_{-60}	$-0.6^{+0.5}_{-0.3}$						PL	Exclude
PTF10qts	Ic-BL	32^{+9}_{-21}	$-0.5^{+0.1}_{-0.1}$						PL	Gold
PTF10xem	Ic-BL	150^{+60}_{-30}	$-0.76^{+0.07}_{-0.17}$						PL	Silver
2010ay	Ic-BL	16^{+7}_{-34}	$0.1^{+0.3}_{-0.2}$						PL	Exclude
PTF11qcj	Ic-BL	27^{+4}_{-15}	$-0.25^{+0.12}_{-0.08}$						PL	Silver
2012ap	Ic-BL (pec.)	60^{+10}_{-10}	$-0.57^{+0.07}_{-0.07}$	17^{+3}_{-5}	$-0.5^{+0.3}_{-0.4}$	$-0.5^{+0.3}_{-0.5}$	12^{+5}_{-6}	20	PL	Gold
PTF12gzk	Ic/Ic-BL	80^{+10}_{-20}	$-0.58^{+0.07}_{-0.07}$	$16.3^{+0.4}_{-0.4}$	$-0.33^{+0.02}_{-0.02}$	$-1.12^{+0.05}_{-0.05}$	$19.0^{+0.7}_{-0.7}$	20	BPL	Gold
iPTF13ebw	Ic-BL	140^{+60}_{-40}	$-0.9^{+0.1}_{-0.2}$						PL	Silver
2013bn	Ic-BL	60^{+40}_{-70}	$-0.6^{+0.3}_{-0.3}$						PL	Exclude
2014ad	Ic-BL	56^{+4}_{-4}	$-0.31^{+0.02}_{-0.02}$						PL	Gold
iPTF15dgg	Ic-BL	110^{+20}_{-30}	$-0.73^{+0.07}_{-0.07}$						PL	Gold
iPTF15eov	Ic-BL	100^{+60}_{-70}	$-0.6^{+0.1}_{-0.3}$						PL	Bronze
2016gox	Ic-BL	110^{+60}_{-60}	$-0.7^{+0.1}_{-0.2}$						PL	Bronze
2016coi	Ic/Ic-BL	58^{+6}_{-7}	$-0.51^{+0.04}_{-0.04}$	$16.4^{+0.4}_{-0.4}$	$-0.21^{+0.02}_{-0.02}$	$-1.18^{+0.04}_{-0.04}$	$17.8^{+0.5}_{-0.5}$	20	BPL	Gold
2016P	Ic/Ic-BL	160^{+40}_{-30}	$-1.23^{+0.06}_{-0.12}$						PL	Silver
2016ilj	Ic-BL	100^{+50}_{-60}	$-0.6^{+0.2}_{-0.2}$						PL	Bronze
2017fwm	Ib/Ic-BL	90^{+60}_{-70}	$-1.1^{+0.2}_{-0.3}$						PL	Bronze
2017dcc	Ic-BL	50^{+10}_{-10}	$-0.6^{+0.1}_{-0.1}$						PL	Silver

Continued on next page

Table B.5. Fit results for the evolution of Si II for Ic-BLs with and without GRBs.

Event name	Type	a [10^3 kms/s]	b	A [10^3 km/s]	α_1	α_2	t_b [days]	s	Best fit	Sample
2017cw	Ic-BL	25^{+4}_{-11}	$-0.18^{+0.12}_{-0.06}$						PL	Silver
2018giu	Ic-BL	50^{+40}_{-80}	$-0.7^{+0.3}_{-0.4}$						PL	Exclude
2018cbz	Ic-BL	80^{+30}_{-50}	$-0.7^{+0.2}_{-0.2}$	14^{+1}_{-2}	$-0.7^{+1.8}_{-0.6}$	$-0.5^{+1.8}_{-0.5}$	16^{+3}_{-3}	20	PL	Bronze
2018gsk	Ic-BL	8^{+4}_{-17}	$0.1^{+0.4}_{-0.2}$						PL	Exclude
2020abdw	Ic/Ic-BL	110^{+70}_{-60}	$-0.9^{+0.2}_{-0.3}$						PL	Bronze